

C. ÖZKAYA

AN ANALYTICAL STUDY ON MINIMUM CONFINEMENT
IN SPIRAL COLUMNS

CENAN ÖZKAYA

JULY 2005

**METU
2005**

AN ANALYTICAL STUDY ON MINIMUM CONFINEMENT IN SPIRAL COLUMNS

A THESIS SUBMITTED TO
THE GRADUATE SCHOOL OF NATURAL AND APPLIED SCIENCES
OF
MIDDLE EAST TECHNICAL UNIVERSITY

BY

CENAN ÖZKAYA

IN PARTIAL FULFILLMENT OF THE REQUIREMENTS
FOR
THE DEGREE OF MASTER OF SCIENCE
IN
CIVIL ENGINEERING

JULY 2005

Approval of the Graduate School of Natural and Applied Sciences

Prof. Dr. Canan Özgen
Director

I certify that this thesis satisfies all the requirements as a thesis for the degree of Master of Science.

Prof. Dr. Erdal Çokça
Head of Department

This is to certify that we have read this thesis and that in our opinion it is fully adequate, in scope and quality, as a thesis for the degree of Master of Science.

Prof. Dr. Ugur Ersoy
Co-Supervisor

Prof. Dr. Güney Özcebe
Supervisor

Examining Committee Members

Prof. Dr. Tugrul Tankut (METU,CE) _____

Prof. Dr. Güney Özcebe (METU,CE) _____

Prof. Dr. Ugur Ersoy (METU,CE) _____

Mr. Ali Terzibasoglu (M.S.C.E.) (Terzibasoglu C. E. Co.) _____

Asst. Prof. Dr. Erdem Canbay (METU,CE) _____

I hereby declare that all information in this document has been obtained and presented in accordance with academic rules and ethical conduct. I also declare that, as required by these rules and conduct, I have fully cited and referenced all material and results that are not original to this work.

Name, Last Name : Cenan Özkaya

Signature :

ABSTRACT

AN ANALYTICAL STUDY ON THE MINIMUM CONFINEMENT IN SPIRAL COLUMNS

Özkaya, Cenan

M.S., Department of Civil Engineering

Supervisor: Prof. Dr. Güney Özcebe

Co-Supervisor: Prof. Dr. Uğur Ersoy

July 2005, 135 pages

The minimum spiral ratio equation given in the codes is derived by equating the strength at the second peak to the strength at the first peak for spiral columns tested under uniaxial load. In this study, specimen behavior under combined bending and axial load was taken as basis while deriving proposed equations. Analyses were carried out by using a Moment-Curvature program.

For normal strength concrete, one regression and one simplified equation giving minimum spiral ratio are proposed. Difference between two equations arises from the number in front of (A_c/A_{ck}) . In regression equation, this number is calculated by means of a function. In simplified equation, this number is a constant.

For high strength concrete, a different regression equation is proposed which is valid for concrete strengths up to 95 MPa. Simplified equation proposed for normal strength concrete is also proposed for high strength concrete up to concrete strengths of 120 MPa.

It was found that; (i) Simplified equation proposed for normal and high strength concrete yielded consistent results in the range of variables studied; (ii) Except some points,

regression equations yielded consistent results; (iii) It is recommended to use simplified equation instead of regression and code equations since it yields more consistent results than code and regression equations.

Keywords: Confined Concrete, Ductility, Moment-Curvature, Minimum Spiral Volumetric Ratio

ÖZ

FRETLİ KOLONLARDA MİNİMUM SARGI DONATISI ÜZERİNE ANALİTİK BİR ÇALIŞMA

Özkaya, Cenan

Yüksek Lisans, İnşaat Mühendisliği Bölümü

Tez Yöneticisi: Prof. Dr. Güney Özcebe

Ortak Tez Yöneticisi: Prof. Dr. Uğur Ersoy

Temmuz 2005, 135 sayfa

Yürürlükte olan Betonarme yönetmeliklerinde minimum fret oranını veren denklem, aksel basınç altındaki kolonun ikinci tepe noktasındaki dayanımın birinci tepe noktasındaki dayanıma eşit olmasına dayanmaktadır. Bu çalışmada ise kesitlerin eğilme ve aksel yük altındaki davranışları esas alınarak minimum fret oranını veren denklemler elde edilmiştir. Analizler bir Moment-Eğrilik programı aracılığı ile gerçekleştirilmiştir.

Normal dayanımlı betonlar için minimum fret oranını veren bir adet regresyon ve bir adet basitleştirilmiş denklem önerilmiştir. Bu iki denklemin farkı, regresyon denkleminde (A_c/A_{ck}) 'in önündeki sayı bir fonksiyon aracılığı ile hesaplanırken basitleştirilmiş denklemde bir sabittir.

Yüksek dayanımlı betonlarda, 95 MPa beton dayanımına kadar geçerli olan farklı bir regresyon denklemi önerilmiştir. Normal dayanımlı betonlar için önerilen basitleştirilmiş denklem 120 MPa beton dayanımına kadar yüksek dayanımlı betonlar için de önerilmiştir.

(i) Çalışılan parametrelerde, basitleştirilmiş denklemin normal ve yüksek dayanımlı betonlarda tutarlı sonuçlar verdiği; (ii) Regresyon denklemlerinin bazı noktalar haricinde

tutarlı sonuçlar verdiđi; (iii) Basitleştirilmiş denklemin çalışılan parametrelerde daha tutarlı sonuçlar verdiđinden dolayı regresyon ve yürürlükte olan denklemlerin kullanılmasından daha avantajlı olduđu sonuçlarına varılmıştır.

Anahtar Sözcükler: Sargılı Beton, Süneklik, Moment-Eğrilik, Minimum Hacimsel Fret Oranı

ACKNOWLEDGEMENTS

This study was conducted under the supervision of Prof. Dr. Güney Özcebe and co-supervision of Prof. Dr. Ugur Ersoy. I wish to express my deepest appreciation to them for their suggestions in the creation of the scope of this study. Moreover, I am indebted to them for their criticism and encouragement throughout the study and my life.

I would like to give my sincere thanks to Prof. Dr. Tugrul Tankut, Assistant Prof. Dr. Erdem Canbay and Consulting Engineer Ali Terzibasoglu (Honorary Dr., M.S.C.E., B.S.C.E.) for their precious contributions.

I owe thanks to Mr. Hakan Ince for the Moment-Curvature program used in this study.

I owe special thanks to people who provided research reports from libraries of Cornell University and University of California at Berkeley.

I would like to give my thanks to those of my friends who helped me throughout this study.

Last, but not least thanks to my family for being with me all the way.

TABLE OF CONTENTS

	Page
PLAGIARISM.....	iii
ABSTRACT	iv
ÖZ.....	vi
ACKNOWLEDGEMENTS	viii
TABLE OF CONTENTS	ix
LIST OF TABLES	xi
LIST OF FIGURES.....	xii
LIST OF SYMBOLS.....	xvii
 CHAPTERS	
1. INTRODUCTION	1
1.1. General	1
1.2. Object and Scope.....	3
 2. LITERATURE SURVEY	5
2.1. General	5
2.2. Spiral Column Database	12
 3. DEFINITION OF THE PROBLEM	14
3.1. General	14
3.2. Mechanics of Spiral Confinement	15
3.3. Derivation of the Code Equations Giving Minimum Spiral Ratio.....	17
3.4. Review of Previous Research on Minimum Spiral Ratio....	19
 4. DERIVATION OF PROPOSED EQUATIONS.....	22
4.1. Information about Computer Program	22

4.2. Derivation of the Proposed Equations for Spiral Columns Having Normal Strength Concrete	24
4.3. Analytical Studies Carried Out for Sections Having Normal Strength Concrete	29
4.4. Derivation of the Proposed Equations for Spiral Columns Having High Strength Concrete.....	35
4.5. Analytical Studies Carried Out for Sections Having High Strength Concrete	39
4.6. Comparison of Eq. (4.42) with Eq.(4.21)	43
 5. ANALYTICAL STUDIES	 45
5.1. Effect of Volumetric Ratio of Spiral Steel on Section Behaviour (NSC)	45
5.2. Effect of Longitudinal Steel Percentage and Axial Load Level	58
5.3. Effect of Number and Orientation of Longitudinal Bars.....	60
5.4. Effect of Volumetric Ratio of Spiral Steel on Section Behaviour (HSC).....	61
 6. SUMMARY AND CONCLUSION.....	 75
6.1. Summary	75
6.2. Conclusion.....	76
6.3. Recommendations for Future Researches	77
 REFERENCES	 79
APPENDICES (Moment-Curvature Comparisons)	86
Appendix A (Effect of Volumetric Ratio of Spiral Steel on Section Behaviour (NSC)).....	86
Appendix B (Effect of Longitudinal Steel Percentage and Axial Load Level)	101
Appendix C (Effect of Number and Orientation of Longitudinal Bars)	108
Appendix D (Effect of Volumetric Ratio of Spiral Steel on Section Behaviour (HSC)).....	121

LIST OF TABLES

		Page
Table 3.1.	K_c Values of 28 Sections Designed According to Eq. (3.13)	20
Table 4.1.	Common Properties of Cross-Sections	30
Table 4.2.	Properties of 28 NSC Sections Designed According to Eq. (3.13)	30
Table 4.3.	Properties of 21 HSC Sections Designed According to Eq. (4.21)	39
Table 5.1.	Spiral Volumetric Ratio Comparisons for 28 NSC Sections	48
Table 5.2.	K_{pN} and $K_{.85N}$ Values of 28 NSC Sections Designed According to Proposed and Code Equations	50
Table 5.3.	Curvature Ductility Index Comparisons for 28 NSC Sections	52
Table 5.4.	M_{R1} and M_{R2} Values of 28 NSC Sections Designed According to Proposed and Code Equations	54
Table 5.5.	Capacity Index Comparisons for 28 NSC Sections	55
Table 5.6.	Strains Used for Calculating CI that are Different than 0.04.....	56
Table 5.7.	Comparisons of Moment Resistances at the Strain of 0.04 for 28 NSC Sections.....	57
Table 5.8.	Properties of Section 57.....	59
Table 5.9.	Spiral Volumetric Ratio Comparisons for 28 HSC Sections	65
Table 5.10.	K_{pH} and $K_{.85H}$ Values of 28 HSC Sections Designed According to Proposed and Code Equations	67
Table 5.11.	Curvature Ductility Index Comparisons for 28 HSC Sections	68
Table 5.12.	M_{R1} and M_{R2} Values of 28 HSC Sections Designed According to Proposed and Code Equations	70
Table 5.13.	Capacity Index Comparisons for 28 HSC Sections	71
Table 5.14.	Strains Used for Calculating CI that are Different than 0.03.....	72
Table 5.15.	Comparisons of Moment Resistances at the Strain of 0.03 for 28 HSC Sections.....	73

LIST OF FIGURES

	Page
Figure 4.1. Spiral Column under Combined Axial Load and Bending (Early Stages)	24
Figure 4.2. Spiral Column under Combined Axial Load and Bending (Later Stages)	25
Figure 4.3. Δ_2 vs. (A_c/A_{ck}) for 28 NSC Sections.....	32
Figure 4.4. Variation of Δ_2/m with (A_c/A_{ck}) for NSC Sections.....	33
Figure 4.5. Variation of Δ_2/m with “m” for NSC Sections.....	33
Figure 4.6. Δ_2 vs. (A_c/A_{ck}) for 21 HSC Sections.....	40
Figure 4.7. Variation of Δ_2/m with (A_c/A_{ck}) for HSC Sections.....	41
Figure 4.8. Variation of Δ_2/m with “m” for HSC Sections.....	41
Figure 4.9. Variation of Δ_2/m with “m” for NSC and HSC Sections.....	43
Figure 4.10. Comparison of Volumetric Ratios of Spiral Steel Required by Eq. (4.21) and Eq. (4.42).....	44
Figure 5.1. Comparison of Volumetric Ratios of Spiral Steel for “m” =0.0595.....	46
Figure 5.2. Comparison of Volumetric Ratios of Spiral Steel for “m” =0.0833.....	46
Figure 5.3. Comparison of Volumetric Ratios of Spiral Steel for “m” =0.0952.....	47
Figure 5.4. Comparison of Volumetric Ratios of Spiral Steel for “m” =0.1333.....	47
Figure 5.5. Different Longitudinal Steel Orientations.....	61
Figure 5.6. Comparison of Volumetric Ratios of Spiral Steel for “m”=0.1548.....	62
Figure 5.7. Comparison of Volumetric Ratios of Spiral Steel for “m” =0.2024.....	63
Figure 5.8. Comparison of Volumetric Ratios of Spiral Steel for “m” =0.2262.....	64
Figure 5.9. Comparison of Volumetric Ratios of Spiral Steel for “m”=0.2857.....	64
Figure A.1. Comparison of Proposed and Code Equations for Section 1.....	86
Figure A.2. Comparison of Proposed and Code Equations for Section 2.....	87
Figure A.3. Comparison of Proposed and Code Equations for Section 3.....	87
Figure A.4. Comparison of Proposed and Code Equations for Section 4.....	88
Figure A.5. Comparison of Proposed and Code Equations for Section 5.....	88

Figure A.6.	Comparison of Proposed and Code Equations for Section 6	89
Figure A.7.	Comparison of Proposed and Code Equations for Section 7.....	89
Figure A.8.	Comparison of Proposed and Code Equations for Section 8.....	90
Figure A.9.	Comparison of Proposed and Code Equations for Section 9.....	90
Figure A.10.	Comparison of Proposed and Code Equations for Section 10.....	91
Figure A.11.	Comparison of Proposed and Code Equations for Section 11.....	91
Figure A.12.	Comparison of Proposed and Code Equations for Section 12.....	92
Figure A.13.	Comparison of Proposed and Code Equations for Section 13.....	92
Figure A.14.	Comparison of Proposed and Code Equations for Section 14.....	93
Figure A.15.	Comparison of Proposed and Code Equations for Section 15.....	93
Figure A.16.	Comparison of Proposed and Code Equations for Section 16.....	94
Figure A.17.	Comparison of Proposed and Code Equations for Section 17.....	94
Figure A.18.	Comparison of Proposed and Code Equations for Section 18.....	95
Figure A.19.	Comparison of Proposed and Code Equations for Section 19.....	95
Figure A.20.	Comparison of Proposed and Code Equations for Section 20.....	96
Figure A.21.	Comparison of Proposed and Code Equations for Section 21.....	96
Figure A.22.	Comparison of Proposed and Code Equations for Section 22.....	97
Figure A.23.	Comparison of Proposed and Code Equations for Section 23.....	97
Figure A.24.	Comparison of Proposed and Code Equations for Section 24.....	98
Figure A.25.	Comparison of Proposed and Code Equations for Section 25.....	98
Figure A.26.	Comparison of Proposed and Code Equations for Section 26.....	99
Figure A.27.	Comparison of Proposed and Code Equations for Section 27.....	99
Figure A.28.	Comparison of Proposed and Code Equations for Section 28.....	100
Figure B.1.	Effect of Longitudinal Steel Percentage on Ductility [Section 4]	101
Figure B.2.	Effect of Longitudinal Steel Percentage on Ductility [Section 4]	102
Figure B.3.	Effect of Longitudinal Steel Percentage on Ductility [Section 4]	102
Figure B.4.	Effect of Longitudinal Steel Percentage on Ductility [Section 25]	103
Figure B.5.	Effect of Longitudinal Steel Percentage on Ductility [Section 25]	103
Figure B.6.	Effect of Longitudinal Steel Percentage on Ductility [Section 25]	104
Figure B.7.	Comparison of Proposed and Code Equations for Section 4.....	104
Figure B.8.	Comparison of Proposed and Code Equations for Section 6.....	105
Figure B.9.	Comparison of Proposed and Code Equations for Section 19.....	105
Figure B.10.	Comparison of Proposed and Code Equations for Section 25.....	106
Figure B.11.	Comparison of Proposed and Code Equations for Section 57.....	106

Figure B.12.	Effect of Axial Load Level on Ductility [Section 57]	107
Figure C.1.	Comparison of Different Number and Orientation of Longitudinal Bars for Section 1	108
Figure C.2.	Comparison of Different Number and Orientation of Longitudinal Bars for Section 1	109
Figure C.3.	Comparison of Different Number and Orientation of Longitudinal Bars for Section 1	109
Figure C.4.	Comparison of Different Number and Orientation of Longitudinal Bars for Section 1	110
Figure C.5.	Comparison of Different Number and Orientation of Longitudinal Bars for Section 1	110
Figure C.6.	Comparison of Different Number and Orientation of Longitudinal Bars for Section 1	111
Figure C.7.	Comparison of Different Number and Orientation of Longitudinal Bars for Section 9	111
Figure C.8.	Comparison of Different Number and Orientation of Longitudinal Bars for Section 9	112
Figure C.9.	Comparison of Different Number and Orientation of Longitudinal Bars for Section 9	112
Figure C.10.	Comparison of Different Number and Orientation of Longitudinal Bars for Section 9	113
Figure C.11.	Comparison of Different Number and Orientation of Longitudinal Bars for Section 9	113
Figure C.12.	Comparison of Different Number and Orientation of Longitudinal Bars for Section 9	114
Figure C.13.	Comparison of Different Number and Orientation of Longitudinal Bars for Section 9	114
Figure C.14.	Comparison of Different Number and Orientation of Longitudinal Bars for Section 9	115
Figure C.15.	Comparison of Different Number and Orientation of Longitudinal Bars for Section 9	115
Figure C.16.	Comparison of Different Number and Orientation of Longitudinal Bars for Section 24	116

Figure C.17.	Comparison of Different Number and Orientation of Longitudinal Bars for Section 24.....	116
Figure C.18.	Comparison of Different Number and Orientation of Longitudinal Bars for Section 24.....	117
Figure C.19.	Comparison of Different Number and Orientation of Longitudinal Bars for Section 24.....	117
Figure C.20.	Comparison of Different Number and Orientation of Longitudinal Bars for Section 24.....	118
Figure C.21.	Comparison of Different Number and Orientation of Longitudinal Bars for Section 24.....	118
Figure C.22.	Comparison of Different Number and Orientation of Longitudinal Bars for Section 24.....	119
Figure C.23.	Comparison of Different Number and Orientation of Longitudinal Bars for Section 24.....	119
Figure C.24.	Comparison of Different Number and Orientation of Longitudinal Bars for Section 24.....	120
Figure D.1.	Comparison of Proposed and Code Equations for Section 29.....	121
Figure D.2.	Comparison of Proposed and Code Equations for Section 30.....	122
Figure D.3.	Comparison of Proposed and Code Equations for Section 31.....	122
Figure D.4.	Comparison of Proposed and Code Equations for Section 32.....	123
Figure D.5.	Comparison of Proposed and Code Equations for Section 33.....	123
Figure D.6.	Comparison of Proposed and Code Equations for Section 34.....	124
Figure D.7.	Comparison of Proposed and Code Equations for Section 35.....	124
Figure D.8.	Comparison of Proposed and Code Equations for Section 36.....	125
Figure D.9.	Comparison of Proposed and Code Equations for Section 37.....	125
Figure D.10.	Comparison of Proposed and Code Equations for Section 38.....	126
Figure D.11.	Comparison of Proposed and Code Equations for Section 39.....	126
Figure D.12.	Comparison of Proposed and Code Equations for Section 40.....	127
Figure D.13.	Comparison of Proposed and Code Equations for Section 41.....	127
Figure D.14.	Comparison of proposed and Code Equations for Section 42.....	128
Figure D.15.	Comparison of Proposed and Code Equations for Section 43.....	128
Figure D.16.	Comparison of Proposed and Code Equations for Section 44.....	129
Figure D.17.	Comparison of Proposed and Code Equations for Section 45.....	129
Figure D.18.	Comparison of Proposed and Code Equations for Section 46.....	130

Figure D.19.	Comparison of Proposed and Code Equations for Section 47.....	130
Figure D.20.	Comparison of Proposed and Code Equations for Section 48.....	131
Figure D.21.	Comparison of Proposed and Code Equations for Section 49.....	131
Figure D.22.	Comparison of Proposed and Code Equations for Section 50.....	132
Figure D.23.	Comparison of Proposed and Code Equations for Section 51.....	132
Figure D.24.	Comparison of Proposed and Code Equations for Section 52.....	133
Figure D.25.	Comparison of Proposed and Code Equations for Section 53.....	133
Figure D.26.	Comparison of Proposed and Code Equations for Section 54.....	134
Figure D.27.	Comparison of Proposed and Code Equations for Section 55.....	134
Figure D.28.	Comparison of Proposed and Code Equations for Section 56.....	135

LIST OF SYMBOLS

A_0	Cross sectional area of the spiral steel
A_c	Total cross-sectional area. (Gross Area)
A_{ck}	Area of core concrete
d_{sp}	Spiral reinforcement diameter
D_o	Overall diameter of the column cross-section
D	Core concrete diameter
E_s	Modulus of elasticity of steel
f_c	Unconfined concrete compressive strength
f_{ck}	Characteristic compressive strength of unconfined concrete
f_{cc}	Strength of confined concrete
f_{su}	Ultimate strength of longitudinal steel
f_{yk}	Characteristic yield strength of longitudinal steel
f_{yw}	Yield strength of spiral steel
f_{ywk}	Characteristic yield strength of spiral steel
F_{c1}	Resultant concrete compressive force at early stages (At the stage of cover crushing)
F_{c2}	Resultant concrete compressive force at later stages (When confinement becomes fully effective)
$K_{.85H}$	Curvature of the cross-section at the 85% of the maximum moment
$K_{.85N}$	Curvature of the cross-section at the 85% of the moment at the extreme fiber strain of 0.004
K_c	Slope of post-peak region of stress–strain curve of confined concrete in Saatcioglu and Razvi model
K_{pH}	Curvature of the cross-section at the maximum moment
K_{pN}	Curvature of the cross-section at the extreme fiber strain of 0.004
k_1	Coefficient for confined concrete in Saatcioglu and Razvi model
k_3	Constant for the ratio of in place unconfined concrete strength to the cylinder strength of unconfined concrete in the Saatcioglu and Razvi model
M_{c1}	Resultant moment of concrete compressive forces about centroid of the cross-section at the stage of cover crushing

M_{c2}	Resultant moment of concrete compressive forces about centroid of the cross-section at later stages
M_{R1}	Moment capacity of the cross-section at the first peak
M_{R2}	Moment capacity of the cross-section at the extreme fiber strain of 0.04 (0.03 for HSC)
M_{s1}	Resultant longitudinal steel moment about centroid of the cross-section at the stage of cover crushing
M_{s2}	Resultant longitudinal steel moment about centroid of the cross-section at later stages
N	Axial load on the column cross-section
s	Spacing of the spiral reinforcement
x_1	Moment arm of F_{c1} with respect to the centroid of the cross-section
x_2	Moment arm of F_{c2} with respect to the centroid of the cross-section
β_1	A factor defining the ratio of average concrete compressive stress to the unconfined concrete strength at the stage of cover crushing
β_2	A factor defining the ratio of average concrete compressive stress to the confined concrete strength at later stages (When confinement becomes fully effective)
ϵ_c	Concrete strain
ϵ_{sh}	Longitudinal steel strain at the onset of strain hardening
ϵ_{su}	Ultimate longitudinal steel strain
ϕ	Steel bar diameter
γ_1	A factor defining the ratio of area of concrete in compression to the total cross-sectional area at the stage of cover crushing
γ_2	A factor defining the ratio of area of concrete in compression to the core area at later stages (When confinement becomes fully effective)
ρ_s	Volumetric ratio of the spiral steel
σ_2	Lateral pressure in the core concrete due to transverse reinforcement
μ_o	Dependable displacement ductility
μ	Displacement ductility

CHAPTER 1

INTRODUCTION

1.1. General

Analytical and experimental research on mechanics of confined concrete goes back to early 1900's. Since then, hundreds of researchers contributed to the developments of mechanics of confined concrete. On the other hand, there is still debate on some subjects which need to be agreed upon.

Lateral confinement reinforcement in reinforced concrete columns can be applied in various forms such as circular spirals, circular hoops, rectangular ties, crossties and square helix. Lateral confinement in reinforced concrete columns is used for shear reinforcement, providing ductility and strength enhancement to the core concrete by applying it lateral confining pressure and preventing buckling of the longitudinal reinforcement at high curvature values. In ordinary structures, rectangular ties are used more frequently than circular spirals since it is easier to construct rectangular columns than circular columns in building structures. However, circular column's omnidirectional strength characteristics under seismic and wind loads make them favorable for bridge piers [1]. In building structures, difficulties associated with detailing beam column intersections occur when circular columns are used.

When designing reinforced concrete frames against seismic attack, it is assumed that plastic hinges occur in the beams and at the bases of the columns. This phenomenon is called "strong column – weak beam". However, under severe seismic attack, plastic hinges are expected to form at other locations of the columns in addition to the bases of them. In this case, lateral confinement is necessary to ensure ductile response associated with large rotations. Large rotations are necessary to dissipate energy, which is in turn, is necessary for the survival of the structure.

There are various confined concrete models developed. Unfortunately, almost all of these models were developed with data of tests on uniaxially loaded specimens. In addition, in

most of these tests, parameters were inadequate to represent the design practice. Some confined concrete models such as models proposed by Scott [2] and Mander [3] take effect of strain rate into account on the stress-strain curve of confined concrete which is quite important in case of seismic excitation and blast.

The current code provisions for spiral reinforcement are based on the ACI Committee 105 recommendations of 1933 [23]. In the derivation of the code equations, uniaxially loaded column behavior was considered. The idea is to equate axial strength lost due to crushing of the concrete cover to the strength gained in the core concrete due to confinement. It is not realistic to consider a column only under uniaxial load in practice. Hence, the validity of the code equations can be argued upon. Columns are subjected to bending moments in addition to axial loads in structures. Therefore, derivation of the equations for minimum spiral ratio should be based on the behaviour under combined bending and axial load rather than the behaviour under uniaxial loading.

In this study, by starting with the equation proposed by Ersoy and Özcebe [5] an equation for the minimum spiral reinforcement ratio was derived by conducting analytical studies. In this equation, called regression equation, the number in front of (A_c/A_{ck}) is a function of the ratio of concrete compressive strength (f_{ck}) to yield strength of spiral steel (f_{ywk}). Then, by using the results obtained from analytical studies, a number was proposed as a constant in front of (A_c/A_{ck}) rather than a regression function. This second equation is called simplified equation. Their comparisons with the code equations were made with varying parameters that are considered to affect the specimen behaviour. Simplified equation yielded satisfactory results in the range of parameters studied. On the other hand, regression equation yielded relatively poor results at some exceptional points.

A different regression equation was derived for high strength concrete. Simplified equation for normal strength concrete was extended to high strength concrete by carrying out further analytical studies. Comparisons were done between these two equations and code equations. Simplified equation yielded satisfactory results up to $f_{ck}=120$ MPa. On the other hand, the upper limit for regression equation for high strength concrete is selected as $f_{ck}=95$ MPa.

1.2. Object and Scope

The minimum spiral ratio equation given in the codes is derived by equating the strength at the second peak to the strength at the first peak for spiral columns tested under uniaxial load. This equation is as follows:

$$\mathbf{r}_s = 0.45 \frac{f_{ck}}{f_{ywk}} \left[\frac{A_c}{A_{ck}} - 1 \right] \quad (1.1)$$

However, realizing that ρ_s approaches zero as (A_c/A_{ck}) approaches 1.0, a second equation is given as the lower limit:

$$\mathbf{r}_s = 0.12 \frac{f_{ck}}{f_{ywk}} \quad (1.2)$$

In the building codes, design of columns under uniaxial loading is not permitted and a minimum eccentricity is specified. For the design engineer, the important thing is the ductility of the column under axial load and bending moment and not the ductility under uniaxial loading. Therefore, the basic philosophy behind the derivation of the code equation becomes debatable. It should also be pointed out that the equation gives unrealistically low spiral ratios when (A_c/A_{ck}) approaches one.

Considering the drawbacks of the code equation, Ersoy and Özcebe [5] derived an equation for minimum spiral ratio not by using the P- Δ curve as in the code equation, but using the Moment-Curvature curves. Ersoy and Özcebe argued that the equation derived was more realistic than the code equation because it was based on moment capacities rather than the axial load. The basic philosophy in the derivation of the equation proposed was to equate the moment at a specified curvature to the maximum moment. Parameters in this equation were based on some assumptions.

The main objective of this study was to make case studies on spiral columns to determine the variation of the basic variables included in Ersoy and Özcebe [5] equation.

- Statistical studies were carried out and a regression equation was proposed for the minimum spiral ratio. Also, using the analytical results obtained, a simplified equation was derived. The derivation was based on Moment-Curvature curves. The Moment-Curvature program developed for this purpose was checked using the test results.

- The equation derived for minimum spiral ratio was then modified for HSC columns using material models proposed for HSC.

- A database was prepared for spiral columns which included 463 tests. The database was mainly used to determine the strains corresponding to maximum moment. The strain at maximum moment was an important parameter in the derivation of the proposed equation.

- Analytical studies were made on 28 circular column sections with spiral reinforcement having NSC. Similar studies were made on 21 circular column sections having HSC. In these studies, Moment-Curvature curves obtained for these columns using the proposed minimum ratio and code equations were compared to observe the behaviour and ductility.

CHAPTER 2

LITERATURE SURVEY

2.1. General

For a long time, it is totally agreed upon by researchers that lateral reinforcement increases both strength and ductility. It is well known that the confining mechanism of circular spirals and rectangular ties are different. It was also stated by Saatcioglu and Razvi [6] that the restraining action of the hoop, between the corners is related to the flexural rigidity of the steel, which depends on the size and unsupported length of the bar in rectangular and square columns. However, the flexural rigidity of the hoop between the laterally supported nodal points and the resulting restraining action is very small as compared to the restraining action of the corners and the other nodal points. If cross ties or inside hoops are used to support the middle bars, additional points of high lateral restraint are generated. On the other hand, in circular hoops and spirals, axial rigidity of the lateral steel dominates the deformation of the lateral steel. Axial rigidity is much higher than flexural rigidity. By using rectangular ties, the deformation of the lateral steel at the midway between the two supported longitudinal steels becomes maximum. Since confining pressure and deformation are inversely related, confining pressure is high only at the locations close to the supported longitudinal bars in case of rectangular ties. Confining pressure is minimum at the midway between the supported longitudinal bars. In case of circular spirals and hoops, confining pressure is uniform through the perimeter of the lateral reinforcement due to uniform hoop tension.

Chan [4] proposed a trilinear stress-strain curve for confined concrete. While first two of these lines have positive slope and same for unconfined and confined concrete, positive or negative slope of the third line is dependent on the amount of confinement reinforcement. Slope of the third line is negative for plain concrete and it turns to positive as confinement reinforcement increases.

Roy and Sozen [4] concluded that using rectangular ties does not enhance the strength of the confined concrete. Authors proposed a bilinear curve for confined concrete. The initial

part of the curve is same for both plain and confined concrete. Slope of the descending branch is dependent upon the volumetric ratio of tie steel to concrete core and the ratio of the shorter side dimension of the compressed concrete section to the tie spacing.

Soliman and Yu [9] proposed a stress-strain relationship for confined concrete. This stress-strain relationship consists of a parabola and two straight lines. The major disadvantage of this model is that it does not take effect of spalling of concrete into account and the stress-strain curve is based upon the total concrete area under compression.

In the initial version of Kent and Park model [4], which is a modification of the Roy and Sozen's model, strength increase due to rectangular confinement is not included. Again, the initial part of the stress-strain curve is identical for both unconfined and confined cross sections. In the modified version of Kent and Park model [11], strength enhancement due to confinement is taken into account.

Sargin [9] proposed a single continuous curve of confined concrete. In this model, strain gradient is taken into account. Sargin's equations are based on regression analysis of tests conducted under concentric and eccentric compression loads. Important feature of this model is that it takes strain gradient into account. It should also be noted longitudinal steel is not taken into account in this model.

In most of the old tests mentioned above, small-scale specimens with simple tie arrangements were tested [4]. This is the most probable reason of noticing no strength increase due to confinement. In these tests, confined concrete strength was barely higher than the unconfined concrete strength.

Bertero, Vallenas and Popov [9] proposed a model for confined concrete which takes the ratio of area of longitudinal steel to the cross-section area into account. Strength increase due to confinement is included in this model.

In Sheikh and Uzumeri model [4], the increase in strength of confined concrete was calculated by using effectively confined concrete area concept. Effectively confined area is less than the core concrete area. Most pronounced feature of this model is that it takes arrangement of longitudinal bars into account in addition to the area of the longitudinal

bars. In this model, both strength and ductility enhancement due to confinement is included.

Scott, Park and Priestley [2] stated that longitudinal strain rate influenced both the peak stress and the slope of the falling branch of the stress-strain curve of the concrete core. For the high strain rate in the tests (0.0167/sec), the peak stress and the slope of the falling branch were increased by about 25 percent compared with those for the low strain rate (0.0000033/sec). Authors noted that an increase in the spacing of hoop sets, while maintaining a constant volume ratio of transverse reinforcement by the use of larger diameter hoop bars, tended to reduce the efficiency of the concrete confinement. Authors also noticed that the presence of strain gradient across the column unit due to eccentric loading increased the peak longitudinal concrete compressive strain measured at first hoop fracture very significantly. The presence of a strain gradient also resulted in a smaller decrease in load and moment carried with increasing strain after peak load than was predicted by analysis using stress-strain curves for concrete obtained from the concentric load tests. When using Modified Kent and Park model for confined sections under high strain rates, applying a multiplying factor of 1.25 to the peak stress, the strain at peak stress and the slope of the falling branch yielded good agreement with Scott's test results.

In the model proposed for confined concrete by Mander, Priestley and Park [3], the increase in the strain at ultimate strength is assumed to be about five times the strength increase. In this model, an allowance for the dynamic response in stress-strain modeling may be incorporated by modifying the quasi-static concrete parameters by dynamic magnification factors which are then used in the stress-strain model.

Dash and Ahmad [12] proposed a model for stress-strain relationship of spirally confined normal and high strength concrete columns. The model proposed is applicable for a wide range of variables including the strength of the concrete, the presence of longitudinal reinforcement, the diameter of the circular section, the amount of lateral reinforcement and the rate of loading. This model utilizes a single fractional equation.

Ngo, Mendis and Kusuma [13] stated that HSC columns perform better than NSC columns (with the same axial load capacity) when subjected to extreme impulsive loading. HSC columns also had higher energy absorption capacity than NSC columns when subjected to

blast loading. A new strain-rate dependent model was proposed by the authors for concrete under dynamic load which can take the strain-rate effect by incorporating multiplying factors for increases in the peak stress, strain at peak strength and the variation in the softening slope into account. Authors also noted that shear failure was the dominant mode of failure for close-range explosion.

Priestley, Park and Potangaroa [14] stated that the portion of the confined column length should be increased when axial load levels are high. Tests indicated that SEAOC (Structural Engineers Association of California) /ACI (American Concrete Institute) volumetric ratios of confining steel are excessive at low axial loads, and slightly unconservative at axial load levels higher than $0.5f_{ck}A_c$. In New Zealand Code, the level of axial load is included in the equations giving the minimum spiral reinforcement ratio as a multiplying factor.

Martinez, Nilson and Slate [15] concluded that effectiveness of the spiral reinforcement in enhancing the compressive strength of lightweight columns is about 60 percent lower than for corresponding normal weight columns. If the spiral is designed with the philosophy of equating the axial load capacity lost due to crushing of cover concrete to the strength gained due to the confinement, then in the lightweight columns about 2.7 times more steel is required than required in the normal weight columns. Martinez, Nilson and Slate's studies on High Strength Concrete columns (HSC) revealed that the load deflection curves of High Strength Concrete columns were much steeper and more linear on the ascending branch than the corresponding Low Strength Concrete (LSC) columns. Authors noticed that the failure of HSC specimens was a shear plane failure which was also reported by Cusson and Paultre [16]. Strain at the peak stress and strain at the failure for HSC columns increase with confinement but their values are much smaller than the corresponding LSC columns. Authors also concluded that ACI design recommendations for spiral reinforcement should not be applied to lightweight concrete columns.

Ahmad and Shah [17] concluded that confining reinforcement is less effective for lightweight concrete than with normal weight concrete of comparable strength and confinement. By using the theoretical model proposed in the study, the authors also noted that steel stresses at the peak of the confined concrete's stress-strain curve are smaller with

higher concrete compressive strength and are not influenced by the yield strength of the spiral reinforcement for the same compressive strength.

Fafitis and Shah [18] concluded that the rate of drop in the moment capacity of the column after the first peak was higher for higher compressive strength concrete.

Fafitis and Shah [19], in a separate study, concluded that a smaller column may be more ductile than a larger one when both are designed according to the current code. Also, everything else being equal, the square columns designed according to the ACI method have higher moment capacities at large strains or curvature values than the circular ones.

Mander, Priestley and Park [20] stated the possibility of reduction of the available ductility of a section confined with high-strength transverse steel due to premature fracture of that steel and a consequent loss of effective confinement. Authors concluded that configuration of transverse reinforcement has a particularly large effect on the confinement effectiveness coefficient. Confinement effectiveness coefficient is in the range of 0.40-0.70 for the rectangular walls and 0.89-1.0 for circular columns. According to the authors, the only significance of the configuration of longitudinal reinforcement was through its effect on confinement effectiveness coefficient. Authors also concluded that the most significant parameter affecting the shape of the stress-strain curve of confined concrete for all section shapes was the quantity of confining reinforcements. As the volumetric ratio of confining reinforcement increased, the longitudinal strain at which hoop fracture occurred increased.

Zahn, Park and Priestley [21] concluded that when higher strength spiral steel is used instead of lower grade spiral steel, the ultimate longitudinal concrete compression strain decreases if both columns are designed according to code equations. The reason is that the reduced quantity of higher strength spiral steel has a smaller capacity to absorb strain energy from the core concrete.

Azizinamini, Corley and Johal [22] stated that square helix as transverse reinforcement is subjected to both bending and axial tension. Therefore, square helix reinforcement provides only partial confinement. Authors concluded that the square helix reinforcement was able to enclose the core concrete more efficiently than the discrete-type transverse

reinforcement. Authors also noted that the use of square helix as transverse reinforcement resulted in extensive cover concrete spalling.

Sheikh and Toklucu [23] concluded that the spiral steel yielded when concrete carried the maximum stress in well-confined columns. According to the authors, in some cases, a large amount of closely spaced spiral steel may result in a lack of stable descending branch of the column behaviour curve due to the longitudinal bars instability. Authors also concluded that the concept of a limit on the specified yield strength of spiral steel is true.

Cusson and Paultre [16] concluded that an increase of the tie yield strength can produce significant strength and toughness gains only in adequately confined columns. Therefore, using high strength steel ties in lightly confined specimens does not translate into strength and ductility gains.

Madi, Deeb and Samra [24] proposed adding a factor to the current ACI code requirements for spiral steel which is a function of the eccentricity-to-column diameter ratio. This factor is multiplied by the original ACI expression for spiral steel. Authors concluded that the current ACI Code requirements for transverse reinforcement are low at high eccentricity levels and high for axially loaded columns.

Saatcioglu and Baingo [25] concluded that individual circular hoops are as effective as continuous circular spirals in confining HSC columns, provided that the ends of the ties are bent and anchored into the confined core. However, the spiral reinforcement appears to be effective in improving stability of longitudinal reinforcement at later stages of deformation. Authors also concluded that the deformability of HSC columns decrease with increasing axial compression. Authors also noted that the ratio $(\rho_s \times f_{yw}) / (f_c)$ can be used as a design parameter for confinement of circular HSC columns.

Considering the drawbacks of the code equations, Ersoy and Özcebe [5] derived an equation for minimum spiral ratio using the Moment-Curvature curves. Baran [7] used the equation proposed by Ersoy and Özcebe in his studies. Baran tested eight spirally reinforced columns. Four of these eight columns were designed according to the code equations and four columns were designed according to the proposed equation. (A_c / A_{ck}) and yield strength of spiral steel (f_{yw}) were taken as variables. It was concluded that

proposed equation yields ductile response in the range of variables studied. However, when high strength spiral steel ($f_{yw}=990$ MPa) was used, rupture of the spiral steel occurred at high curvature values in some specimens. Rupture of spiral reinforcement would lead to a complete unwinding of the spiral [25]. Also, rupture of the spiral steel having yield strength of 650 MPa occurred in some specimens at high curvature values.

Dinçer [8] modified the equation proposed by Ersoy and Özcebe [5] by carrying out some analytical studies. Dinçer tested four spirally reinforced columns. Two of these columns were designed according to the code equations and the other two were designed according to the modified proposed equation. (A_c/A_{ck}) was the variable in his studies. In Baran's and Dincer's studies, (A_c/A_{ck}) ratios equal to 1.1 and 1.29 were used.

According to Razvi and Saatcioglu [26], if the same percentage of strength enhancement is desired, higher-strength concrete columns are required to be confined proportionately more than those with lower-strength concretes. Higher grades of confinement reinforcement, with yield strengths of up to 1000 MPa, were found to be effective in circular columns with spirals, provided a minimum volumetric ratio of spiral steel is maintained. Strength and ductility enhancements in circular columns, with up to 124 MPa concrete strength, showed approximately linear variation with $(\rho_s \times f_{yw}) / (f_c)$ when confined by circular spirals.

According to Bing, Park and Tanaka [27], in order to prevent a relatively early loss of strength of high-strength concrete caused by both buckling of reinforcing bars and excessively deep arching of the confined concrete in between the spirals and hoops, all specimens should have sufficiently close spacing of transverse reinforcement.

Esmaily and Xiao [28] reported the effect of axial force level and the loading pattern on the flexural strength and the deformation capacity of the column.

Ersoy and Özcebe [5] proposed an equation giving the minimum spiral reinforcement ratio. In the derivation of the proposed equation, behaviour of the column under combined bending and axial load was considered. Ersoy and Özcebe criticized three points in the code equations giving the minimum spiral reinforcement ratio that are as follows:

1. If the basic theory behind the code equation is true, why it does not give realistic results when $(A_c/A_{ck}) < 1.20$ and a second equation is needed?
2. Do code equations give realistic results? Can using same volumetric ratio of spiral reinforcement when (A_c/A_{ck}) is between 1.0 and 1.27 be realistic?
3. In practice, no column is under uniaxial load only. Do code equations give realistic results for the columns under combined bending and axial load? Do the columns having minimum volumetric ratio of spiral reinforcement according to code equations behave in a ductile manner?

2.2. Spiral Column Database

A spiral column database was developed by the author which contains data for 463 test columns. One hundred twenty nine of these columns were tested under reversed bending. One hundred seventy one of these columns were tested under concentric loading. One hundred forty eight of these columns were CFT (Concrete Filled Tube) and tubed columns tested under concentric loading, reversed bending and under eccentric loading. Twelve of these columns were tested under combined bending and axial load. Three of these columns have interlocking spirals as transverse reinforcement and tested under reversed bending. The parameters included in the database are diameter of the column, cover concrete thickness, loading type, cross-section type, length of the test region, compressive strength of concrete, number and diameter of longitudinal bars, yield and ultimate strength of longitudinal bars, longitudinal and transverse reinforcement ratio, diameter of the transverse reinforcement, yield strength of the transverse reinforcement, hoop spacing, configuration of the test column, value of the axial load applied, failure type, tube thickness of the steel tube for CFT (Concrete Filled Tube) and tubed columns, yield and ultimate strength of the tube. Author could not reach few parameters for some columns. For this reason, some data is missing for some columns. Author believes that international usage of the spiral column database can make unaccessible data accessible. Sometimes spacing of the transverse reinforcement was back substituted from volumetric ratio and diameter of the transverse reinforcement and vice versa. The reason for back substitution is the inadequate information about the test specimens in the original papers.

As long as the author could reach them, actual material strengths at the test day were used instead of nominal material strengths. For some columns, on the other hand, nominal material strengths were used due to inadequate information. For few columns, yield and ultimate strengths of longitudinal and transverse reinforcement were derived from stress-strain curves of the reinforcing bars by the author. Therefore, small variations from the actual values may occur for these few columns.

Another thing to be mentioned is the failure types included in the database. For the columns under reversed bending, response curves were used in order to determine the failure type. Following failure criterion was used:

- Flexural failure $6 \leq \mu_0$ (Satisfactory Displacement Ductility)
- Failure with moderate ductility, dominated by shear $4 \leq \mu_0 \leq 6$
- Shear Failure with restricted ductility $2 \leq \mu_0 \leq 4$
- (Brittle) Shear Failure $\mu_0 \leq 2$

It should be noted that this classification was proposed by Ang, Paulay and Priestley [1]. However, the term “satisfactory displacement ductility” was not fully utilized for some columns in this study. If strength degradation larger than 15 % between different cycles at a displacement ductility level or between two consecutive displacement levels occurred, then this displacement ductility level was considered to be not satisfactory in this study. Ang, Paulay and Priestley defined satisfactory displacement ductility as the maximum displacement ductility at which at least 80 percent of the ideal flexural strength was still developed after several cycles of earthquake-induced displacements. The reason for not using the original proposal by Ang, Paulay and Priestley for some columns was the lack of data for these columns. On the other hand, for columns where required data was present, their method of evaluation was also applied. It should be noted that these two approaches yielded almost identical results. In addition, failure with moderate ductility ($4 \leq \mu \leq 6$), dominated by shear and shear failure with restricted ductility ($2 \leq \mu \leq 4$) were defined as Flexural-Shear failure in this study. It should be mentioned that failure pattern of some columns had to be interpreted by the author. In some column tests, test was terminated without any degradation in response. Above classification was applied to those columns regardless of the stage of termination of the test. Spiral column database is included in the CD attached to the back of this thesis.

CHAPTER 3

DEFINITION OF THE PROBLEM

3.1. General

Current code equations for minimum spiral ratio are based on column behaviour under uniaxial load. In this approach, the idea is to equate strength lost due to the crushing of cover concrete to the strength gained in the core concrete due to confinement. In reality, there is no column under uniaxial load. In the building codes, minimum eccentricity is specified so there is always bending moment acting on the column. In the derivation of the code equations, whole cover is considered to crush at the same strain. In reality, for columns under combined bending and axial load, cover crushing is gradual because of the strain gradient present in the column cross-section. Therefore, in this study, section behaviour under combined bending and axial load is taken as basis. In this study, two regression equations and one simplified equation for minimum spiral ratio are derived for columns having normal and high strength concrete. In the regression equations, the number in front of (A_c/A_{ck}) is defined as a function of (f_{ck}/f_{yk}) . In the simplified equation, the number in front of (A_c/A_{ck}) is defined as a constant. This constant was obtained by using the results obtained through analytical studies. One regression and one simplified equation are derived for normal strength concrete. One different regression equation is derived for high strength concrete. Simplified equation for normal strength concrete was proven to be valid for high strength concrete by carrying out analytical studies.

Moment-Curvature curves of the columns are considered to represent the real behaviour of the columns under normal and earthquake loads [29]. In practice, primary curve of hysteretic response can be best represented by the Moment-Curvature relationship under monotonic loading up to the onset of strength decay. Therefore, construction of a realistic Moment-Curvature relationship under monotonic loading is an important step in the seismic response analysis of reinforced concrete structures. The relationship between moment and curvature will demonstrate the strength, ductility and energy dissipation capacity of the section under question.

It should be strongly emphasized that the derived equations are not modification to the equation proposed by Ersoy and Özcebe [5]. However, method of study and parameters are similar to the previous researches on this subject. Hence, mechanics of spiral confinement, derivation of the code equations and review of previous research on minimum spiral ratio will be discussed in the subsequent sections.

3.2. Mechanics of Spiral Confinement

It is well known that circular spirals or circular hoops are more effective than the rectangular ties in confining the core concrete. Under axial load, due to poisson effect, concrete tends to expand laterally. Confinement reinforcement restrains this expansion by exerting compression to the core concrete. In turn, tension forces are produced in confinement reinforcement. In case of circular hoops and spirals, these tension forces are uniform and are called “uniform hoop tension”. Derivation of the equation giving the uniform lateral pressure can be done by using thin-walled cylinder analogy. Lateral pressure in case of circular hoops and spirals can be expressed as:

$$s_2 = \frac{2A_0 f_{yw} k}{D_s} \quad (3.1)$$

Richart proposed the following relation for the increased concrete strength due to lateral pressure [8];

$$f_{cc} = f_{ck} + k_1 s_2 \quad (3.2)$$

It should be noted that using $k_3 f_{ck}$ instead of f_{ck} gives better results. Value of the constant k_3 in the Saatcioglu and Razvi [6] model can be taken between 0.85-1.00. Baran [7] and Dinçer [8] took this constant as 1.00 since their analytical and experimental studies were carried on 200 mm diameter sections and material strengths were well controlled. On the other hand, in this study, 0.85 was used for constant k_3 since 320 mm diameter sections were used in the analytical studies. In high strength concrete sections, k_3 values greater than 0.85 could be used. On the other hand, Razvi and Saatcioglu [10] used 0.85 in their model for high strength concrete. For HSC sections, Razvi and Saatcioglu noted that using

$0.85f_{ck}$ yielded good agreement between analytical and experimental confined concrete strengths. Hence, 0.85 for constant k_3 is used for both NSC and HSC sections.

It is also reported by Saatcioglu and Razvi [6] that k_1 assume low values for high values of lateral pressure, approaching a constant value in the high-pressure range. Authors obtained the value of k_1 from regression analysis of Richart's test result as:

$$k_1 = \frac{6.7}{(\sigma_2)^{0.17}} \quad (3.3)$$

In this equation, the lateral pressure σ_2 is expressed in terms of MPa. It is easily seen that k_1 approaches 4.0 as lateral pressure exceeds 19 MPa. In the analytical studies carried out by the author, attaining a value of 19 MPa for the lateral pressure seems to be quite difficult especially for the columns whose spiral reinforcement is designed according to the code equations for minimum spiral ratio. This conclusion is particularly true for low (A_c/A_{ck}) ratios and normal strength concrete.

Behaviour of a spiral column under uniaxial load should be discussed before proceeding to the derivation of the code equations. Cover concrete crushing initiates approximately at a strain of 0.002. Since there is no strain gradient, whole cover concrete starts to crush at this strain. Therefore, a rapid decrease in the axial load capacity of the column occurs. Longitudinal bars either yield or they are at the verge of yielding at this point. At this strain, strain hardening of the longitudinal steel will not occur. With further deformation, confinement starts to become effective. Strength increase in the core concrete due to confinement results in the second peak. Position of the second peak relative to the first peak depends on the confinement of the column. The second peak can be higher, at the same level or lower than the first peak. While deriving code equations, it is aimed to have the second peak at the same level as the first peak. Hence, setting strength lost due to the crushing of cover concrete equal to the strength gained in the core concrete due to confinement is the idea in the derivation of the code equations.

3.3. Derivation of the Code Equations Giving Minimum Spiral Ratio

Equating the strength lost due to crushing of cover concrete to the strength gained in the core concrete due to confinement is the philosophy behind the derivation of the code equations giving minimum spiral ratio. While doing this, the constant k_1 was taken as 4.0. The derivation is as follows [30]:

$$\text{Strength Lost Due to Crushing of Cover Concrete} = \Delta N_1 = 0.85f_{ck}(A_c - A_{ck}) \quad (3.4)$$

$$\text{Strength Gained Due to Confinement of Core Concrete} = \Delta N_2 = A_{ck} (4\sigma_2) \quad (3.5)$$

By equating ΔN_1 to ΔN_2 ;

$$0.85f_{ck}(A_c - A_{ck}) = A_{ck}(4\sigma_2) \quad (3.6)$$

$$0.85f_{ck} \left[\frac{A_c}{A_{ck}} - 1 \right] = (4\sigma_2) \quad (3.7)$$

The expression for uniform lateral pressure was given in Eq. (3.1). For normal strength spiral and concrete, steel yields at the peak concrete stress. Collecting terms together, following expression is obtained for minimum spiral reinforcement area:

$$A_0 = \frac{0.85f_{ck}D(s) \left[\frac{A_c}{A_{ck}} - 1 \right]}{8f_{yk}} \quad (3.8)$$

Volumetric ratio of spiral reinforcement is then found by dividing the volume of spiral reinforcement for one hoop to the volume of core concrete having a height of s . Expression for volumetric ratio of spiral reinforcement can be written as follows:

$$r_s = \frac{\rho D A_0}{\frac{\rho D^2 (s)}{4}} = \frac{4A_0}{Ds} \quad (3.9)$$

Where;

A_o : Cross sectional area of the spiral steel

A_{ck} : Area of core concrete.

A_c : Total cross-sectional area (Gross Area)

D : Core concrete diameter

f_{ck} : Characteristic compressive strength of unconfined concrete

f_{ywk} : Characteristic yield strength of spiral steel

s : Spacing of the spiral reinforcement

σ_2 : Lateral pressure in the core concrete due to transverse reinforcement

Substitution of Eq. (3.9) into Eq. (3.8) yields the minimum volumetric spiral reinforcement ratio as follows:

$$r_s = 0.425 \frac{f_{ck}}{f_{ywk}} \left[\frac{A_c}{A_{ck}} - 1 \right] \quad (3.10)$$

In the codes, 0.425 was taken as 0.45 and the equation giving the minimum spiral ratio is expressed as:

$$r_s = 0.45 \frac{f_{ck}}{f_{ywk}} \left[\frac{A_c}{A_{ck}} - 1 \right] \quad (3.11)$$

As (A_c/A_{ck}) approaches to 1.0, volumetric ratio of spiral steel calculated according to Eq. (3.11) approaches zero. Since this is not realistic, a second equation is given as the lower limit:

$$\mathbf{r}_s = 0.12 \frac{f_{ck}}{f_{ywk}} \quad (3.12)$$

It should be strongly emphasized that there is no theoretical background of Eq. (3.12). It is an empirical equation. Eq. (3.12) governs when (A_c/A_{ck}) is smaller than 1.27.

3.4. Review of Previous Research on Minimum Spiral Ratio

It is more realistic to consider columns under combined bending and axial load rather than considering uniaxially loaded columns in the derivation of the equations for minimum lateral reinforcement ratio. In the derivation of the equation proposed by Ersoy and Özcebe [5], column behaviour under combined bending and axial load was considered. The equation was derived considering partial areas rather than the total gross and core areas. Also, reduced moment arms for confined and unconfined concrete were taken into account. Equation proposed by Ersoy and Özcebe is given below:

$$\mathbf{r}_s = 0.425 \frac{f_{ck}}{f_{ywk}} \left[1.25 \left(\frac{A_c}{A_{ck}} \right)^{0.5} - 1 \right] \quad (3.13)$$

The constants and the power were determined by intuition and limited statistical analysis. Later Dinçer modified Ersoy and Özcebe's equation. Dinçer proposed the following equation [8]:

$$\mathbf{r}_s = 0.425 \frac{f_{ck}}{f_{ywk}} \left[1.4 \left(\frac{A_c}{A_{ck}} \right)^{0.125} - 1 \right] \quad (3.14)$$

Eq. (3.13) and Eq. (3.14) are criticized by the author due to their semi-empirical derivation. In the derivation of the equation proposed by Ersoy and Özcebe [5], K_c was taken as 5.0, where K_c is the post-peak slope of the stress-strain curve of confined concrete as defined by Saatcioglu and Razvi [6]. Dinçer [8] concluded that satisfactory confinement is observed when $K_c = 7.14$. It is true that when $K_c = 5.0$ or 7.14, satisfactory confinement is obtained. On the other hand, it would be unconservative to assume $K_c = 5.0$ or 7.14

especially at low (A_c/A_{ck}) ratios. K_c values of 28 sections designed according to Eq. (3.13) are given in Table 3.1.

Table 3.1. K_c Values of 28 Sections Designed According to Eq. (3.13)

Section No.	A_c/A_{ck}	ρ_s^* (Eq. (3.13))	f_{ck} (MPa)	f_{ywk} (MPa)	f_{ck}/f_{ywk}	K_c
1	1.1	0.0110	25	300	0.0833	22.32
2	1.1	0.0176	40	300	0.1333	12.41
3	1.1	0.0079	25	420	0.0595	38.27
4	1.1	0.0126	40	420	0.0952	19.06
5	1.2	0.0131	25	300	0.0833	16.52
6	1.2	0.0209	40	300	0.1333	9.37
7	1.2	0.0093	25	420	0.0595	27.88
8	1.2	0.0149	40	420	0.0952	14.40
9	1.3	0.0151	25	300	0.0833	13.42
10	1.3	0.0241	40	300	0.1333	7.40
11	1.3	0.0108	25	420	0.0595	20.92
12	1.3	0.0172	40	420	0.0952	11.30
13	1.4	0.0170	25	300	0.0833	10.27
14	1.4	0.0271	40	300	0.1333	6.07
15	1.4	0.0121	25	420	0.0595	16.93
16	1.4	0.0194	40	420	0.0952	9.11
17	1.5	0.0188	25	300	0.0833	8.60
18	1.5	0.0300	40	300	0.1333	5.08
19	1.5	0.0134	25	420	0.0595	13.93
20	1.5	0.0215	40	420	0.0952	7.61
21	1.6	0.0206	25	300	0.0833	7.28
22	1.6	0.0329	40	300	0.1333	4.33
23	1.6	0.0147	25	420	0.0595	11.62
24	1.6	0.0235	40	420	0.0952	6.47
25	1.7	0.0223	25	300	0.0833	6.28
26	1.7	0.0357	40	300	0.1333	3.75

Table 3.1. K_c Values of 28 Sections Designed According to Eq. (3.13) (Continued)

Section No.	A_c/A_{ck}	ρ_s^* (Eq. (3.13))	f_{ck} (MPa)	f_{ywk} (MPa)	f_{ck}/f_{ywk}	K_c
27	1.7	0.0159	25	420	0.0595	9.93
28	1.7	0.0255	40	420	0.0952	5.59

$$* r_s = \frac{4A_0}{D(s)}$$

It should be noted that these 28 NSC sections are used for deriving proposed equations. K_c values of 28 NSC sections are calculated using Saatcioglu and Razvi [6] model. As seen in Table 3.1, there are few sections having K_c values smaller than or equal to 5.00. Especially at low (f_{ck}/f_{ywk}) ratios, K_c values came out to be significantly greater than either 5.00 or 7.14. In addition to these, at low (A_c/A_{ck}) ratios, attaining K_c values of 5.00 or 7.14 seems almost impossible as indicated by Section 1 to Section 8.

According to the author, effect of (A_c/A_{ck}) on the minimum spiral ratio is underestimated by using 0.5 and 0.125 as power in Eq. (3.13) and Eq. (3.14) respectively. Another point to be mentioned is that the proposed equations require significantly higher volumetric ratios of spiral steel than the code equations at low (A_c/A_{ck}) ratios and lower volumetric ratios of spiral steel at high (A_c/A_{ck}) ratios. Therefore, assumptions and derivations become debatable for Eq. (3.13) and Eq. (3.14).

CHAPTER 4

DERIVATION OF PROPOSED EQUATIONS

4.1. Information about Computer Program

A Moment-Curvature program was used in the analytical studies carried out. This program was developed by Mr. Hakan Ince. On the other hand, the author extended the output diversity of the program and made it applicable to high strength concrete. There are two executable programs as .exe files in the CD provided at the back of this thesis. One of these, MCC 120.exe is applicable to NSC spiral columns. On the other hand, MCC 1313.exe is applicable to HSC spiral columns. It should be noted that confined concrete model proposed by Razvi and Saatcioglu [10] for HSC columns is also applicable to NSC columns having concrete strengths greater than 30 MPa. On the other hand, MCC 120.exe was used by the author in developing the Moment-Curvature curves of NSC columns. Code of the program was written in Visual Basic.

In the program used, the cross-section can be divided into desired number of strips. In a strip, both confined and unconfined areas are present. By satisfying force equilibrium by iteration for a given strain at the extreme fiber in compression, depth of the neutral axis is found. Unconfined and confined stresses in each strip are calculated by using appropriate material models. Strain compatibility is used in calculating strain at each strip. By multiplying these stresses by areas, force in each strip is found. Steel strains are also found by strain compatibility requirements. Then, moments of these strips with respect to the centroid of the cross-section are found by multiplying the forces of the strips with the moment arms of the strips with respect to centroid of the section. Also, steel forces are multiplied by their moment arms in order to calculate their moment with respect to the centroid of the cross-section. In the Moment-Curvature program, gradual crushing of cover concrete is taken into account. As strain at a strip exceeds crushing strain, contribution of the unconfined concrete in this strip to axial force and moment capacity is taken as zero. Curvature of the cross-section is found by dividing the strain at the extreme compression fiber to the neutral axis depth. This procedure is repeated at every strain increment. Hognestad [30] model is used for the unconfined portion and Saatcioglu - Razvi [6] model

is used for confined part. Tri-linear stress-strain model is used for longitudinal steel which takes strain hardening into account. Hence, for longitudinal steel bars, user should define strain at the onset of strain hardening (ϵ_{sh}) and ultimate steel strain (ϵ_{su}) as input.

It should be noted that the program is developed for circular cross-sections. It can be made applicable to rectangular and hexagonal cross-sections having spiral reinforcement by some effort. There is a textbox in the settings submenu in which the accuracy desired in the equilibrium of the axial load is entered. It is recommended by the author to use an accuracy of ± 1 kN or ± 2 kN. Also, strain increment that is defined as input should be selected carefully by the user. Using a strain increment of 0.001 can cause omitting some characteristic points of the Moment-Curvature curves. It is recommended by the author to use a strain increment of 0.0002-0.0005 for normal strength concrete and 0.0002 for high strength concrete. In the program developed, core dimensions are defined from centers of spiral steel. Clear cover thickness is defined by the user as input. However, user should enter the clear cover measured to outside of the spiral steel as input. There is a line in the code of the program that adds half of the spiral diameter to the clear cover thickness. The user should enter location of the top bar as input. Then, program distributes remaining longitudinal bars around the core concrete by equal angles to each other. User can define location of each and every bar by defining its distance from column ends as input. Strain at the extreme compression fiber, curvature, neutral axis depth, total moment, resultant concrete force, resultant steel force, resultant concrete moment about centroid of the cross-section and resultant steel moment about the centroid of the cross-section can be obtained at every strain increment as output. Following the analysis, "Send to Excel" button may be utilized in order to obtain this data. Axial load should be entered in kN units. Material strengths should be given in terms of MPa. All other dimensions should be given in mm.

Ultimate strain and ultimate curvature values can be defined as input. On the other hand, program terminates when resultant concrete moment comes out to be near zero. Hence, sometimes predetermined strain and curvature values may not be reached by the program. Regional settings of the computer should be O.K in order to run the program properly.

4.2. Derivation of the Proposed Equations for Spiral Columns Having Normal Strength Concrete

In this study, derivation of the equations for minimum spiral ratio is based on section behaviour under combined bending and axial load. In the Figure 4.1, prior but close to cover crushing, whole concrete section in compression is contributing to the moment resistance. At this stage, there is no cover crushing and confinement is not fully effective. Figure 4.2 shows what happens beyond the peak under large curvatures. Here, a large portion of the cover concrete in compression has crushed. Also, confinement at this stage is fully effective. Small portion of cover concrete is effective due to gradual crushing of cover concrete. A considerable decrease in the moment resistance should be expected due to crushing of cover concrete since outermost cover concrete fibers with largest moment arm become ineffective.

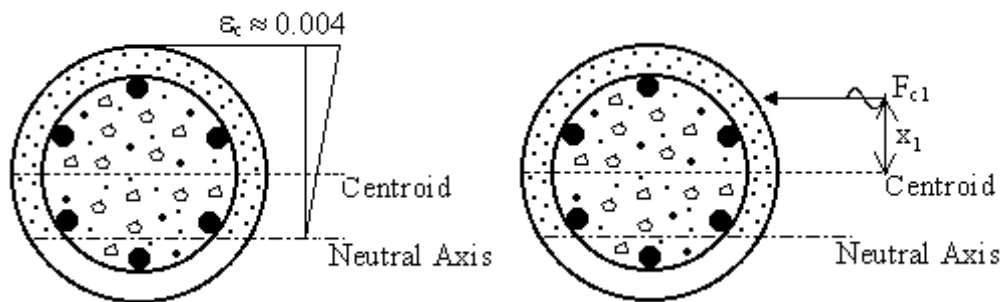


Figure 4.1. Spiral Column under Combined Axial Load and Bending
(Early Stages) [8]

In the derivation of the equations for minimum spiral reinforcement, Figures 4.1 and 4.2 will be taken as basis. It should be noted that Figure 4.1 represents the stage where cover crushing has not yet occurred. Although cover crushing initiates at a strain value of approximately 0.002, spalling of cover can be assumed to take place at about $\epsilon_c = 0.004$.

Figure 4.2 represents the case where a large portion of the cover has crushed. After some analytical studies, it was decided to consider this case at a strain value of $\epsilon_c = 0.04$. After some analytical studies on test columns, the author concluded that strain value of $\epsilon_c = 0.04$ can be attained at the plastic hinge regions of flexure dominated well-confined columns.

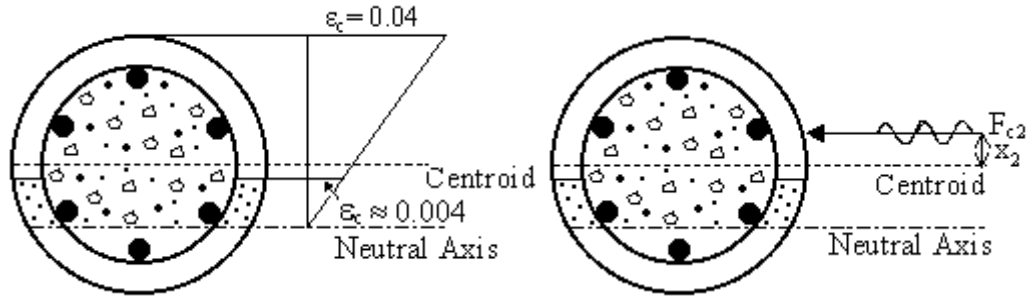


Figure 4.2. Spiral Column under Combined Axial Load and Bending
(Later Stages) [8]

After examining the Moment-Curvature diagrams of spiral columns, it was observed that reasonable ductility would be obtained if the moment capacity corresponding to an extreme fiber strain of 0.04 was at least 85% of the moment capacity corresponding to an extreme fiber strain of 0.004 which corresponds to cover crushing. Derivation of the equation for minimum spiral ratio will be initiated by equating M_{c2} to $0.85M_{c1}$:

$$(M_{c2}) = 0.85(M_{c1}) \quad (4.1)$$

Here it would be more reasonable to include the contribution of longitudinal reinforcement as, $M_{c2} + M_{s2} = 0.85(M_{c1} + M_{s1})$. However analytical studies made by the author indicated that when N is close to about $0.5f_{ck}A_c$, M_{s2} is not very different from M_{s1} . The assumption of $M_{s2} = M_{s1}$ is not strictly correct since the moment capacity provided by the longitudinal reinforcement changes with changing of the neutral axis.

Needless to say, taking extreme fiber strain of 0.04 as basis and defining ductility as indicated by Eq. (4.1) are open to discussion. It should be mentioned that ratio given in Eq. (4.1) is dependent on the confinement of the column. For poorly confined columns, this ratio comes out be smaller and for well-confined columns the opposite is true.

For each of these two cases parameters representing concrete stress, area under compression and moment arm of the concrete stress are defined as given below:

At the stage of cover crushing ($\epsilon_c = 0.004$); Figure 4.1:

$$M_{c1} = F_{c1}x_1 \quad (4.2)$$

$$F_{c1} = \mathbf{b}_1 f_{ck} \mathbf{g}_1 A_c \quad (4.3)$$

$$\mathbf{b}_1 = \left(\frac{\Sigma F_{c1}}{\Sigma A_{c1}} \right) \left(\frac{1}{f_{ck}} \right) \quad (4.4)$$

where $\frac{\Sigma F_{c1}}{\Sigma A_{c1}}$ is average concrete stress.

$$\mathbf{g}_1 = \frac{\Sigma A_{c1}}{\Sigma A_c} \quad (4.5)$$

$$x_1 = \frac{\Sigma M_{c1}}{\Sigma F_{c1}} \quad (4.6)$$

At the extreme fiber strain of 0.04 ($\epsilon_c=0.04$); Figure 4.2:

$$M_{c2} = F_{c2}x_2 \quad (4.7)$$

$$F_{c2} = \mathbf{b}_2 f_{cc} \mathbf{g}_2 A_{ck} \quad (4.8)$$

$$\mathbf{b}_2 = \left(\frac{\Sigma F_{c2}}{\Sigma A_{c2}} \right) \left(\frac{1}{f_{cc}} \right) \quad (4.9)$$

$$\mathbf{g}_2 = \frac{\Sigma A_{c2}}{\Sigma A_{ck}} \quad (4.10)$$

$$x_2 = \frac{\Sigma M_{c2}}{\Sigma F_{c2}} \quad (4.11)$$

Where;

- ΣA_{c1} : Area of concrete in compression for extreme fiber strain of 0.004.
- ΣA_{c2} : Area of concrete in compression for extreme fiber strain of 0.04.
- ΣF_{c1} : Resultant concrete compressive force for extreme fiber strain of 0.004.
- ΣF_{c2} : Resultant concrete compressive force for extreme fiber strain of 0.04.
- ΣM_{c1} : Resultant moment of concrete compressive forces about centroid of the cross-section for extreme fiber strain of 0.004.
- ΣM_{c2} : Resultant moment of concrete compressive forces about centroid of the cross-section for extreme fiber strain of 0.04.
- β_1 : A factor defining the ratio of average concrete compressive stress to the unconfined concrete strength for extreme fiber strain of 0.004.
- β_2 : A factor defining the ratio of average concrete compressive stress to the confined concrete strength for extreme fiber strain of 0.04.
- γ_1 : A factor defining the ratio of area of concrete in compression to the gross area for extreme fiber strain of 0.004.
- γ_2 : A factor defining the ratio of area of concrete in compression to the cross-sectional area of the core for extreme fiber strain of 0.04.
- x_1 : Defines the moment arm of resultant concrete force to the centroid of the cross-section for extreme fiber strain of 0.004.
- x_2 : Defines the moment arm of resultant concrete force to the centroid of the cross-section for extreme fiber strain of 0.04.
- A_{ck} : Area of core concrete. Diameter of the core concrete is measured from centers of spirals or hoops.

A_c : Total cross-sectional area. (Gross area)

When $\epsilon_c=0.004$, it is reasonable to use unconfined concrete strength f_{ck} and use confined concrete strength when $\epsilon_c=0.04$.

By putting Eq. (4.7) and Eq. (4.2) into Eq. (4.1):

$$\mathbf{b}_2 \mathbf{g}_2 x_2 f_{cc} A_{ck} = 0.85 \mathbf{b}_1 \mathbf{g}_1 x_1 f_{ck} A_c \quad (4.12)$$

As given in Eq. (3.3), k_1 varies as a function of σ_2 . However, analytical case studies made by the author indicated that for columns having the minimum spiral reinforcement as defined by the codes or by Ersoy and Özcebe [5] k_1 varies between 5.0 and 5.5. Therefore, it is reasonable to assume $k_1=5.25$ and take constant $k_3=0.85$. Substituting these values into Eq. (4.12), equality obtained is as follows:

$$\mathbf{b}_2 \mathbf{g}_2 x_2 [0.85 f_{ck} + 2.625 r_s f_{ywk}] A_{ck} = 0.85 \mathbf{b}_1 \mathbf{g}_1 x_1 f_{ck} A_c \quad (4.13)$$

Eq. (4.13) can be rewritten as,

$$1 + 3.09 \frac{r_s f_{ywk}}{f_{ck}} = \left(\frac{\mathbf{b}_1}{\mathbf{b}_2} \right) \left(\frac{\mathbf{g}_1}{\mathbf{g}_2} \right) \left(\frac{x_1}{x_2} \right) \left(\frac{A_c}{A_{ck}} \right) \quad (4.14)$$

By rearranging the terms,

$$r_s = 0.32 \frac{f_{ck}}{f_{ywk}} \left[\left(\frac{\mathbf{b}_1}{\mathbf{b}_2} \right) \left(\frac{\mathbf{g}_1}{\mathbf{g}_2} \right) \left(\frac{x_1}{x_2} \right) \left(\frac{A_c}{A_{ck}} \right) - 1 \right] \quad (4.15)$$

Eq. (4.15) can be written in a simpler form by defining new parameters. New parameters are as follows:

$$m = \frac{f_{ck}}{f_{ywk}} \quad (4.16)$$

$$\begin{pmatrix} \mathbf{b}_1 \\ \mathbf{b}_2 \end{pmatrix} \begin{pmatrix} \mathbf{g}_1 \\ \mathbf{g}_2 \end{pmatrix} \begin{pmatrix} x_1 \\ x_2 \end{pmatrix} = \Delta_2 \quad (4.17)$$

Substituting Eq. (4.17) into Eq. (4.15), the following relationship is obtained for minimum volumetric spiral ratio:

$$\mathbf{r}_s = 0.32 \frac{f_{ck}}{f_{ywk}} \left[\Delta_2 \left(\frac{A_c}{A_{ck}} \right) - 1 \right] \quad (4.18)$$

In the following section, case studies will be carried on in order to determine Δ_2 .

The derivation of Eq. (4.18) is based on the decision made relating the moment at $\epsilon_c=0.004$ to the moment at $\epsilon_c=0.04$ (Eq. (4.1)). A strength reduction of 15% is generally used in defining ductility.

4.3 Analytical Studies Carried Out for Sections Having Normal Strength Concrete

Analytical studies were carried out in order to obtain Δ_2 . In these analytical studies, spiral steel ratio was calculated according to Eq. (3.13). Common properties of the 28 cross-sections are listed in Table 4.1 and the variables are listed in Table 4.2. In the selection of these cross-sections, it was intended to take all important parameters that are considered to effect column behaviour into account. As can be followed from Table 4.2, (A_c/A_{ck}) ratios ranging from 1.1 to 1.7 were included in the analytical studies. Yield strength of the steel was limited to 420 MPa due to restrictions in the codes. In the analytical studies carried on 28 sections, only normal strength concrete was considered. Also, it should be noted that in all sections 8 longitudinal bars placed at 45° to each other with one bar at the top and one at the bottom.

In the analytical studies, it was intended to use the axial load as high as possible since confinement becomes more important as the axial load increases. The upper limit given for the axial load in the Turkish code [31] was used, $N=0.5f_{ck}A_c$.

Table 4.1. Common Properties of Cross-Sections

Diameter of the Column (D)	320 mm
Number and Diameter of Longitudinal Steel	8- ϕ 14 mm
Spiral Steel Diameter (d_{sp})	8 mm
Yield Strength of Longitudinal Steel (f_{yk})	420 MPa
Ultimate Strength of Longitudinal Steel (f_{su})	525 MPa
Longitudinal Steel Strain at the Onset of Strain Hardening (ϵ_{sh})	0.01
Ultimate Longitudinal Steel Strain (ϵ_{su})	0.1
Modulus of Elasticity of Steel (E_s)	200000 MPa
Axial Load on The Cross-Section (N)	$0.5f_{ck}A_c$

Table 4.2. Properties of 28 NSC Sections Designed According to Eq. (3.13)

Section No.	A_c/A_{ck}	ρ_s^* (Eq. (3.13))	f_{ck} (MPa)	f_{ywk} (MPa)	$m=f_{ck}/f_{ywk}$
1	1.1	0.0110	25	300	0.0833
2	1.1	0.0176	40	300	0.1333
3	1.1	0.0079	25	420	0.0595
4	1.1	0.0126	40	420	0.0952
5	1.2	0.0131	25	300	0.0833
6	1.2	0.0209	40	300	0.1333
7	1.2	0.0093	25	420	0.0595
8	1.2	0.0149	40	420	0.0952
9	1.3	0.0151	25	300	0.0833
10	1.3	0.0241	40	300	0.1333
11	1.3	0.0108	25	420	0.0595

Table 4.2. Properties of 28 NSC Sections Designed According to Eq. (3.13) (Continued)

Section No.	A_c/A_{ck}	ρ_s^* (Eq. (3.13))	f_{ck} (MPa)	f_{ywk} (MPa)	$m=f_{ck}/f_{ywk}$
12	1.3	0.0172	40	420	0.0952
13	1.4	0.0170	25	300	0.0833
14	1.4	0.0271	40	300	0.1333
15	1.4	0.0121	25	420	0.0595
16	1.4	0.0194	40	420	0.0952
17	1.5	0.0188	25	300	0.0833
18	1.5	0.0300	40	300	0.1333
19	1.5	0.0134	25	420	0.0595
20	1.5	0.0215	40	420	0.0952
21	1.6	0.0206	25	300	0.0833
22	1.6	0.0329	40	300	0.1333
23	1.6	0.0147	25	420	0.0595
24	1.6	0.0235	40	420	0.0952
25	1.7	0.0223	25	300	0.0833
26	1.7	0.0357	40	300	0.1333
27	1.7	0.0159	25	420	0.0595
28	1.7	0.0255	40	420	0.0952

$$* r_s = \frac{4A_0}{D(s)}$$

These 28 sections are used throughout this study while comparing code equations with proposed equations, investigating validity of proposed equations with different number and orientation of longitudinal bars, investigating validity of the proposed equations with different longitudinal steel percentage and axial load level.

In Figure 4.3, Δ_2 vs. (A_c/A_{ck}) for 28 NSC sections are presented. As can be seen from the Figure 4.3, Δ_2 values do not possess a representative distribution. It can be seen from Figure 4.4 that variation of Δ_2/m with respect to (A_c/A_{ck}) for 28 sections show better distribution as compared to Δ_2 vs. (A_c/A_{ck}) . However, the difference between the sections

having “m”=0.0595 and other sections should be noted. Four data groups are shown for four different “m” values. In general, the trend is same for all “m” values except for Section 3 and Section 7 when “m”=0.0595. The divergence in this case is believed to be due to the poor confinement of these sections. Section 3 was excluded while obtaining simplified equation since it is thought by the author that it represents misbehaviour. Since Δ_2 value of Section 3 is about 2.5 times the average of the other sections, it increases the total average.

It was found out by analytical studies that Δ_2/m varies as a power function of “m” as can be seen from Figure 4.5. These Δ_2/m values are obtained by averaging five Δ_2/m values for each “m” value. It should be emphasized that while using Δ_2/m values in the derivation of the regression equations, sections with $(A_c/A_{ck}) \geq 1.3$ were taken into consideration. As can be seen in the Figure 4.5, fit of the regression equation is quite good.

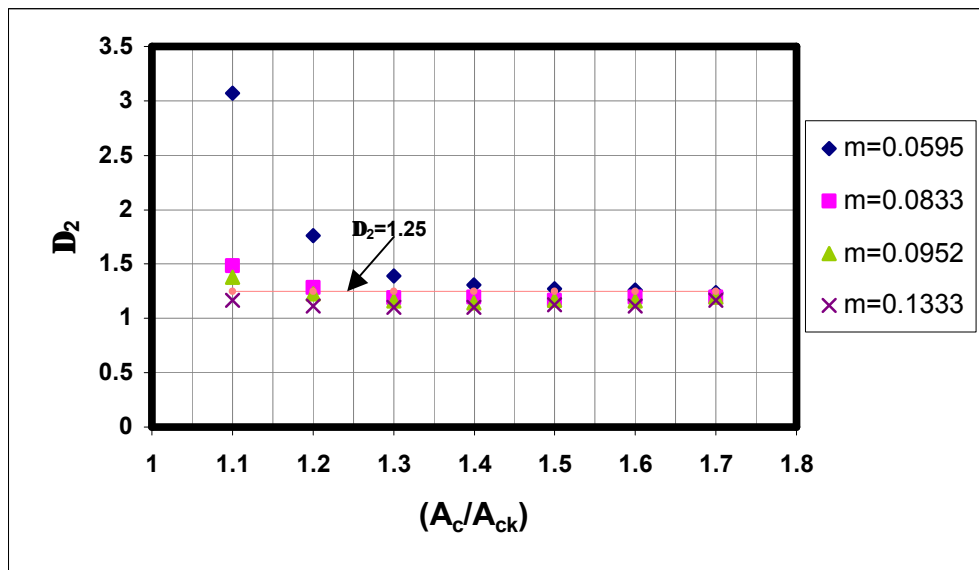


Figure 4.3. Δ_2 vs. (A_c/A_{ck}) for 28 NSC Sections

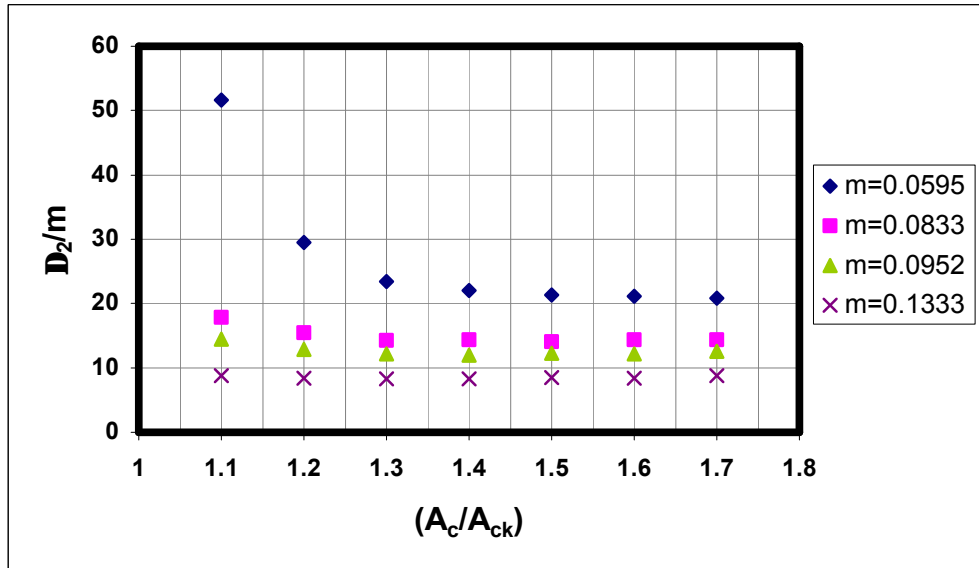


Figure 4.4. Variation of Δ_2/m with (A_c/A_{ck}) for NSC Sections

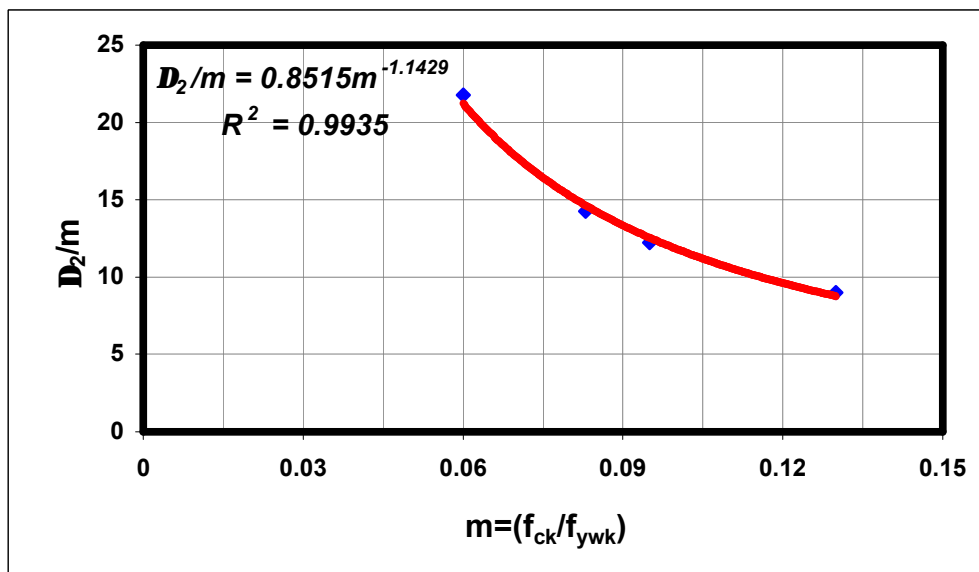


Figure 4.5. Variation of Δ_2/m with “m” for NSC Sections

If the regression equation shown in Figure 4.5 is taken as basis, then Δ_2 in Eq. (4.18) can be written as follows:

$$\Delta_2 = 0.85(m)^{-0.1429} \quad (4.19)$$

By putting Eq. (4.19) into Eq. (4.18),

$$\mathbf{r}_s = 0.32 \frac{f_{ck}}{f_{ywk}} \left[0.85 \left(\frac{f_{ck}}{f_{ywk}} \right)^{-0.1429} \left(\frac{A_c}{A_{ck}} \right) - 1 \right] \quad (4.20)$$

Figure 4.3 shows the variation of Δ_2 with the (A_c/A_{ck}) ratio. If Section 3 is disregarded, Δ_2 can approximately be expressed as a constant, $\Delta_2=1.25$. This constant for Δ_2 was found by averaging 27 Δ_2 values. If this value is substituted into Eq. (4.18), following linear equation is obtained for the minimum spiral ratio:

$$\mathbf{r}_s = 0.32 \frac{f_{ck}}{f_{ywk}} \left[1.25 \left(\frac{A_c}{A_{ck}} \right) - 1 \right] \quad (4.21)$$

Eq. (4.20) is called regression equation and Eq. (4.21) is called simplified equation. It should be strongly emphasized that in the analytical studies made in order to derive the proposed equations Eq (4.20) and Eq. (4.21), normal strength concrete was taken into account. Also, yield strength of both longitudinal and transverse steel was limited to 420 MPa as stated in the current Turkish and ACI codes.

It is considered that size of the cross-section would not change the results as long as the ratios of other parameters are kept constant. Hence, in the analytical studies, only 320 mm diameter sections were used.

Single value for diameter of spiral steel was used in the analytical studies. Changing diameter of spiral steel changes the spacing of the spiral steel while using constant volumetric ratio of transverse reinforcement. This would not affect the results obtained in the analytical studies since volumetric ratio of the transverse reinforcement effects stress-strain curve of the confined concrete in Saatcioglu and Razvi model. However, in reality, increasing the spiral pitch may result in premature buckling of longitudinal bars and poor confinement effect.

4.4. Derivation of the Proposed Equations for Spiral Columns Having High Strength Concrete

In the derivation of equations proposed in Section 4.2, 28 NSC sections were used. Hence, Eq. (4.20) and Eq. (4.21) are valid for normal strength concrete at this stage. After deriving equations for minimum spiral ratio for normal strength concrete, additional analytical studies were carried out in order to derive equations for minimum spiral ratio for high strength concrete. Main philosophy is same in derivation of the equations for NSC and HSC sections. On the other hand, there are significant differences for the values of the parameters used in the derivation of the equations for normal and high strength concrete. Brittle nature of high strength concrete was taken into account in the derivations. It is important to note that cover crushing strain is dependent on concrete compressive strength in case of high strength concrete [10]. In the derivation of equations for high strength concrete, this fact was also taken into account by defining a variable strain at the first peak. Cover crushing strain for HSC sections was calculated by using the equation proposed by Razvi and Saatcioglu [10] in their confinement model for high strength concrete. It should be mentioned that Razvi and Saatcioglu confinement model for high strength concrete was derived using data on test specimens having concrete compressive strengths in the range of 30 MPa to 130 MPa. Therefore, conclusions and equations derived for HSC will be valid for concrete compressive strengths up to 130 MPa. In this study, the upper limit for normal strength concrete is 50 MPa. Concrete compressive strengths larger than 50 MPa are classified as high strength concrete. This classification is also valid in TS-500 [32]. Terms and symbols used in the derivation of equations for minimum spiral reinforcement ratio for HSC columns is same as the terms and symbols used in the derivation of the equations for minimum spiral ratio for NSC columns. Reader can refer to Section 4.2 for terms and symbols used in this section. By using Razvi and Saatcioglu model for high strength concrete, cover crushing strain was approximately obtained and used as 0.0028, 0.0030 and 0.0032 for concrete compressive strengths of 120 MPa, 85 MPa and 65 MPa respectively. These values were used as the strains at the extreme compression fiber at the verge of cover crushing, instead of 0.004 used in the case of NSC sections. Also, strain at the extreme compression fiber of 0.04 in the derivation of equations for normal strength concrete was shifted to 0.03 in case of high strength concrete in order to take brittle nature of high strength concrete into account.

As indicated by Eq. (4.22), at a strain of 0.03, it is intended to have a total concrete moment about 112.5% of the total concrete moment at the verge of cover crushing. It should be reminded that factor 1.125 was obtained by the author while carrying out analytical studies with HSC sections. Cover crushing at lower strains for HSC sections is the reason of the difference between factors used in Eq. (4.1) and Eq. (4.22). After examining the Moment-Curvature diagrams of spiral columns having high strength concrete, it was observed that reasonable ductility would be obtained if the moment capacity corresponding to an extreme fiber strain of 0.03 was at least 112.5% of the moment capacity at the verge of cover crushing. Derivation of the equation for minimum spiral ratio will be initiated by equating M_{c2} to $1.125M_{c1}$:

The derivation of the proposed equations for high strength concrete is as follows;

$$(M_{c2})=1.125(M_{c1}) \quad (4.22)$$

As in NSC, moments of concrete forces are taken as basis assuming the moment capacity supplied by the longitudinal reinforcement is same at the first peak and $\epsilon_c=0.03$. This of course is not strictly correct since the moment capacity provided by the longitudinal reinforcement changes with changing position of the neutral axis. Since this change in moment capacity is small, it is neglected as in NSC.

As in the case of NSC sections, taking extreme fiber strain of 0.03 as basis and defining ductility as indicated by Eq. (4.22) are open to discussion.

For each of these two cases parameters representing concrete stress, area under compression and moment arm of the concrete stress are defined as given below:

At the stage of cover crushing (ϵ_c =Variable)

$$M_{c1} = F_{c1}x_1 \quad (4.23)$$

$$F_{c1} = b_1f_{ck}g_1A_c \quad (4.24)$$

$$\mathbf{b}_1 = \left(\frac{\sum F_{c1}}{\sum A_{c1}} \right) \left(\frac{1}{f_{ck}} \right) \quad (4.25)$$

$$\mathbf{g}_1 = \frac{\sum A_{c1}}{\sum A_c} \quad (4.26)$$

$$x_1 = \frac{\sum M_{c1}}{\sum F_{c1}} \quad (4.27)$$

At the extreme fiber strain of 0.03 ($\epsilon_c=0.03$);

$$M_{c2} = F_{c2}x_2 \quad (4.28)$$

$$F_{c2} = \mathbf{b}_2 f_{cc} \mathbf{g}_2 A_{ck} \quad (4.29)$$

$$\mathbf{b}_2 = \left(\frac{\sum F_{c2}}{\sum A_{c2}} \right) \left(\frac{1}{f_{cc}} \right) \quad (4.30)$$

$$\mathbf{g}_2 = \frac{\sum A_{c2}}{\sum A_{ck}} \quad (4.31)$$

$$x_2 = \frac{\sum M_{c2}}{\sum F_{c2}} \quad (4.32)$$

At the first peak, it is reasonable to use unconfined concrete strength f_{ck} and use confined concrete strength when $\epsilon_c=0.03$.

By putting Eq. 4.23 and Eq. 4.28 into Eq. 4.22,

$$\mathbf{b}_2 \mathbf{g}_2 x_2 f_{cc} A_{ck} = 1.125 \mathbf{b}_1 \mathbf{g}_1 x_1 f_{ck} A_c \quad (4.33)$$

In the case of NSC sections, k_1 was taken as 5.25. The reason of this was explained in Section 4.2. In case of HSC sections, a smaller value for k_1 should be used since σ_2 values

are greater in case of HSC sections. Analytical case studies made by the author indicated that for columns having the minimum spiral reinforcement as defined by Eq. (4.21), k_1 varies between 4.25 and 4.75. Therefore, it is reasonable to assume $k_1=4.5$ and take constant $k_3=0.85$. Substituting these values into Eq. (4.33), equality obtained is as follows:

$$\mathbf{b}_2 \mathbf{g}_2 x_2 [0.85 f_{ck} + 2.25 r_s f_{yw}] A_{ck} = 1.125 \mathbf{b}_1 \mathbf{g}_1 x_1 f_{ck} A_c \quad (4.34)$$

Eq. (4.34) can be rewritten as,

$$0.756 + 2.00 \frac{r_s f_{yw}}{f_{ck}} = \left(\frac{\mathbf{b}_1}{\mathbf{b}_2} \right) \left(\frac{\mathbf{g}_1}{\mathbf{g}_2} \right) \left(\frac{x_1}{x_2} \right) \left(\frac{A_c}{A_{ck}} \right) \quad (4.35)$$

By rearranging the terms:

$$r_s = 0.378 \frac{f_{ck}}{f_{yw}} \left[1.322 \left(\frac{\mathbf{b}_1}{\mathbf{b}_2} \right) \left(\frac{\mathbf{g}_1}{\mathbf{g}_2} \right) \left(\frac{x_1}{x_2} \right) \left(\frac{A_c}{A_{ck}} \right) - 1 \right] \quad (4.36)$$

Eq. (4.36) can be written in a simpler form by using the same parameters as in the case of NSC. These parameters are as follows:

$$m = \frac{f_{ck}}{f_{yw}} \quad (4.37)$$

$$\left(\frac{\mathbf{b}_1}{\mathbf{b}_2} \right) \left(\frac{\mathbf{g}_1}{\mathbf{g}_2} \right) \left(\frac{x_1}{x_2} \right) = \Delta_2 \quad (4.38)$$

Substituting Eq. (4.38) into Eq. (4.36), the following relationship is obtained for minimum volumetric spiral ratio:

$$r_s = 0.378 \frac{f_{ck}}{f_{yw}} \left[1.322 \Delta_2 \left(\frac{A_c}{A_{ck}} \right) - 1 \right] \quad (4.39)$$

In the following section, case studies will be carried on in order to determine Δ_2 .

4.5. Analytical Studies Carried Out for Sections Having High Strength Concrete

Analytical studies were carried out in order to obtain Δ_2 . Concrete compressive strengths of 21 sections are between 65 MPa and 120 MPa. This range covers important extent of the high strength concrete used in practice. Common properties of 28 NSC sections are also valid for these 21 HSC sections. Therefore, reader can refer to Table 4.1 for common properties of these 21 sections. Properties of 21 sections are listed in Table 4.3.

Table 4.3. Properties of 21 HSC Sections Designed According to Eq. (4.21)

Section No:	A_c/A_{ck}	ρ_s (Eq. (4.21))	f_{ck} (MPa)	f_{ywk} (MPa)	$m=f_{ck}/f_{ywk}$
29	1.1	0.0186	65	420	0.1548
30	1.2	0.0248	65	420	0.1548
31	1.3	0.0310	65	420	0.1548
32	1.4	0.0371	65	420	0.1548
33	1.5	0.0433	65	420	0.1548
34	1.6	0.0495	65	420	0.1548
35	1.7	0.0557	65	420	0.1548
36	1.1	0.0243	85	420	0.2024
37	1.2	0.0324	85	420	0.2024
38	1.3	0.0405	85	420	0.2024
39	1.4	0.0485	85	420	0.2024
40	1.5	0.0570	85	420	0.2024
41	1.6	0.0647	85	420	0.2024
42	1.7	0.0728	85	420	0.2024
43	1.1	0.0340	120	420	0.2857
44	1.2	0.0457	120	420	0.2857
45	1.3	0.0571	120	420	0.2857
46	1.4	0.0686	120	420	0.2857
47	1.5	0.0800	120	420	0.2857
48	1.6	0.0914	120	420	0.2857
49	1.7	0.1030	120	420	0.2857

In Figure 4.6, Δ_2 vs. (A_c/A_{ck}) for 21 HSC sections are presented. As can be seen from the Figure 4.6, Δ_2 values do not possess a representative distribution. Three data groups are shown for three different “m” values. As can be seen from Figure 4.7, variation of Δ_2/m with respect to (A_c/A_{ck}) for 21 sections show better distribution as compared to Δ_2 vs. (A_c/A_{ck}) . For each “m”, there is a distinct trend as can be seen from Figure 4.7. Also, distribution of Δ_2 values are better in case of 21 HSC sections than the NSC sections as can be seen from Figure 4.6 and Figure 4.3. It should be noted that in case of HSC sections, there is no divergence in Δ_2 values as Section 3 in case of normal strength concrete.

As for normal strength concrete, it was found that Δ_2/m varies as a power function of “m”. These Δ_2/m values are obtained by averaging five Δ_2/m values for each “m” value. While obtaining Δ_2/m values used in Figure 4.8, Δ_2/m values of the sections having $(A_c/A_{ck}) \geq 1.3$ were used as in the case of NSC sections.

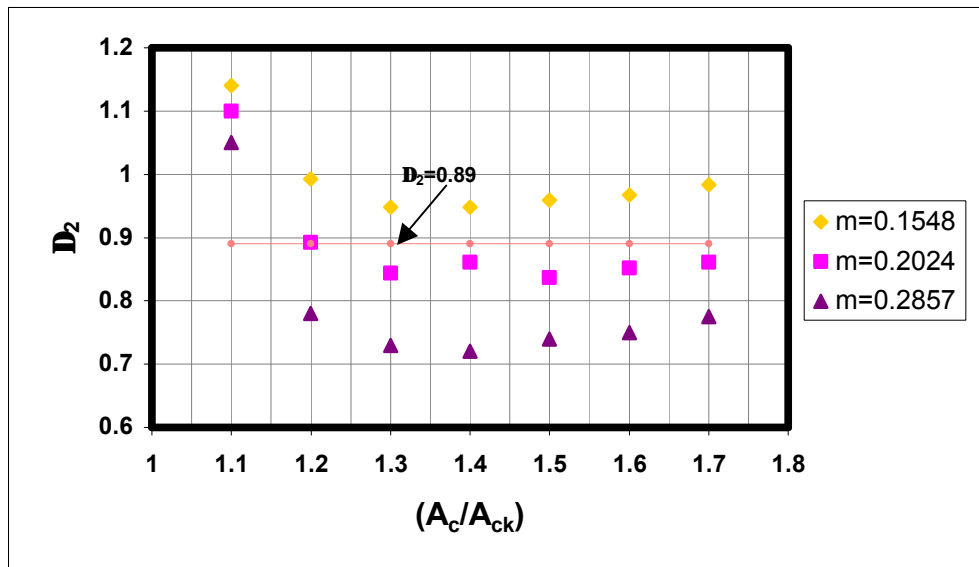


Figure 4.6. Δ_2 v.s. (A_c/A_{ck}) for 21 HSC Sections

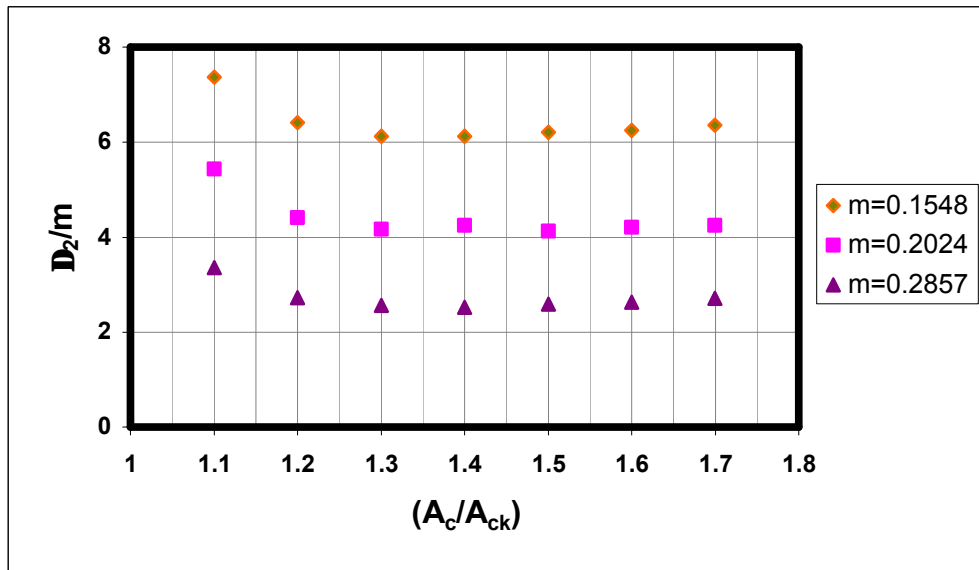


Figure 4.7. Variation of Δ_2/m with (A_c/A_{ck}) for HSC Sections

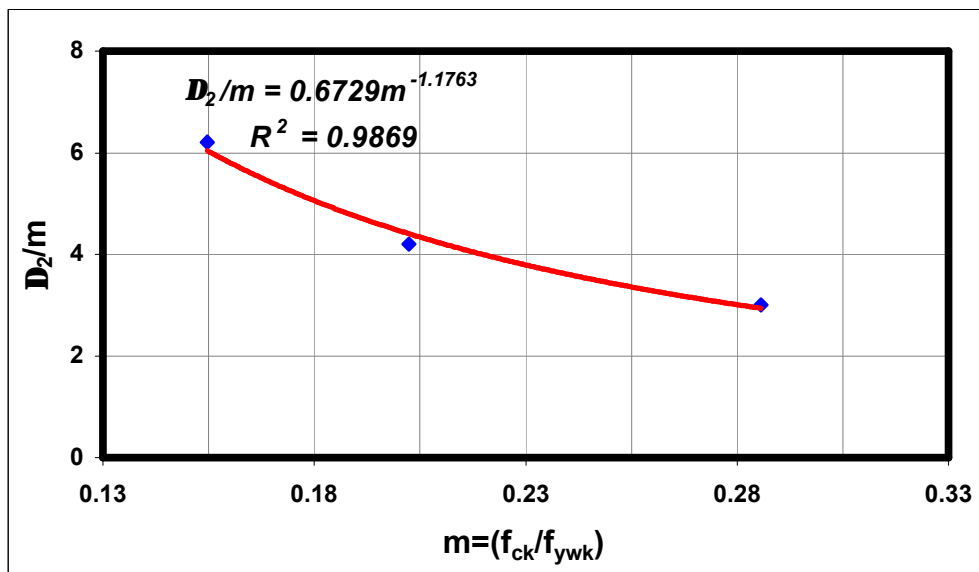


Figure 4.8. Variation of Δ_2/m with “m” for HSC Sections

If the regression equation shown in Figure 4.8 is taken as basis, then Δ_2 in Eq. (4.38) can be written as follows:

$$\Delta_2 = 0.6729(m)^{-0.1763} \quad (4.40)$$

By putting Eq. (4.40) into Eq. (4.39),

$$\mathbf{r}_s = 0.378 \frac{f_{ck}}{f_{ywk}} \left[0.890 \left(\frac{f_{ck}}{f_{ywk}} \right)^{-0.1763} \left(\frac{A_c}{A_{ck}} \right) - 1 \right] \quad (4.41)$$

Figure 4.6 shows the variation of Δ_2 with the (A_c/A_{ck}) ratio. Δ_2 can approximately be expressed as a constant, $\Delta_2=0.89$. This constant for Δ_2 was found by averaging 21 Δ_2 values. If this value is substituted into Eq. (4.39), following linear equation is obtained for the minimum spiral ratio:

$$\mathbf{r}_s = 0.378 \frac{f_{ck}}{f_{ywk}} \left[1.18 \left(\frac{A_c}{A_{ck}} \right) - 1 \right] \quad (4.42)$$

Eq. (4.41) is called regression equation for high strength concrete. Eq. (4.42) is called simplified equation for high strength concrete. In derivation of both Eq. (4.20) and Eq. (4.41), lowest ρ_2/m values were shifted upward at a small percentage in order to obtain more reasonable volumetric ratios of spiral steel at different (A_c/A_{ck}) ratios and “m” values. This normalization slightly decreases ρ_2 values for low “m” values and it slightly increases ρ_2 values for high “m” values, which is quite desirable.

It is seen from Figure 4.9 that variation of Δ_2/m with “m” can be expressed as a power function of “m” if both NSC and HSC are included. It is seen that fit of the regression equation is quite good confirming the previous studies. Different derivations and assumptions for NSC and HSC sections make defining a single regression equation valid for both normal and high strength concrete impossible.

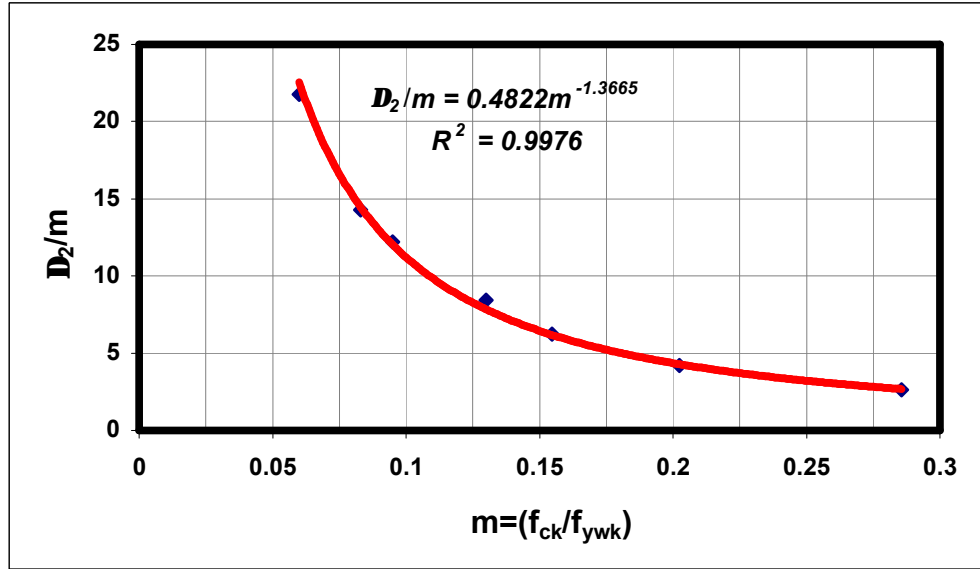


Figure 4.9. Variation of Δ_2/m with “m” for NSC and HSC Sections

4.6 Comparison of Eq. (4.42) with Eq. (4.21).

Eq. (4.21) was proposed for normal strength concrete in Section 4.3. Eq. (4.42) is the simplified equation valid for high strength concrete. In Figure 4.10, it can easily be seen that these two equations require very close volumetric ratios of spiral steel as (A_c/A_{ck}) varies. Eq. (4.21) requires slightly higher volumetric ratios of spiral steel than Eq. (4.42) at low (A_c/A_{ck}) ratios. On the other hand, Eq. (4.42) requires slightly higher volumetric ratios of spiral steel than Eq. (4.21) at moderately high and high (A_c/A_{ck}) ratios. Using Eq. (4.21) instead of Eq. (4.42) is advantageous since it requires higher volumetric ratios of spiral steel at low (A_c/A_{ck}) ratios and lower volumetric ratios at high (A_c/A_{ck}) ratios. Practically, these two equations may be considered as identical. To avoid extra work and confusion, Eq. (4.21) will be called as simplified equation and is proposed for both normal and high strength concrete. In contrast, there are two regression equations (Eq. (4.20) and Eq. (4.41)) one valid for normal strength concrete and one valid for high strength concrete. Eq. (4.42) will not be used from now on for comparison purposes.

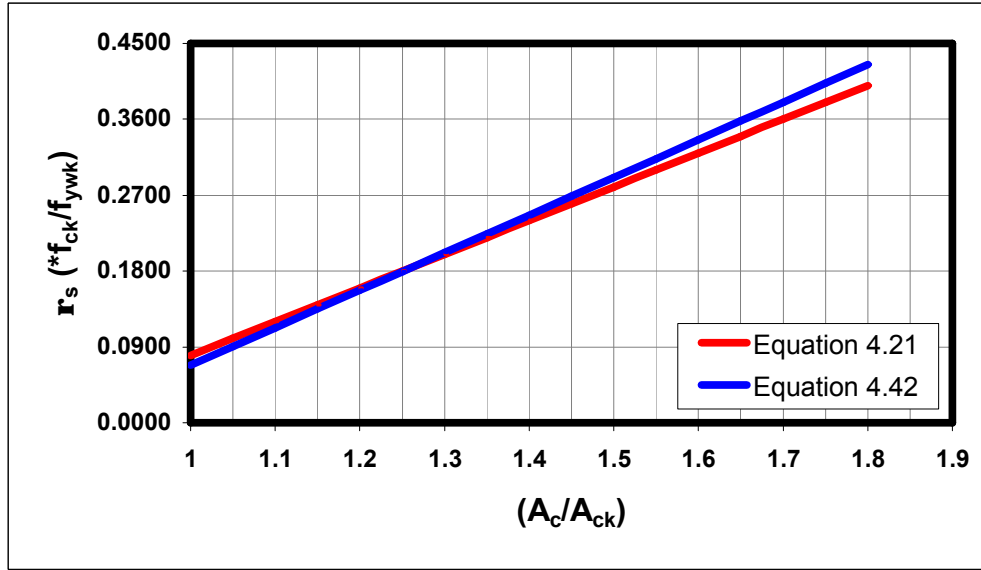


Figure 4.10. Comparison of Volumetric Ratios of Spiral Steel Required by Eq. (4.21) and Eq. (4.42)

CHAPTER 5

ANALYTICAL STUDIES

5.1. Effect of Volumetric Ratio of Spiral Steel on Section Behaviour (NSC)

Following the derivations of the equations, volumetric ratios of spiral steel required by Eqs. (3.11), (3.12), (4.20) and (4.21) should be compared in order to make further discussion. It is widely known and accepted that volumetric ratio of the spiral steel is the most important parameter affecting cross-section ductility. Therefore, comparison of the volumetric ratios of spiral steel required by proposed and code equations should be made for different “m” values in order to obtain a sound judgement on the proposed equations before proceeding into analytical comparisons. Comparisons of volumetric ratios of spiral steel can be seen from Figures 5.1 to 5.4. In these figures, (A_c/A_{ck}) ratios up to 1.8 were used. Compared to larger columns, higher (A_c/A_{ck}) ratios for small columns are obtained if the code requirement concerning minimum cover thickness is applied. On the other hand, attaining a (A_c/A_{ck}) ratio of 1.8 is an exceptional case.

It can be seen from Figure 5.1 and Figure 5.2 that Eq. (4.20) and Eq. (4.21) require very close volumetric ratios of spiral steel. It should be noted that calculated volumetric ratios of spiral steel by using the regression and simplified equations are both above the volumetric ratios required by the code equations at moderate and high (A_c/A_{ck}) ratios.

As can be seen from Figure 5.4, for section having “m”=0.1333 and (A_c/A_{ck})=1.1, ρ_s obtained by using Eq. (4.20) is very low.

Eq. (4.20) requires slightly higher volumetric ratios of spiral steel than the Eq. (4.21) at “m”=0.0595 and both require higher spiral ratios than the code equations except at (A_c/A_{ck}) ratios equal to and smaller than 1.1. In the Saatcioglu and Razvi model [6], post-peak slope of the stress-strain curve of confined concrete is dependent upon the volumetric ratio of spiral steel. Therefore, decreasing the volumetric ratio of transverse reinforcement while

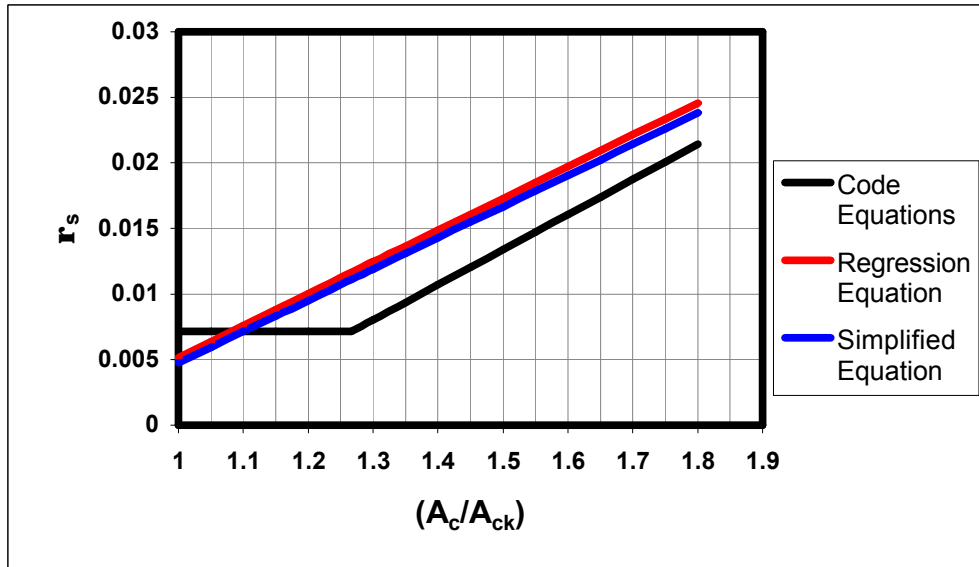


Figure 5.1. Comparison of Volumetric Ratios of Spiral Steel for “m”=0.0595

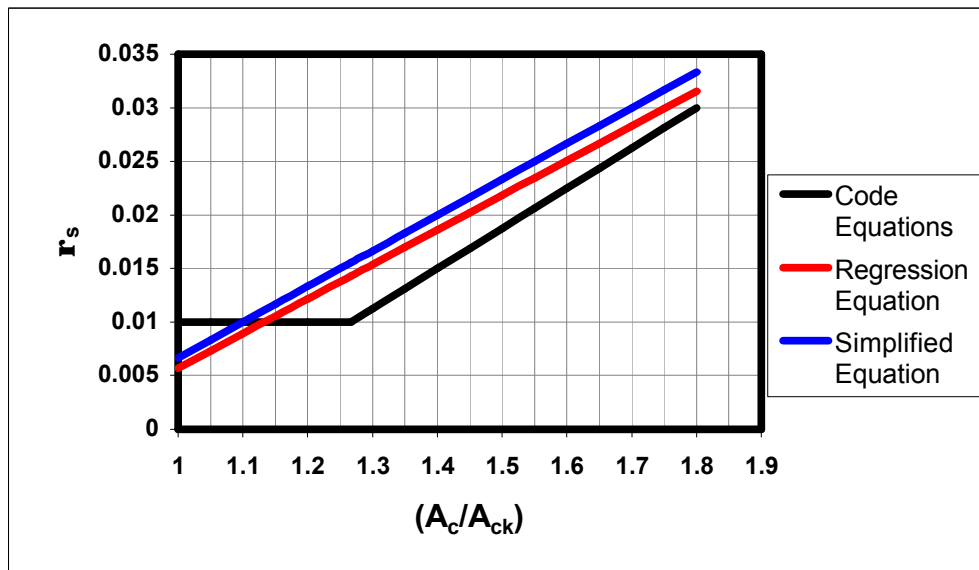


Figure 5.2. Comparison of Volumetric Ratios of Spiral Steel for “m” = 0.0833

increasing the yield strength of spiral steel makes post-peak of the stress-strain curve steeper. Consequently, relatively brittle stress-strain curves for confined concrete are obtained by using code equations especially at low (A_c/A_{ck}) ratios and at small “m” values. Eq. (4.20) and Eq. (4.21) solved this problem and yielded acceptable results. At medium

“m” values like 0.0833 and 0.0952, Eq. (4.21) requires higher volumetric ratios of spiral steel than Eq. (4.20).

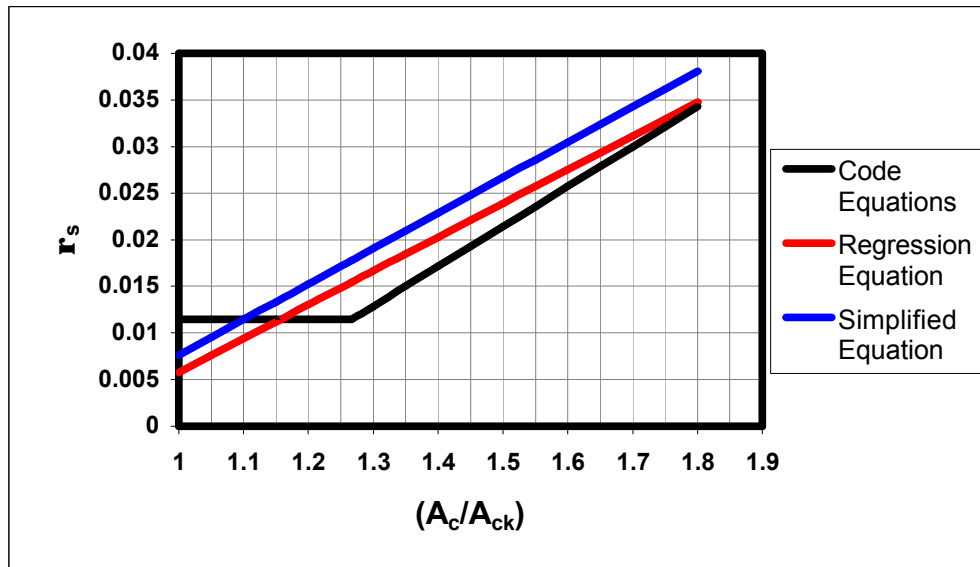


Figure 5.3. Comparison of Volumetric Ratios of Spiral Steel for “m” = 0.0952

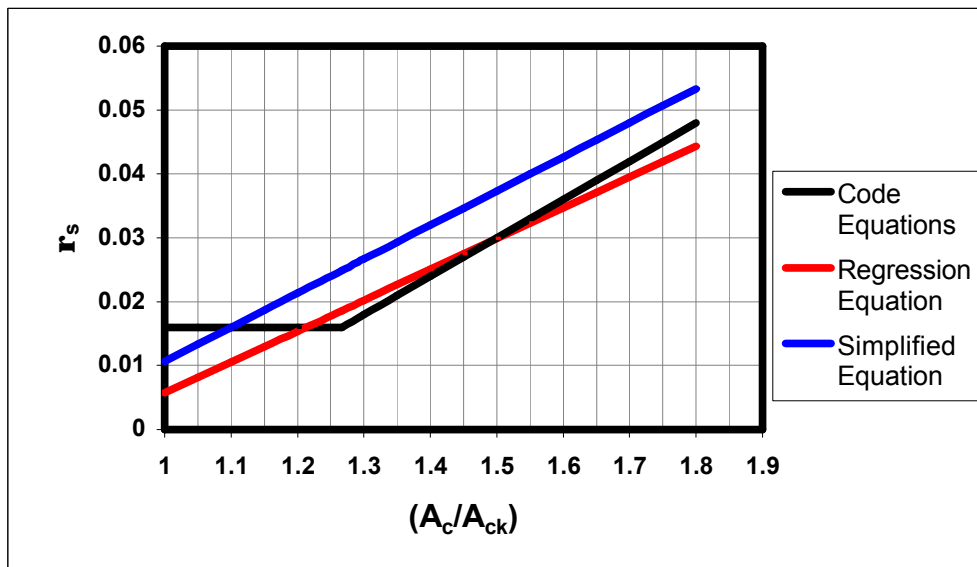


Figure 5.4. Comparison of Volumetric Ratios of Spiral Steel for “m” = 0.1333

Eq. (4.20) and Eq. (4.21) require smaller volumetric ratios of spiral steel than the code equations at (A_c/A_{ck}) ratios smaller than approximately 1.1. In practice, columns having (A_c/A_{ck}) ratios smaller than 1.1 are quite uncommon due to minimum clear cover requirements in the codes. Exceptions may be the piers of long span bridges and base floor columns of tall buildings.

In this study, comparisons of Moment-Curvature curves of 28 sections whose spiral reinforcement are designed according to Eqs. (3.11), (3.12), (4.20) and (4.21) will be made. Details of 28 sections were presented at Section 4.3 in Table 4.1 and Table 4.2. In this study, only volumetric ratio of spiral steel was the variable for each of the 28 sections. All other parameters were kept constant. All Moment-Curvature curves are presented in Appendix A. In this study, the aim is to investigate the effect of volumetric ratios of spiral steel in the code, the regression and simplified equations on ductility. Volumetric ratios of spiral steel for 28 sections obtained using Eqs. (3.11), (3.12), (4.20) and (4.21) are presented at Table 5.1.

Table 5.1. Spiral Volumetric Ratio Comparisons for 28 NSC Sections

Section No:	(A_c/A_{ck})	$m=f_{ck}/f_{ywk}$	r_s (Code)	r_s (Regr.)	r_s (Simp.)	$\frac{r_s(\text{Re gr.})}{r_s(\text{Code})}$	$\frac{r_s(\text{Simp.})}{r_s(\text{Code})}$
1	1.1	0.0833	0.0100	0.0089	0.0100	0.89	1.00
2	1.1	0.1333	0.0160	0.0105	0.0160	0.66	1.00
3	1.1	0.0595	0.0071	0.0076	0.0071	1.07	1.00
4	1.1	0.0952	0.0114	0.0094	0.0114	0.83	1.00
5	1.2	0.0833	0.0100	0.0121	0.0133	1.21	1.33
6	1.2	0.1333	0.0160	0.0154	0.0213	0.96	1.33
7	1.2	0.0595	0.0071	0.0100	0.0095	1.41	1.33
8	1.2	0.0952	0.0114	0.0130	0.0152	1.14	1.33
9	1.3	0.0833	0.0113	0.0154	0.0167	1.36	1.48
10	1.3	0.1333	0.0180	0.0202	0.0267	1.12	1.48
11	1.3	0.0595	0.0080	0.0124	0.0119	1.55	1.48
12	1.3	0.0952	0.0129	0.0166	0.0190	1.29	1.48
13	1.4	0.0833	0.0150	0.0186	0.0200	1.24	1.33
14	1.4	0.1333	0.0240	0.0250	0.0320	1.04	1.33

Table 5.1. Spiral Volumetric Ratio Comparisons for 28 NSC Sections (Continued)

Section No:	(A_c/A_{ck})	$m=f_{ck}/f_{ywk}$	r_s (Code)	r_s (Regr.)	r_s (Simp.)	$\frac{r_s(Regr.)}{r_s(Code)}$	$\frac{r_s(Simp.)}{r_s(Code)}$
15	1.4	0.0595	0.0107	0.0149	0.0143	1.39	1.33
16	1.4	0.0952	0.0171	0.0203	0.0228	1.19	1.33
17	1.5	0.0833	0.0187	0.0218	0.0233	1.17	1.24
18	1.5	0.1333	0.0300	0.0299	0.0373	1.00	1.24
19	1.5	0.0595	0.0134	0.0173	0.0167	1.29	1.24
20	1.5	0.0952	0.0214	0.0239	0.0267	1.12	1.24
21	1.6	0.0833	0.0225	0.0251	0.0267	1.11	1.19
22	1.6	0.1333	0.0360	0.0347	0.0427	0.96	1.19
23	1.6	0.0595	0.0161	0.0197	0.0190	1.22	1.19
24	1.6	0.0952	0.0257	0.0275	0.0305	1.07	1.19
25	1.7	0.0833	0.0262	0.0283	0.0300	1.08	1.14
26	1.7	0.0420	0.0420	0.0396	0.0480	0.94	1.14
27	1.7	0.0187	0.0187	0.0221	0.0214	1.18	1.14
28	1.7	0.0300	0.0300	0.0311	0.0343	1.04	1.14

An examination of Table 5.1 will reveal that the proposed regression equation generally yields somewhat higher spiral ratios as compared to the code equations. However, in some cases, regression equation results in smaller spiral ratios.

As can be seen from figures in Appendix A, sections designed according to Eq. (4.21) behaved in a ductile manner in all cases. It should be emphasized that at $(A_c/A_{ck})=1.1$, code equation and Eq. (4.21) require the same volumetric ratio of spiral steel. Therefore, these two Moment-Curvature curves overlap each other. The blue colour represents both code and simplified equations in this case. In addition, for Section 18, the regression and code equations require the same volumetric ratio of spiral steel. Therefore, these two overlap with each other as can be seen from Figure A.18. Regression and code equations are represented by red colour in this case.

In order to compare code equations with proposed equations, a curvature ductility index is defined as follows:

$$m = \frac{K_{.85N}}{K_{pN}} \quad (5.1)$$

Where;

$K_{.85N}$ = Curvature of the cross-section at the 85% of the moment at the extreme fiber strain of 0.004

K_{pN} = Curvature of the cross-section at the extreme fiber strain of 0.004

In some sections, 15% strength degradation did not occur until $\epsilon_c=0.05$. In this case, symbol “>” is put in front of the curvature ductility index in order to emphasize that 15% strength degradation did not occur until $\epsilon_c=0.05$. This generally occurs at high (A_c/A_{ck}) ratios and well-confined sections. Curvature ductility index is an important indicator of the ductility. Hence, comparing curvature ductility indexes gives information about the ductility of the sections designed according to either code or proposed equations. $K_{.85N}$ and K_{pN} values of 28 NSC sections designed according to Eqs. (3.11), (3.12), (4.20) and (4.21) are presented at Table 5.2. These values are used in order to calculate curvature ductility indexes presented at Table 5.3. Curvature ductility indexes for 28 NSC sections are presented at Table 5.3.

Table 5.2. K_{pN} and $K_{.85N}$ Values of 28 NSC Sections Designed According to Proposed and Code Equations

Section No:	(A_c/A_{ck})	$m=f_{ck}/f_{ywk}$	K_{pNC}	K_{pNR}	K_{pNS}	$K_{.85NC}$	$K_{.85NR}$	$K_{.85NS}$
1	1.1	0.0833	0.0208	0.0207	0.0208	0.223	0.184	0.223
2	1.1	0.1333	0.0202	0.0200	0.0202	>0.286	0.155	>0.286
3	1.1	0.0595	0.0208	0.0210	0.0208	0.153	0.171	0.153
4	1.1	0.0952	0.0202	0.0200	0.0202	0.216	0.158	0.216

Table 5.2. K_{pN} and $K_{.85N}$ Values of 28 NSC Sections Designed According to Proposed and Code Equations (Continued)

Section No:	(A_c/A_{ck})	$m=f_{ck}/f_{ywk}$	K_{pNC}	K_{pNR}	K_{pNS}	$K_{.85NC}$	$K_{.85NR}$	$K_{.85NS}$
5	1.2	0.0833	0.0208	0.0211	0.0213	0.202	>0.287	>0.301
6	1.2	0.1333	0.0202	0.0201	0.0207	0.266	0.250	>0.304
7	1.2	0.0595	0.0207	0.0214	0.0212	0.140	0.259	0.234
8	1.2	0.0952	0.0201	0.0204	0.0207	0.189	0.242	>0.293
9	1.3	0.0833	0.0209	0.0216	0.0218	0.225	>0.305	>0.308
10	1.3	0.1333	0.0201	0.0204	0.0211	>0.277	>0.291	>0.309
11	1.3	0.0595	0.0209	0.0220	0.0218	0.156	>0.304	>0.302
12	1.3	0.0952	0.0203	0.0208	0.0211	0.203	>0.293	>0.304
13	1.4	0.0833	0.0214	0.0221	0.0223	>0.298	>0.308	>0.310
14	1.4	0.1333	0.0207	0.0208	0.0216	>0.294	>0.298	>0.309
15	1.4	0.0595	0.0213	0.0224	0.0223	0.245	>0.308	>0.307
16	1.4	0.0952	0.0207	0.0212	0.0216	>0.283	>0.301	>0.307
17	1.5	0.0833	0.0219	0.0221	0.0227	>0.304	>0.309	>0.311
18	1.5	0.1333	0.0213	0.0213	0.0220	>0.301	>0.301	>0.309
19	1.5	0.0595	0.0219	0.0229	0.0227	>0.300	>0.311	>0.309
20	1.5	0.0952	0.0213	0.0216	0.0220	>0.296	>0.303	>0.308
21	1.6	0.0833	0.0224	0.0228	0.0231	>0.306	>0.311	>0.312
22	1.6	0.1333	0.0218	0.0216	0.0224	>0.303	>0.301	>0.308
23	1.6	0.0595	0.0224	0.0233	0.0231	>0.304	>0.312	>0.310
24	1.6	0.0952	0.0218	0.0220	0.0223	>0.301	>0.304	>0.308
25	1.7	0.0833	0.0229	0.0232	0.0234	>0.307	>0.310	>0.311
26	1.7	0.1333	0.0222	0.0219	0.0227	>0.303	>0.303	>0.308
27	1.7	0.0595	0.0229	0.0236	0.0233	>0.306	>0.312	>0.312
28	1.7	0.0952	0.0221	0.0222	0.0226	>0.304	>0.305	>0.309

Table 5.3. Curvature Ductility Index Comparisons for 28 NSC Sections

Section No:	(A_c/A_{ck})	$m=f_{ck}/f_{yw}$	m_{Code}	$m_{Regression}$	$m_{Simplified}$	$\frac{m_{Re gr.}}{m_{Code}}$	$\frac{m_{Simp.}}{m_{Code}}$
1	1.1	0.0833	10.72	8.89	10.72	0.83	1.00
2	1.1	0.1333	>14.16	7.75	>14.16	<0.55	1.00
3	1.1	0.0595	7.36	8.14	7.36	1.11	1.00
4	1.1	0.0952	10.69	7.90	10.69	0.74	1.00
5	1.2	0.0833	9.71	>13.60	>14.13	>1.40	>1.45
6	1.2	0.1333	13.17	12.43	>14.69	0.94	>1.12
7	1.2	0.0595	6.76	12.10	11.04	1.79	1.63
8	1.2	0.0952	9.40	11.86	>14.15	1.26	>1.51
9	1.3	0.0833	10.77	>14.12	>14.12	>1.31	>1.31
10	1.3	0.1333	>13.70	>14.30	>14.30	-	-
11	1.3	0.0595	7.46	>13.80	>13.80	>1.85	>1.85
12	1.3	0.0952	10.00	>14.10	>14.10	>1.41	>1.41
13	1.4	0.0833	>13.90	>13.90	>13.90	-	-
14	1.4	0.1333	>14.20	>14.20	>14.20	-	-
15	1.4	0.0595	11.50	>13.75	>13.75	>1.20	>1.20
16	1.4	0.0952	>13.65	>14.20	>14.20	-	-
17	1.5	0.0833	>13.70	>13.70	>13.70	-	-
18	1.5	0.1333	>14.00	>14.00	>14.00	-	-
19	1.5	0.0595	>13.50	>13.50	>13.50	-	-
20	1.5	0.0952	>13.90	>13.90	>13.90	-	-
21	1.6	0.0833	>13.50	>13.50	>13.50	-	-
22	1.6	0.1333	>13.75	>13.75	>13.75	-	-
23	1.6	0.0595	>13.40	>13.40	>13.40	-	-
24	1.6	0.0952	>13.80	>13.80	>13.80	-	-
25	1.7	0.0833	>13.40	>13.40	>13.40	-	-
26	1.7	0.1333	>13.60	>13.60	>13.60	-	-
27	1.7	0.0595	>13.30	>13.30	>13.30	-	-
28	1.7	0.0952	>13.60	>13.60	>13.60	-	-

As can be seen from Table 5.3, Eq. (4.21) yielded significantly higher curvature ductility indexes than the code equations especially at (A_c/A_{ck}) ratios of 1.2 and 1.3. For $(A_c/A_{ck}) \geq 1.4$, both code and proposed equations resulted in very ductile behaviour. Hence, curvature ductility index comparisons are not made for these sections.

Since curvature ductility index does not give reasonable information for some sections, a capacity index is defined in this study.

Capacity index is defined as:

$$CI = \frac{M_{R2}}{M_{R1}} \quad (5.2)$$

Where;

M_{R2} = Moment capacity of the cross-section at the extreme fiber strain of 0.04

M_{R1} = Moment capacity of the cross-section at the extreme fiber strain of 0.004

It should be strongly emphasized that some sections designed according to proposed and code equations having low (A_c/A_{ck}) ratios could not reach the strain of 0.04. It should be reminded that when resultant concrete moment comes out to be near zero, the computer program terminates. Hence, for these few sections, the strains given in Table 5.6 are used. M_{R1} and M_{R2} values of 28 NSC sections designed according to Eqs. (3.11), (3.12), (4.20) and (4.21) are presented at Table 5.4. These values are used in order to calculate capacity indexes presented at Table 5.5.

While Eq. (5.2) was called as “capacity index”, it is also a measure of ductility. Since “ M_{R2} ” is an indicator of the post-peak slope, capacity index gives information about both strength and ductility of the section.

Table 5.4. M_{R1} and M_{R2} Values of 28 NSC Sections Designed According to Proposed and Code Equations

Section No:	(A_c/A_{ck})	$m=f_{ck}/f_{ywk}$	M_{R1C}	M_{R1R}	M_{R1S}	M_{R2C}	M_{R2R}	M_{R2S}
1	1.1	0.0833	100.1	99.1	100.1	84.2	71.0	84.2
2	1.1	0.1333	134.0	128.6	134.0	134.8	89.4	134.8
3	1.1	0.0595	100.1	100.8	100.1	70.3	79.0	70.3
4	1.1	0.0952	132.5	131.7	132.5	120.7	92.6	120.7
5	1.2	0.0833	95.7	97.7	98.8	75.8	92.0	96.6
6	1.2	0.1333	128.0	127.5	132.6	117.7	115.0	136.4
7	1.2	0.0595	94.0	98.0	97.3	68.7	97.5	94.6
8	1.2	0.0952	127.9	129.9	132.6	97.5	115.1	128.3
9	1.3	0.0833	93.0	97.1	98.3	79.5	95.8	99.1
10	1.3	0.1333	122.0	123.9	129.8	114.8	122.2	135.7
11	1.3	0.0595	93.1	99.1	98.3	65.9	98.1	93.2
12	1.3	0.0952	124.8	129.3	132.2	102.1	123.6	131.2
13	1.4	0.0833	92.7	96.3	97.0	87.5	95.2	97.4
14	1.4	0.1333	124.1	124.8	131.0	119.3	120.9	131.6
15	1.4	0.0595	91.8	97.8	97.0	80.3	96.0	94.4
16	1.4	0.0952	124.0	127.7	131.0	114.0	123.0	129.2
17	1.5	0.0833	93.2	94.3	96.9	88.4	92.9	94.7
18	1.5	0.1333	125.8	125.8	130.6	118.4	118.4	126.9
19	1.5	0.0595	93.2	97.8	97.0	85.2	94.4	93.0
20	1.5	0.0952	125.8	128.9	131.5	115.7	120.8	125.4
21	1.6	0.0833	92.0	94.1	96.5	87.5	90.5	92.1
22	1.6	0.1333	126.7	125.8	130.6	116.4	115.3	122.7
23	1.6	0.0595	92.0	97.3	96.4	85.8	92.1	90.9
24	1.6	0.0952	126.7	128.7	129.1	114.9	117.7	121.6
25	1.7	0.0833	93.6	95.1	94.6	85.9	87.9	89.0
26	1.7	0.1333	127.5	123.6	131.4	113.7	111.7	118.5
27	1.7	0.0595	93.7	96.9	94.9	85.0	89.6	88.6
28	1.7	0.0952	125.2	126.4	129.3	112.8	114.2	117.8

Table 5.5. Capacity Index Comparisons for 28 NSC Sections

Section No:	(A_c/A_{ck})	$m=f_{ck}/f_{ywk}$	CI_{Code}	$CI_{Regression}$	$CI_{Simplified}$	$\frac{CI_{Regr.}}{CI_{Code}}$	$\frac{CI_{Simp.}}{CI_{Code}}$
1	1.1	0.0833	0.84	0.72	0.84	0.86	1.00
2	1.1	0.1333	1.01	0.70	1.01	0.70	1.00
3	1.1	0.0595	0.70	0.78	0.70	1.11	1.00
4	1.1	0.0952	0.91	0.70	0.91	0.77	1.00
5	1.2	0.0833	0.79	0.94	0.98	1.19	1.24
6	1.2	0.1333	0.92	0.90	1.03	0.98	1.12
7	1.2	0.0595	0.73	0.99	0.97	1.36	1.33
8	1.2	0.0952	0.76	0.89	0.97	1.17	1.28
9	1.3	0.0833	0.85	0.99	1.01	1.16	1.19
10	1.3	0.1333	0.94	0.99	1.05	1.05	1.12
11	1.3	0.0595	0.71	0.99	0.95	1.39	1.34
12	1.3	0.0952	0.82	0.96	0.99	1.17	1.21
13	1.4	0.0833	0.94	0.99	1.00	1.06	1.06
14	1.4	0.1333	0.96	0.97	1.02	1.01	1.05
15	1.4	0.0595	0.87	0.98	0.97	1.13	1.12
16	1.4	0.0952	0.92	0.96	0.99	1.04	1.08
17	1.5	0.0833	0.95	0.98	0.98	1.03	1.03
18	1.5	0.1333	0.94	0.94	0.97	1.00	1.03
19	1.5	0.0595	0.91	0.97	0.96	1.07	1.05
20	1.5	0.0952	0.92	0.94	0.95	1.02	1.03
21	1.6	0.0833	0.95	0.96	0.95	1.01	1.00
22	1.6	0.1333	0.92	0.92	0.94	1.00	1.02
23	1.6	0.0595	0.93	0.95	0.94	1.02	1.01
24	1.6	0.0952	0.91	0.92	0.94	1.01	1.03
25	1.7	0.0833	0.92	0.92	0.94	1.00	1.02
26	1.7	0.1333	0.89	0.89	0.90	1.00	1.01
27	1.7	0.0595	0.91	0.92	0.93	1.01	1.02
28	1.7	0.0952	0.90	0.90	0.91	1.00	1.01

As can be followed from Table 5.3, Table 5.5 and Table 5.7, proposed equations resulted in more ductile behaviour than the code equations except few points. At $(A_c/A_{ck})=1.1$, Section 1, Section 2 and Section 4 are the ones for which Eq. (4.20) yielded poor results. Relatively brittle behaviour of the Section 2 designed according to Eq. (4.20) is presented in Figure A.2. Also, Eq. (4.20) resulted in brittle behaviour of the Section 6. At (A_c/A_{ck}) ratios of 1.2 and 1.3, proposed equations resulted in significantly more ductile behaviour than the code equations. Brittle behaviour of the section designed according to code equations can be seen in Figure A.11. On the other hand, as seen from Table 5.5 and Table 5.7, relative development in response is higher for low values of “m” and lower for high values of “m”. This is expected since code equations yield relatively brittle results at “m”=0.0595. However, as can be seen from Table 5.1, proposed equations require significantly higher volumetric ratios of spiral steel at (A_c/A_{ck}) ratios equal to 1.2 and 1.3. At high (A_c/A_{ck}) ratios like 1.6 and 1.7, difference between proposed and code equations becomes smaller than 10%. At these (A_c/A_{ck}) ratios, both code and proposed equations yield stable and ductile post-peak behaviour. This is considered to be the reason for relatively small differences between proposed and code equations at high (A_c/A_{ck}) ratios.

Table 5.6. Strains Used for Calculating CI that are Different than 0.04

Section No:	ϵ_c
2	0.036
3	0.033
4	0.035
7	0.030
11	0.035

It should be strongly emphasized that capacity index ratios listed in Table 5.5 may not represent the real behaviour completely. Confinement becomes fully effective after cover crushing. On the other hand, at the first peak of the Moment-Curvature curves, some small differences between Eqs. (3.11), (3.12), (4.20) and (4.21) are present due to confinement. This event can also be seen in the analytical studies of the previous researcher [8] on this subject. Hence, capacity index may be low for some sections implying that the section

could not provide adequate strength increase. This may create confusion if these sections had higher volumetric ratios of spiral steel. Ratios of the moment resistances at the strain of 0.04 can also be considered as a comparison parameter. It should be reminded that Table 5.3, Table 5.5 and Table 5.7 should be considered in conjunction with each other.

Table 5.7. Comparisons of Moment Resistances at the Strain of 0.04 for 28 NSC Sections

Section No:	(A_c/A_{ck})	$m=f_{ck}/f_{ywk}$	$\frac{M_{R2}(Re\ gr.)}{M_{R2}(Code)}$	$\frac{M_{R2}(Simp.)}{M_{R2}(Code)}$
1	1.1	0.0833	0.84	1.00
2	1.1	0.1333	0.66	1.00
3	1.1	0.0595	1.12	1.00
4	1.1	0.0952	0.77	1.00
5	1.2	0.0833	1.21	1.27
6	1.2	0.1333	0.98	1.16
7	1.2	0.0595	1.42	1.38
8	1.2	0.0952	1.18	1.32
9	1.3	0.0833	1.21	1.25
10	1.3	0.1333	1.06	1.18
11	1.3	0.0595	1.49	1.41
12	1.3	0.0952	1.21	1.29
13	1.4	0.0833	1.09	1.11
14	1.4	0.1333	1.01	1.10
15	1.4	0.0595	1.20	1.18
16	1.4	0.0952	1.08	1.13
17	1.5	0.0833	1.05	1.07
18	1.5	0.1333	1.00	1.07
19	1.5	0.0595	1.11	1.09
20	1.5	0.0952	1.04	1.08
21	1.6	0.0833	1.03	1.05
22	1.6	0.1333	0.99	1.05
23	1.6	0.0595	1.07	1.06
24	1.6	0.0952	1.02	1.06

Table 5.7. Comparisons of Moment Resistances at the Strain of 0.04 for 28 NSC Sections
(Continued)

Section No:	(A_c/A_{ck})	$m=f_{ck}/f_{ywk}$	$\frac{M_{R2}(Re\ gr.)}{M_{R2}(Code)}$	$\frac{M_{R2}(Simp.)}{M_{R2}(Code)}$
25	1.7	0.0833	1.02	1.04
26	1.7	0.1333	0.98	1.04
27	1.7	0.0595	1.05	1.04
28	1.7	0.0952	1.01	1.05

Although some numerical comparisons are presented at Table 5.3, Table 5.5 and Table 5.7, Moment-Curvature curves presented at Appendix A should also be compared as a whole. It is concluded at the end of Section 5.1 that especially Eq. (4.21) can be used safely for normal strength concrete. Cost increases due to increased amount of spiral steel are counteracted to an important extent by the development in the responses of the sections. However, development in the response is not linearly related to increase in the transverse steel content.

5.2. Effect of Longitudinal Steel Percentage and Axial Load Level

Eq. (4.20) and Eq. (4.21) were derived for sections having a longitudinal steel percentage of 0.015. This percentage of longitudinal steel is common in practice. On the other hand, TS-500 [32] allows longitudinal steel percentages up to 0.04 outside the lapped splice region. Hence, behaviour of the sections having longitudinal steel content close to this limit should also be investigated. For some sections defined in Table 4.1 and Table 4.2, effect of longitudinal steel percentage is investigated. In these sections, 8- ϕ 20 is used as longitudinal reinforcement instead of 8- ϕ 14, corresponding to a longitudinal steel percentage of 0.038. All other parameters are kept constant for each section. Moment-Curvature curves are presented at Appendix B.

It should be noted that relative moment drop due to cover crushing came out to be smaller when $\rho_l=0.038$. Minor reason for this is the changes in neutral axis position as longitudinal steel percentage changes. However, this effect is rather insignificant. The main reason is

the ratio of steel moments to resultant concrete moments. If longitudinal steel percentage is small, major part of the moment capacity is supplied by confined and unconfined concrete fibers. In such sections, as concrete crushing starts, the drop in the moment is significant. On the other hand, in case of sections having high longitudinal steel percentage, the moment capacity supplied by steel bars becomes more significant.

As can be followed from Moment-Curvature curves in Appendix B, the trend in ductility does not change when longitudinal steel percentage is changed from 0.015 to 0.038. It is found out that Eq. (4.20) and Eq. (4.21) yield consistent results as longitudinal steel percentage is changed.

Performance of column sections having low axial load levels should also be investigated. Bridge piers generally have relatively low axial loads as compared to columns in the buildings. In addition, an important extent of the bridge piers have (A_c/A_{ck}) ratios about 1.1. These bridge piers have longitudinal steel percentage about one. Properties of a column section designed in order to investigate size effect and axial load level is given in Table 5.8. It should be noted that this column section is analysed under two axial load levels, $N=0.25f_{ck}A_c$ and $N=0.5f_{ck}A_c$.

Table 5.8. Properties of Section 57

Diameter of the Column (D)	3000 mm
Number and Diameter of Longitudinal Steel	100- ϕ 32 mm
Spiral Steel Diameter (d_{sp})	16 mm
Concrete Compressive Strength	25 MPa
Yield Strength of Transverse Steel (f_{ywk})	420 MPa
r_s (Code)	0.00714
r_s (Regression)	0.00708
r_s (Simplified)	0.00666
Axial Load on The Cross-Section (N)	$0.25f_{ck}A_c$ - $0.5f_{ck}A_c$

As can be seen from Figure B.11, proposed equations yielded acceptable results when (A_c/A_{ck}) is smaller than 1.1. It can be seen that size effect does not have significant effect on section behaviour. As expected, when there is lower axial load on the column section, ductile response is obtained (see Figure B.12). Proposed equations yielded acceptable results when axial load level is lower than $0.5f_{ck}A_c$. It is seen that conclusions drawn in Section 5.1 are equally valid for the cases studied.

5.3. Effect of Number and Orientation of Longitudinal Bars

Eq. (4.20) and Eq. (4.21) were derived for sections having 8- ϕ 14 as longitudinal bars. Section behaviour should be investigated with different longitudinal steel orientations, keeping ρ_t constant. In this study, Moment-Curvature comparisons will be derived for sections having longitudinal steel of 6- ϕ 16, 8- ϕ 14 or 12 ϕ 11.5. As can be seen from Figure 5.5, sections with 8 or 12 bars behave omnidirectional. It means that these sections behave in the same manner whether they are bent about axes A or B which are defined in Figure 5.5. On the other hand, sections with 6 longitudinal bars behave in a different manner as they are bent about different axes. This fact was also reported by Dinçer [8]. Moment-Curvature curves are presented at Appendix C. Properties of the sections can be found in Table 4.1 and Table 4.2.

In the analytical studies carried out in this study, it is assumed that sections having 6 longitudinal bars are bent about axis A unless otherwise stated. In 12 bars case, bar diameter is 11.5 mm. This bar is not available in Turkey.

It is seen from the Moment-Curvature curves in Appendix C that the number and orientations of the bars do not have significant effect on the section behaviour up to peak point. Deviations between curves begin approximately at the peak point. It should be noted that as (A_c/A_{ck}) increases, effect of number and orientation of longitudinal bars on section behaviour decreases. At high (A_c/A_{ck}) ratios like 1.6 and 1.7, effect of number and orientation of longitudinal bars on section behaviour can almost be neglected as can be seen from Figures C.16 to C.24. At low (A_c/A_{ck}) ratios like 1.1, number and orientation of longitudinal bars have significant effect on the post – peak behaviour as can be seen from Figures C.1 to C.6. This fact is thought to be due to changes in neutral axis position and well confinement of columns at high (A_c/A_{ck}) ratios. It can also be concluded from the

curves in Appendix C that there is significant difference between 6 bars case as it is bent about axes A or B. This difference is most pronounced again at low (A_c/A_{ck}) ratios. At high (A_c/A_{ck}) ratios, this phenomenon becomes less significant as in the previous case. It is concluded that Eq. (4.20) and Eq. (4.21) yield consistent results as number and orientation of longitudinal bars is changed.

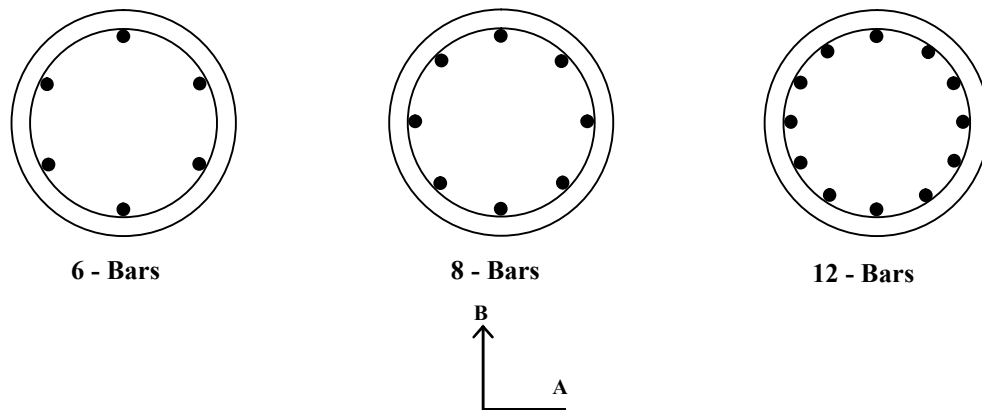


Figure 5.5. Different Longitudinal Steel Orientations

5.4. Effect of Volumetric Ratio of Spiral Steel on Section Behaviour (HSC)

Volumetric ratios of spiral steel required by Eqs. (3.11), (3.12), (4.21), (4.41) are compared in Figures 5.6 to 5.9. It should be strongly emphasized that Eq. (4.20) and Eq. (4.41) require significantly different volumetric ratios of spiral steel at the points close to transition between normal and high strength concrete. The reason for this is the two different derivation processes followed for sections having normal and high strength concrete. For normal strength concrete, these “m” values were the upper limit points and for high strength case, these “m” values were the lower limit points. While using 51 MPa concrete instead of 49 MPa, such a sharp transition as indicated by Eq. (4.20) and Eq. (4.41) is not expected in behaviour. However, code limits [32] enforce to separate normal strength concrete from high strength concrete. It is recommended by the author to use Eq. (4.21) at transition points. On the other hand, user should also be aware of using Eq. (4.21) instead of Eq. (4.20) and Eq. (4.41) is an average solution to the problem in terms of spiral volumetric ratios. As can be seen from Figure 5.6, the regression equation

for high strength concrete requires higher volumetric ratios of spiral steel than Eq. (4.21) at all (A_c/A_{ck}) ratios for this relatively small “m” value. If Eq. (4.41) is used, this may lead to unduly conservative results at the boundary between normal and high strength concrete.

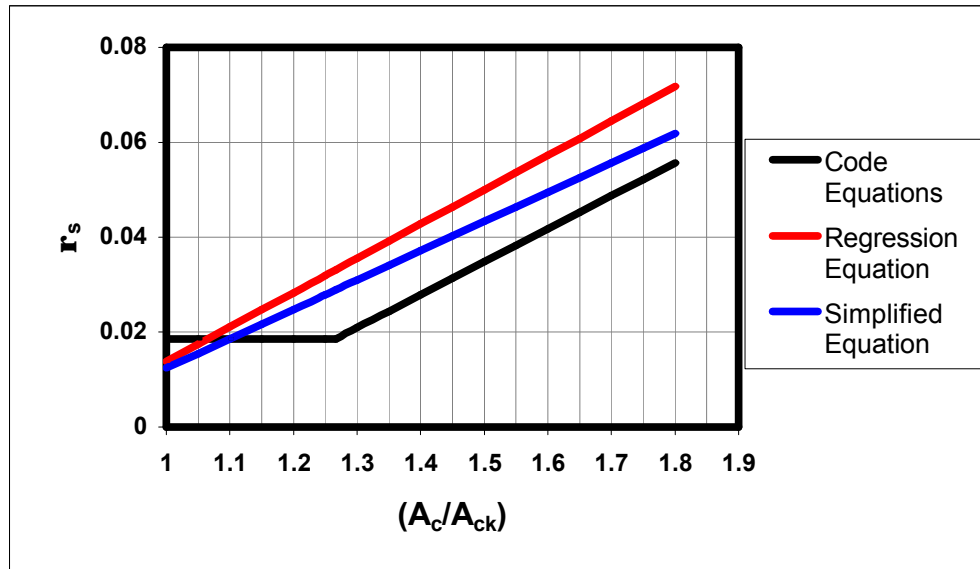


Figure 5.6 Comparison of Volumetric Ratios of Spiral Steel for “m”= 0.1548

On the other hand, difference between volumetric ratios of spiral steel required by Eq. (4.21) and Eq. (4.41) is at most 15% for “m”=0.1548.

As can be seen from Figure 5.7, difference between Eq. (4.21) and Eq. (4.41) is quite small at this “m” value corresponding to concrete compressive strength of 85 MPa. Both equations can be used safely at this “m” value.

As can be seen from Figure 5.8, Eq. (4.41) requires quite low volumetric ratios of spiral steel at $(A_c/A_{ck}) = 1.1$. This is the reason for choosing upper limit as “m” =0.2262 for Eq. (4.41). Eq. (4.21) and Eq. (4.41) require almost same volumetric ratios of spiral steel for $(A_c/A_{ck}) \geq 1.3$. Hence, Eq. (4.41) may yield relatively poor results only at $(A_c/A_{ck}) = 1.1$ for this “m” value corresponding to concrete compressive strength of 95 MPa.

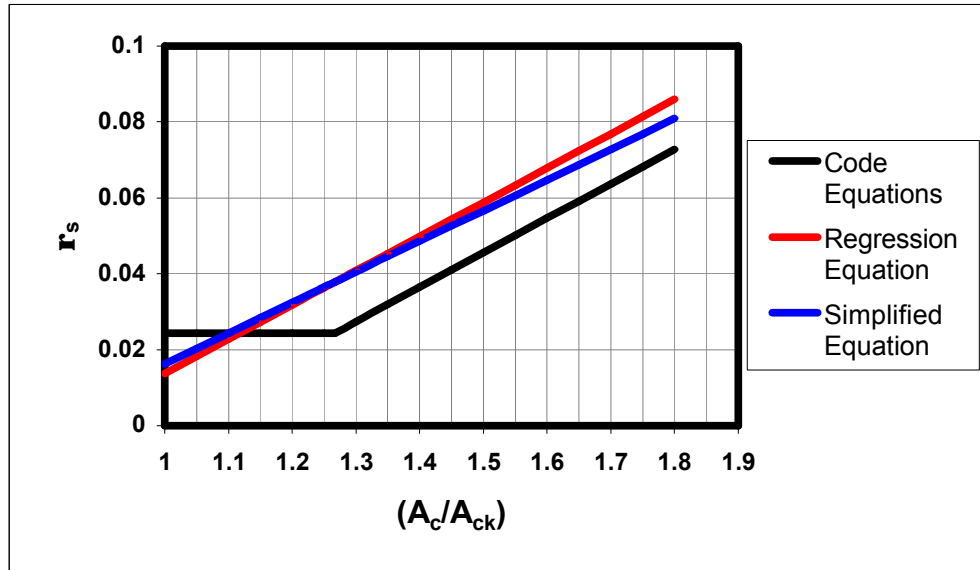


Figure 5.7. Comparison of Volumetric Ratios of Spiral Steel for “m” = 0.2024

As seen from Figure 5.9, Eq. (4.41) requires very small volumetric ratios of spiral steel at low (A_c/A_{ck}) ratios at this “m” value corresponding to concrete compressive strength of 120 MPa. Hence, Eq. (4.41) is proposed for concrete strengths up to 95 MPa. On the other hand, extension for Eq. (4.21) can be made for higher concrete strengths up to 120 MPa.

It should be reminded that Razvi-Saatcioglu [10] confined concrete model for high strength concrete was derived using data from test specimens having concrete strengths between 30 MPa-130 MPa. Hence, validity of Eq. (4.21) for columns having concrete strengths greater than 130 MPa cannot be guaranteed. However, in practice, concrete strengths greater than 130 MPa are quite rare. In TS-500 [32], the upper limit for concrete compressive strength is stated as 50 MPa corresponding to C50. In ACI [33], there is no upper limit for concrete strength as in TS-500. Instead, ACI states that Eq. (3.11) and Eq. (3.12) can be used for concrete strengths greater than 2500 psi. There is no upper limit in concrete strength for Eq. (3.11) and Eq. (3.12) in ACI.

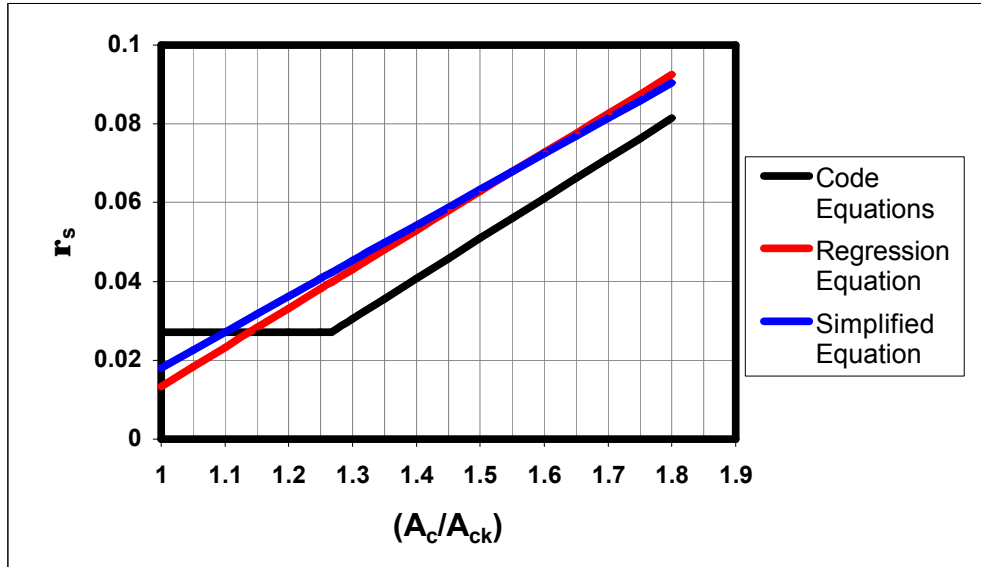


Figure 5.8. Comparison of Volumetric Ratios of Spiral Steel for “m” = 0.2262

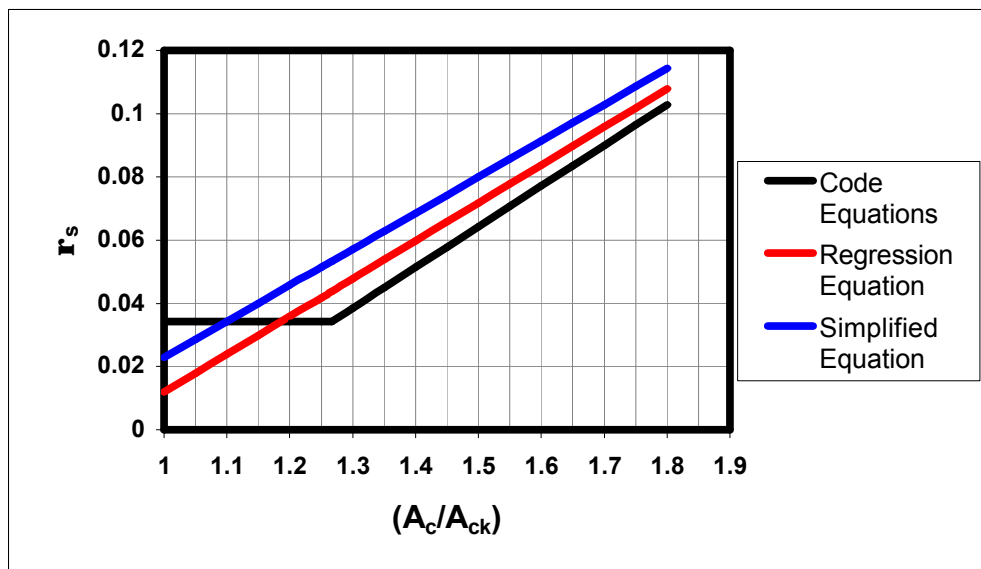


Figure 5.9. Comparison of Volumetric Ratios of Spiral Steel for “m”= 0.2857

In this study, comparison of column sections having spiral reinforcement designed according to either proposed equations or code equations are made by using the Moment-Curvature program. All other parameters except the volumetric ratio of transverse reinforcement were kept constant for each section. Common properties of sections can be

found in Table 4.1. In Table 5.9, properties are listed for 28 sections. It should be noted that sections having concrete compressive strength of 95 MPa were included in the comparison.

Table 5.9. Spiral Volumetric Ratio Comparisons for 28 HSC Sections

Section No:	(A_c/A_{ck})	$m=f_{ck}/f_{ywk}$	r_s (Code)	r_s (Regr.)	r_s (Simp.)	$\frac{r_s(\text{Regr.})}{r_s(\text{Code})}$	$\frac{r_s(\text{Simp.})}{r_s(\text{Code})}$
29	1.1	0.1548	0.0186	0.0211	0.0186	1.13	1.00
30	1.2	0.1548	0.0186	0.0283	0.0248	1.52	1.33
31	1.3	0.1548	0.0209	0.0356	0.0310	1.70	1.48
32	1.4	0.1548	0.0279	0.0428	0.0371	1.53	1.33
33	1.5	0.1548	0.0348	0.0500	0.0433	1.44	1.24
34	1.6	0.1548	0.0418	0.0573	0.0495	1.37	1.19
35	1.7	0.1548	0.0488	0.0645	0.0557	1.32	1.14
36	1.1	0.2024	0.0243	0.0228	0.0243	0.94	1.00
37	1.2	0.2024	0.0243	0.0318	0.0324	1.31	1.33
38	1.3	0.2024	0.0273	0.0409	0.0405	1.50	1.48
39	1.4	0.2024	0.0364	0.0499	0.0485	1.37	1.33
40	1.5	0.2024	0.0455	0.0589	0.0567	1.29	1.24
41	1.6	0.2024	0.0546	0.0679	0.0647	1.24	1.19
42	1.7	0.2024	0.0638	0.0770	0.0728	1.21	1.14
43	1.1	0.2857	0.0343	-	0.0343	-	1.00
44	1.2	0.2857	0.0343	-	0.0457	-	1.33
45	1.3	0.2857	0.0386	-	0.0571	-	1.48
46	1.4	0.2857	0.0514	-	0.0686	-	1.33
47	1.5	0.2857	0.0643	-	0.0800	-	1.24
48	1.6	0.2857	0.0771	-	0.0914	-	1.19
49	1.7	0.2857	0.0900	-	0.1030	-	1.14
50	1.1	0.2262	0.0271	0.0233	0.0271	0.86	1.00
51	1.2	0.2262	0.0271	0.0332	0.0362	1.23	1.33
52	1.3	0.2262	0.0305	0.0431	0.0452	1.41	1.48

Table 5.9. Spiral Volumetric Ratio Comparisons for 28 HSC Sections (Continued)

Section No:	(A_c/A_{ck})	$m=f_{ck}/f_{ywk}$	r_s (Code)	r_s (Regr.)	r_s (Simp.)	$\frac{r_s(\text{Re gr.})}{r_s(\text{Code})}$	$\frac{r_s(\text{Simp.})}{r_s(\text{Code})}$
53	1.4	0.2262	0.0407	0.0530	0.0543	1.30	1.33
54	1.5	0.2262	0.0509	0.0629	0.0633	1.24	1.24
55	1.6	0.2262	0.0611	0.0728	0.0724	1.19	1.18
56	1.7	0.2261	0.0713	0.0827	0.0814	1.16	1.14

It should be stated that section numbers between 50 and 56 have concrete compressive strength of 95 MPa and spirals with yield strength of 420 MPa. Moment-Curvature curves for the HSC sections are presented at Appendix D. It should be noted that high volumetric ratios of spiral steel required by proposed and code equations may lead to difficulties in construction. Sometimes, spiral pitch decreases to eight or nine millimetres that is almost impossible to construct. Increasing the diameter of transverse reinforcement while keeping its volumetric ratio constant or using high strength transverse steel may be the solutions of this problem. However, these two alternatives have also major disadvantages as mentioned in Chapter 2.

Curvature ductility index comparisons are also made for HSC sections. Hence, Eq. (5.3) is used for HSC sections. $K_{.85H}$ and K_{pH} values of 28 HSC sections designed according to Eqs. (3.11), (3.12), (4.41) and (4.21) are presented at Table 5.10. These values are used in order to calculate curvature ductility indexes presented at Table 5.11. Curvature ductility indexes for 28 HSC sections are listed at Table 5.11.

$$m = \frac{K_{.85H}}{K_{pH}} \quad (5.3)$$

$K_{.85H}$ = Curvature of the cross-section at the 85% of the maximum moment

K_{pH} = Curvature of the cross-section at the maximum moment

Table 5.10. K_{pH} and $K_{.85H}$ Values of 28 HSC Sections Designed According to Proposed and Code Equations

Section No:	(A_c/A_{ck})	$m=f_{ck}/f_{ywk}$	ϵ_c at K_{pH}	K_{pHC}	K_{pHR}	K_{pHS}	$K_{.85HC}$	$K_{.85HR}$	$K_{.85HS}$
29	1.1	0.1548	0.0090	0.0505	0.0513	0.0505	0.155	0.191	0.155
30	1.2	0.1548	0.0090	0.0483	0.0504	0.0497	0.142	>0.297	0.238
31	1.3	0.1548	0.0090	0.0470	0.0495	0.0488	0.161	>0.306	>0.294
32	1.4	0.1548	0.0100	0.0540	0.0550	0.0540	>0.299	>0.308	>0.299
33	1.5	0.1548	0.0100	0.0519	0.0538	0.0530	>0.281	>0.308	>0.300
34	1.6	0.1548	0.0120	0.0635	0.0657	0.0647	>0.287	>0.308	>0.301
35	1.7	0.1548	0.0120	0.0628	0.0647	0.0637	>0.289	>0.307	>0.300
36	1.1	0.2024	0.0070	0.0367	0.0365	0.0367	0.134	0.121	0.134
37	1.2	0.2024	0.0070	0.0351	0.0358	0.0358	0.124	0.198	0.204
38	1.3	0.2024	0.0070	0.0342	0.0351	0.0351	0.142	>0.283	>0.282
39	1.4	0.2024	0.0090	0.0453	0.0467	0.0466	0.206	>0.291	>0.289
40	1.5	0.2024	0.0090	0.0447	0.0457	0.0456	>0.270	>0.295	>0.292
41	1.6	0.2024	0.0100	0.0501	0.0512	0.0509	>0.278	>0.296	>0.292
42	1.7	0.2024	0.0120	0.0613	0.0627	0.0623	>0.281	>0.296	>0.291
43	1.1	0.2857	0.0070	0.0353	-	0.0353	0.110	-	0.110
44	1.2	0.2857	0.0070	0.0338	-	0.0346	0.106	-	0.167
45	1.3	0.2857	0.0070	0.0329	-	0.0339	0.119	-	0.240
46	1.4	0.2857	0.0100	0.0496	-	0.0513	0.161	-	0.280
47	1.5	0.2857	0.0100	0.0492	-	0.0504	0.225	-	>0.279
48	1.6	0.2857	0.0100	0.0487	-	0.0496	>0.266	-	>0.281
49	1.7	0.2857	0.0120	0.0595	-	0.0606	>0.270	-	>0.281
50	1.1	0.2262	0.0070	0.0363	0.0358	0.0363	0.125	0.100	0.125
51	1.2	0.2262	0.0070	0.0347	0.0353	0.0355	0.117	0.162	0.191
52	1.3	0.2262	0.0070	0.0338	0.0347	0.0348	0.133	0.253	0.280
53	1.4	0.2262	0.0100	0.0507	0.0523	0.0525	0.187	>0.282	>0.284
54	1.5	0.2262	0.0100	0.0502	0.0514	0.0514	0.266	>0.287	>0.287
55	1.6	0.2262	0.0100	0.0497	0.0505	0.0505	>0.274	>0.289	>0.289
56	1.7	0.2262	0.0120	0.0607	0.0619	0.0618	>0.278	>0.289	>0.288

Table 5.11. Curvature Ductility Index Comparisons for 28 HSC Sections

Section No:	(A_c/A_{ck})	$m=f_{ck}/f_{ywk}$	ϵ_c at K_{pH}	m_{Code}	$m_{Regression}$	$m_{Simplified}$	$\frac{m_{Re gr.}}{m_{Code}}$	$\frac{m_{Simp.}}{m_{Code}}$
29	1.1	0.1548	0.0090	3.07	3.72	3.07	1.21	1.00
30	1.2	0.1548	0.0090	2.94	>5.89	4.79	>2.00	1.63
31	1.3	0.1548	0.0090	3.43	>6.15	>6.00	>1.79	>1.75
32	1.4	0.1548	0.0100	>5.50	>5.50	>5.50	-	-
33	1.5	0.1548	0.0100	>5.40	>5.40	>5.40	-	-
34	1.6	0.1548	0.0120	>4.50	>4.50	>4.50	-	-
35	1.7	0.1548	0.0120	>4.60	>4.60	>4.60	-	-
36	1.1	0.2024	0.0070	3.65	3.32	3.65	0.91	1.00
37	1.2	0.2024	0.0070	3.53	5.53	5.69	1.57	1.61
38	1.3	0.2024	0.0070	4.15	>8.05	>8.05	>1.94	>1.94
39	1.4	0.2024	0.0090	4.55	>6.20	>6.20	>1.36	>1.36
40	1.5	0.2024	0.0090	>6.00	>6.40	>6.40	-	-
41	1.6	0.2024	0.0100	>5.50	>5.70	>5.70	-	-
42	1.7	0.2024	0.0120	>4.50	>4.65	>4.65	-	-
43	1.1	0.2857	0.0070	3.12	-	3.12	-	1.00
44	1.2	0.2857	0.0070	3.14	-	4.83	-	1.54
45	1.3	0.2857	0.0070	3.62	-	7.08	-	1.96
46	1.4	0.2857	0.0100	3.24	-	5.46	-	1.69
47	1.5	0.2857	0.0100	4.57	-	>5.54	-	>1.21
48	1.6	0.2857	0.0100	>5.45	-	>5.65	-	-
49	1.7	0.2857	0.0120	>4.50	-	>4.60	-	-
50	1.1	0.2262	0.0070	3.44	2.79	3.44	0.81	-
51	1.2	0.2262	0.0070	3.37	4.59	5.38	1.36	1.60
52	1.3	0.2262	0.0070	3.93	7.29	8.05	1.85	2.05
53	1.4	0.2262	0.0100	3.69	>5.40	>5.40	>1.46	>1.46
54	1.5	0.2262	0.0100	>5.30	>5.55	>5.55	-	-
55	1.6	0.2262	0.0100	>5.50	>5.70	>5.70	-	-
56	1.7	0.2262	0.0120	>4.60	>4.60	>4.60	-	-

As can be seen from Table 5.11, proposed equations yielded significantly higher curvature ductility indexes than the code equations especially at (A_c/A_{ck}) ratios of 1.2 and 1.3. It should be strongly emphasized that curvature ductility indexes listed in Table 5.11 give notion about the behaviour of the sections. It should be reminded that curvature ductility index as defined by Eq. (5.3) is an approximate way of comparing results since strain corresponding to maximum moment is interpreted in most cases. Hence, curvature ductility index comparisons are not as absolute as capacity index comparisons. Curvature ductility index comparison is not made for some sections since 15% strength degradation did not occur until $\epsilon_c=0.05$.

In case of HSC sections, K_{pH} is the curvature of the cross-section at the maximum moment. The reason for this definition can be seen from figures in Appendix D. Since cover crushing occurs at a lower strain in case of HSC sections, moment capacity at the first peak is relatively small. Hence, in case of HSC sections, maximum moments are used instead of the moments at the initiation of cover crushing in calculating K_{pH} . As can be seen from figures in Appendix D, as concrete strength increases, relative difference between maximum moment and the moment at the first peak increases. Therefore, the values given in Table 5.11 should not be compared directly with those given in Table 5.3.

Capacity index is used to compare Moment-Curvature curves numerically as in the case of NSC sections. Eq. (5.2) is also valid for high strength concrete sections except the strain values at which “ M_{R1} ” and “ M_{R2} ” are calculated. As mentioned before, cover crushing strain is dependent on concrete compressive strength in case of high strength concrete as also included in the Razvi-Saatcioglu [10] model for high strength concrete. Therefore, strain values at the extreme compression fiber were taken as 0.0028 for concrete compressive strengths of 95 MPa and 120 MPa in calculating “ M_{R1} ”. Strain value at the extreme compression fiber was taken as 0.0030 for concrete compressive strength of 85 MPa in calculating “ M_{R1} ”. Finally, strain value at the extreme compression fiber was taken as 0.0032 for concrete compressive strength of 65 MPa in calculating “ M_{R1} ”. While calculating “ M_{R2} ”, strain at the extreme fiber 0.04 in case of NSC sections was shifted to 0.03 in case of HSC sections which is consistent with the derivation made at Section 4.4. It should be emphasized that one section having $(A_c/A_{ck})=1.1$ could not reach the strain of 0.03. The strain value used for this section can be found in Table 5.14.

Table 5.12. M_{R1} and M_{R2} Values of 28 HSC Sections Designed According to Proposed and Code Equations

Section No:	(A_c/A_{ck})	$m=f_{ck}/f_{ywk}$	M_{R1C}	M_{R1R}	M_{R1S}	M_{R2C}	M_{R2R}	M_{R2S}
29	1.1	0.1548	168.8	169.4	168.8	174.5	191.6	174.5
30	1.2	0.1548	162.9	164.6	164.0	153.1	199.0	187.4
31	1.3	0.1548	159.0	161.1	160.5	150.7	197.6	187.5
32	1.4	0.1548	156.2	157.9	157.3	161.2	191.2	181.9
33	1.5	0.1548	153.9	155.3	154.7	161.4	184.2	175.5
34	1.6	0.1548	152.1	153.2	152.5	159.4	178.1	169.5
35	1.7	0.1548	150.4	151.3	150.8	155.7	171.6	163.3
36	1.1	0.2024	183.4	183.4	183.4	196.0	179.6	196.0
37	1.2	0.2024	177.3	177.5	177.8	168.2	218.0	220.7
38	1.3	0.2024	173.8	174.0	174.1	168.7	225.2	224.1
39	1.4	0.2024	171.0	171.3	171.2	188.1	221.3	218.7
40	1.5	0.2024	169.0	169.2	169.2	191.2	214.9	212.1
41	1.6	0.2024	167.3	167.4	167.4	190.1	208.5	204.6
42	1.7	0.2024	166.1	166.2	166.2	186.5	201.6	197.2
43	1.1	0.2857	199.0	-	199.0	220.5	-	220.5
44	1.2	0.2857	197.9	-	196.4	185.0	-	271.9
45	1.3	0.2857	197.6	-	195.6	192.7	-	282.4
46	1.4	0.2857	197.2	-	194.1	229.6	-	278.4
47	1.5	0.2857	197.3	-	196.2	238.8	-	270.5
48	1.6	0.2857	197.7	-	196.8	239.8	-	262.3
49	1.7	0.2857	198.4	-	197.7	236.4	-	253.3
50	1.1	0.2262	188.5	188.8	188.5	215.6	170.2	215.6
51	1.2	0.2262	185.6	185.2	184.9	173.6	220.7	236.1
52	1.3	0.2262	183.6	182.8	182.7	176.3	235.1	241.3
53	1.4	0.2262	181.5	181.0	181.0	200.8	233.8	236.5
54	1.5	0.2262	180.3	179.9	179.9	205.6	228.3	228.9
55	1.6	0.2262	179.5	179.2	179.2	205.0	222.2	221.7
56	1.7	0.2262	179.1	178.8	178.9	201.3	215.1	213.7

M_{R1} and M_{R2} values of 28 HSC sections designed according to Eqs. (3.11), (3.12), (4.41) and (4.21) are presented at Table 5.12. These values are used in order to calculate capacity indexes presented at Table 5.13.

Table 5.13. Capacity Index Comparisons for 28 HSC Sections

Section No:	(A_c/A_{ck})	$m=f_{ck}/f_{ywk}$	CI_{Code}	$CI_{Regression}$	$CI_{Simplified}$	$\frac{CI_{Regr.}}{CI_{Code}}$	$\frac{CI_{Simp.}}{CI_{Code}}$
29	1.1	0.1548	1.03	1.13	1.03	1.10	1.00
30	1.2	0.1548	0.94	1.21	1.14	1.29	1.21
31	1.3	0.1548	0.95	1.23	1.17	1.29	1.23
32	1.4	0.1548	1.03	1.21	1.16	1.17	1.13
33	1.5	0.1548	1.05	1.19	1.13	1.13	1.08
34	1.6	0.1548	1.05	1.16	1.11	1.10	1.06
35	1.7	0.1548	1.03	1.13	1.08	1.10	1.05
36	1.1	0.2024	1.07	0.98	1.07	0.92	1.00
37	1.2	0.2024	0.95	1.23	1.24	1.29	1.30
38	1.3	0.2024	0.97	1.29	1.29	1.33	1.33
39	1.4	0.2024	1.10	1.29	1.28	1.17	1.16
40	1.5	0.2024	1.13	1.27	1.25	1.12	1.11
41	1.6	0.2024	1.14	1.25	1.22	1.10	1.07
42	1.7	0.2024	1.12	1.21	1.19	1.08	1.06
43	1.1	0.2857	1.11	-	1.11	-	1.00
44	1.2	0.2857	0.93	-	1.38	-	1.48
45	1.3	0.2857	0.98	-	1.44	-	1.47
46	1.4	0.2857	1.16	-	1.43	-	1.23
47	1.5	0.2857	1.21	-	1.38	-	1.14
48	1.6	0.2857	1.21	-	1.33	-	1.10
49	1.7	0.2857	1.19	-	1.28	-	1.08
50	1.1	0.2262	1.14	0.90	1.14	0.79	1.00
51	1.2	0.2262	0.94	1.19	1.28	1.27	1.36
52	1.3	0.2262	0.96	1.29	1.32	1.34	1.38
53	1.4	0.2262	1.11	1.29	1.31	1.16	1.18

Table 5.13. Capacity Index Comparisons for 28 HSC Sections (Continued)

Section No:	(A_c/A_{ck})	$m=f_{ck}/f_{ywk}$	CI_{Code}	$CI_{Regression}$	$CI_{Simplified}$	$\frac{CI_{Regr.}}{CI_{Code}}$	$\frac{CI_{Simp.}}{CI_{Code}}$
54	1.5	0.2262	1.14	1.27	1.27	1.11	1.11
55	1.6	0.2262	1.14	1.24	1.24	1.09	1.09
56	1.7	0.2262	1.12	1.20	1.19	1.07	1.06

As can be followed from Table 5.11, Table 5.13 and Table 5.15, proposed equations resulted in more ductile behaviour than the code equations except Section 36 and Section 50 designed according to Eq. (4.41). It should be reminded that these two sections have $(A_c/A_{ck})=1.1$. At (A_c/A_{ck}) ratios of 1.2 and 1.3, proposed equations resulted in more ductile behaviour than the code equations. However, as can be seen from Table 5.9, proposed equations require significantly higher volumetric ratios of spiral steel at these (A_c/A_{ck}) ratios. As concrete strength increases, difference in response between code and proposed equations increases. Reader can compare the capacity indexes for “m”=0.1548 and “m” =0.2857 for this purpose from Table 5.13. At high (A_c/A_{ck}) ratios like 1.6 and 1.7, difference between proposed and code equations becomes equal to or smaller than 10%. At these (A_c/A_{ck}) ratios, both code and proposed equations yield stable and ductile post-peak behaviour. This is considered to be the reason for relatively small differences between proposed and code equations at high (A_c/A_{ck}) ratios.

Table 5.14. Strains Used for Calculating CI that are Different than 0.03

Section No:	ϵ_c
50	0.028

As can be seen in Table 5.14, Section 50 designed according to Eq. (4.41) could not reach the strain value of 0.03 at the extreme compression fiber. In addition, relatively brittle behaviour of the Section 50 designed according to Eq. (4.41) can be seen from

Figure D.22. Hence, concrete compressive strength limit of 95 MPa for Eq. (4.41) is verified.

Table 5.15. Comparisons of Moment Resistances at the Strain of 0.03 for 28 HSC Sections

Section No:	(A_c/A_{ck})	$m=f_{ck}/f_{ywk}$	$\frac{M_{R2}(Re\ gr.)}{M_{R2}(Code)}$	$\frac{M_{R2}(Simp.)}{M_{R2}(Code)}$
29	1.1	0.1548	1.10	1.00
30	1.2	0.1548	1.30	1.22
31	1.3	0.1548	1.31	1.24
32	1.4	0.1548	1.19	1.13
33	1.5	0.1548	1.14	1.09
34	1.6	0.1548	1.12	1.06
35	1.7	0.1548	1.10	1.05
36	1.1	0.2024	0.92	1.00
37	1.2	0.2024	1.30	1.31
38	1.3	0.2024	1.33	1.33
39	1.4	0.2024	1.18	1.16
40	1.5	0.2024	1.12	1.11
41	1.6	0.2024	1.10	1.08
42	1.7	0.2024	1.08	1.06
43	1.1	0.2857	-	1.00
44	1.2	0.2857	-	1.47
45	1.3	0.2857	-	1.47
46	1.4	0.2857	-	1.21
47	1.5	0.2857	-	1.13
48	1.6	0.2857	-	1.09
49	1.7	0.2857	-	1.07
50	1.1	0.2262	0.79	1.00
51	1.2	0.2262	1.27	1.36
52	1.3	0.2262	1.33	1.37
53	1.4	0.2262	1.16	1.18
54	1.5	0.2262	1.11	1.11

Table 5.15. Comparisons of Moment Resistances at the Strain of 0.03 for 28 HSC Sections
(Continued)

Section No:	(A_c/A_{ck})	$m=f_{ck}/f_{ywk}$	$\frac{M_{R2}(Re\ gr.)}{M_{R2}(Code)}$	$\frac{M_{R2}(Simp.)}{M_{R2}(Code)}$
55	1.6	0.2262	1.08	1.08
56	1.7	0.2262	1.07	1.06

Although some numerical comparisons are presented at Table 5.11, Table 5.13 and Table 5.15, Moment-Curvature curves presented at Appendix D should also be compared as a whole. As can be seen from Moment-Curvature curves in Appendix D, sections designed according to Eq. (4.21) behaved in a ductile manner up to concrete strength of 120 MPa. Therefore, no limitation for concrete strength is necessary for Eq. (4.21). Eq. (4.41) behaved satisfactorily at other points studied, up to concrete compressive strengths of 95 MPa.

It is concluded at the end of Section 5.4 that especially Eq. (4.21) can be used safely for high strength concrete up to concrete compressive strength of 120 MPa. Cost increases due to increased amount of spiral steel are counteracted by the development in the responses of the sections. However, development in the response is not linearly related to increase in the transverse steel content as in the case of NSC.

CHAPTER 6

SUMMARY AND CONCLUSION

6.1. Summary

The minimum spiral ratio equation in the codes is derived by equating the strength at the second peak to the strength at the first peak for spiral columns tested under uniaxial load. On the other hand, in practice, no column is only under axial load. In this study, behaviour of the circular sections under combined bending and axial load was taken as basis.

A spiral column database was formed including data of 463 column tests. In this database, various column types under various loading schemes were included. Material strengths in the database range from lower limit to upper limit used in practice. Also, (A_v/A_{ck}) ratios of the test columns included in the database possess diversity. Well-confined columns and poorly confined columns were also included in the database.

By carrying out analytical studies on 28 NSC sections, one regression equation and one simplified equation were derived. While Eq. (4.20) is only valid for normal strength concrete, it was proved that Eq. (4.21) is also applicable to high strength concrete by carrying out analytical studies.

Analytical studies on 21 HSC sections lead to one regression equation and one simplified equation. In order to reduce number of equations proposed, Eq. (4.21) instead of Eq. (4.42) was recommended. Concrete strength limit of 95 MPa was established for Eq. (4.41). There is not such a limit for Eq. (4.21). It is proposed for concrete strengths up to 120 MPa. In this study, the upper limit for normal strength concrete was 50 MPa as in TS-500 [32].

Comparisons of code equations and proposed equations were made for NSC sections by using the Moment-Curvature program. Number and orientation of longitudinal bars, longitudinal steel percentage and axial load level were taken as variables.

Comparisons of proposed equations and code equations for HSC sections were also made by using the Moment-Curvature program.

6.2. Conclusion

The following conclusions were drawn based on studies presented in this thesis;

-Eq. (4.21) called simplified equation yielded consistent results at all (A_c/A_{ck}) ratios and “m” values studied.

$$r_s = 0.32 \frac{f_{ck}}{f_{ywk}} \left[1.25 \left(\frac{A_c}{A_{ck}} \right) - 1 \right] \quad (4.21)$$

-Eq. (4.21) yielded consistent results for concrete strengths between 25 MPa and 120 MPa.

-Eq. (4.21) yielded consistent results for yield strength of spiral steel varying between 300 MPa and 420 MPa.

-Eq. (4.21) yielded more consistent results than code equations at (A_c/A_{ck}) ratios greater than 1.1, independent of material strengths.

-Except few points, the regression equation (Eq. (4.20)) yielded consistent results at all (A_c/A_{ck}) ratios and “m” values studied.

$$r_s = 0.32 \frac{f_{ck}}{f_{ywk}} \left[0.85 \left(\frac{f_{ck}}{f_{ywk}} \right)^{-0.1429} \left(\frac{A_c}{A_{ck}} \right) - 1 \right] \quad (4.20)$$

-Except few points, the regression equation (Eq. (4.41)) yielded consistent results for concrete compressive strengths up to 95 MPa.

$$r_s = 0.378 \frac{f_{ck}}{f_{ywk}} \left[0.890 \left(\frac{f_{ck}}{f_{ywk}} \right)^{-0.1763} \left(\frac{A_c}{A_{ck}} \right) - 1 \right] \quad (4.41)$$

-Increasing yield strength of spiral steel decreases volumetric ratio of spiral steel. This results in relatively brittle behaviour.

- For spiral columns, volumetric ratio of the transverse reinforcement is the most significant parameter affecting section ductility.

-Conclusions drawn above were proven to be valid while changing number and orientation of longitudinal bars and longitudinal steel percentage.

- As the last conclusion, one equation for all (A_c/A_{ck}) ranges and derivation based on Moment-Curvature of the sections under $N=0.5f_{ck}A_c$ rather than P- Δ are the advantages of the equations proposed.

6.3. Recommendations for Future Researches

Following recommendations are made for future researches and researchers:

- All conclusions in this study are based on Moment-Curvature diagrams obtained analytically using proper material models. Therefore, validity of these conclusions should be checked by tests.

- Experimental behaviour of the columns designed according to Eqs. (4.20), (4.21) and (4.41) should be investigated at different (A_c/A_{ck}) ratios and “m” values under simulated seismic loading.

- Effect of different loading patterns on columns designed according to Eqs. (4.20), (4.21) and (4.41) should be investigated experimentally.

- Experimental behaviour of the columns designed according to proposed equations should be investigated with different number and orientation of longitudinal bars and different longitudinal steel percentages.

- Experimental behaviour of the columns designed according to Eq. (4.21) while having ultra high strength reinforcement and concrete strengths greater than 120 MPa may be investigated.

- Philosophy of this study may be used for rectangular and square columns having rectilinear ties in order to derive equations for minimum transverse reinforcement ratio.

REFERENCES

- [1] Ang, B.G., Priestley, M.J.N., and Paulay, T., “Seismic Shear Strength of Circular Reinforced Concrete Columns,” *ACI Structural Journal*, January-February 1989, pp. 45- 59.
- [2] Scott, B.D., Park R., and Priestley, M.J.N., “Stress-Strain Behavior of Concrete Confined by Overlapping Hoops at Low and High Strain Rates,” *ACI Journal*, Proceedings V.79, No.1, January-February 1982, pp. 13-27.
- [3] Mander, J.B., Priestley, M.J.N., and Park, R., “Theoretical Stress-Strain Model for Confined Concrete,” *Journal of Structural Engineering*, ASCE, V.114, No. 8, Aug. 1988, pp.1805-1826.
- [4] Sheikh, S.A., “A Comparative Study of Confinement Models,” *ACI Journal*, July-August 1982, pp. 296-305.
- [5] Ersoy, U., Özcebe, G., “Confinement Effect in Spiral Columns – A Discussion,” Fourth National Conference on Earthquake Engineering, Turkish National Society of Earthquake Engineering, Ankara, Turkey, September, 321, 1997 [In Turkish].
- [6] Saatcioglu, M., and Razvi, S.R., “Strength and Ductility of Confined Concrete,” *Journal of Structural Engineering*, ASCE, Vol.118, No.6, June 1992, pp. 1590-1607.
- [7] Baran, M., “An Experimental Investigation on the Minimum Confinement Reinforcement Requirement of Spiral Columns,” MS Thesis, METU, Civil Engineering Department, 1999.
- [8] Dinçer, S., “A Study on the Minimum Confinement in Spiral Columns”, MS Thesis, METU, Civil Engineering Department, 1999.
- [9] Korkmaz, S., “A Comparative Study On Confinement Models for Concrete”, MS Thesis, METU, Civil Engineering Department, 1992.
- [10] Razvi, S.R., and Saatcioglu, M., “Confinement Model for High-Strength Concrete,” *Journal of Structural Engineering*, ASCE, March 1999, pp. 281-288.

- [11] Park, R., Priestley, M.J.N., and Gill, W.D., "Ductility of Square-Confined Concrete Columns," *Journal of the Structural Division, Proceedings of the American Society of Civil Engineers*, Vol.108, No. ST4, April 1982, pp. 929-950.
- [12] El Dash, K.M., and Ahmad, S.H., "A Model for Stress-Strain Relationship of Spirally Confined Normal and High-Strength Concrete Columns," *Magazine of Concrete Research*, 47, No 171, June 1995, pp. 177-184.
- [13] Ngo, T.D, Mendis, P.A., Teo, D., and Kusuma, G., "Behaviour of High-Strength Concrete Columns Subjected to Blast Loading," *Proceedings of the ASSCCA'03 International Conference*, Eds. Hancock, GJ; Bradford, MA; Wilkinson, TJ; UY, B & Rasmussen, KJR, Vol. 2, pp. 1057-1063.
- [14] Priestley, M.J.N., Park, R., and Potangaroa, R.T., "Ductility of Spirally-Confined Concrete Columns," *Journal of the Structural Division, ASCE*, January 1981, pp. 181- 202.
- [15] Martinez, S., Nilson, A., and Slate, F. "Spirally Reinforced High-Strength Concrete Columns," *ACI Journal*, September-October 1984, pp. 431-442.
- [16] Cusson, D., and Paultre, P., "Stress-Strain Model for Confined High-Strength Concrete," *Journal of Structural Engineering, ASCE*, 121 (3) 1995, pp. 468-477.
- [17] Ahmad, S.H., and Shah, S.P., "Stress-Strain Curves of Concrete Confined by Spiral Reinforcement," *ACI Journal*, November-December 1982, pp. 484-490.
- [18] Fafitis, A., and Shah, S.P., "Lateral Reinforcement for High Strength Concrete Columns," *ACI Special Publication, SP-87-12*, 1985, pp.213-232.
- [19] Fafitis, A., and Shah, S.P., "Predictions of Ultimate Behaviour of Confined Columns Subjected to Large Deformations," *ACI Journal*, July-August 1985, pp. 423-433.
- [20] Mander, J.B., Priestley, M.J.N., and Park, R., "Observed Stress-Strain Behaviour of Confined Concrete," *Journal of Structural Engineering, ASCE*, 114 (8) 1988, pp. 1827-1849.
- [21] Zahn, F.A., Park, R. and Priestley, M.J.N., "The Use of Grade 380 Steel for Transverse Confining Reinforcement in Columns," *Bulletin of the New Zealand National Society for Earthquake Engineering*, Vol. 20, No.2, June 1987, pp. 99-115.

- [22] Azizinamini, A., Corley, W. G., and Johal, L.S.P., "Effect of Transverse Reinforcement on Seismic Performance of Columns," ACI Structural Journal, July-August 1992, pp. 442-450.
- [23] Sheikh, S.A., and Toklucu, M.T., "Reinforced Concrete Columns Confined by Circular Spirals and Hoops," ACI Structural Journal, September-October 1993, pp. 542-552.
- [24] Samra, R., Nidal, D. A. A., Madi, U.R., "Transverse Steel Content in Spiral Concrete Columns Subjected To Eccentric Loading," ACI Structural Journal, July-August 1996, pp. 1-7.
- [25] Saatcioglu, M., and Baingo, D., "Circular High-Strength Concrete Columns under Simulated Seismic Loading," Journal of Structural Engineering, ASCE, March 1999, pp. 272-280.
- [26] Razvi, S.R., and Saatcioglu, M., "Circular High-Strength Concrete Columns under Concentric Compression," ACI Structural Journal, September-October 1999, pp. 817-826.
- [27] Bing, L., Park, R., and Tanaka, H., "Stress-Strain Behaviour of High-Strength Concrete Confined by Ultra-High and Normal Strength Transverse Reinforcements," ACI Structural Journal, May-June 2001, pp. 395-406.
- [28] Esmaily, A., and Xiao, Y., "Behaviour of Reinforced Concrete Columns Under Variable Axial Loads," ACI Structural Journal, January-February 2004, pp. 124-132.
- [29] Ersoy, U., and Özcebe, G., "Moment-Curvature Relationship of Confined Concrete Sections," First Japan-Turkey Workshop on Earthquake Engineering, Istanbul, Volume 1, March 1997, pp. 9-21.
- [30] Ersoy, U., and Özcebe, G., "Reinforced Concrete," Expanded New Edition, Evrim Publishing Co., Ankara, 2001.
- [31] _____, "Specification for Structures to be Built in Disaster Areas," Government of Republic of Turkey, Ministry of Public Works and Settlement, Ankara, 1997. [English Translation Prepared Under Direction of Aydinoglu, M.N.]

- [32] _____, “TS-500 February 2000, Requirements for Design and Construction of Reinforced Concrete Structures,” Middle East Technical University, Ankara, 2003. [Translated and Printed with Permission from Turkish Standards Institute]
- [33] ACI Committee 318, “Building Code Requirements for Structural Concrete (ACI 318-02) and Commentary (318R-02),” American Concrete Institute, Farmington Hills, Michigan, 2002, 443 pp.

REFERENCES USED IN THE SPIRAL COLUMN DATABASE AND NOT MENTIONED IN THE MANUSCRIPT

- [34] Tanaka, H., and Park, R., “Seismic Design and Behaviour of Reinforced Concrete Columns with Interlocking Spirals,” ACI Structural Journal, March-April 1993, pp. 192-203.
- [35] Pessiki, S., and Pieroni, A., “Axial Load Behaviour of Large-Scale Spirally-Reinforced High Strength Concrete Columns,” ACI Structural Journal, May-June 1997, pp. 304-314.
- [36] Wong, Y.L., Paulay, T., and Priestley, M.J.N., “Response of Circular Reinforced Concrete Columns to Multi-Directional Seismic Attack,” ACI Structural Journal, March-April 1993, pp. 180-191.
- [37] Naito, C.J., Moehle, J.P., and Mosalam, K.M., “Evaluation of Bridge-Column Joints Under Simulated Seismic Loading,” ACI Structural Journal, January-February 2002, pp. 62-71.
- [38] Ziehl, P.H., Cloyd, J.E., and Kreger, M.E., “Investigation of Minimum Longitudinal Reinforcement for Concrete Columns Using Present-Day Construction Materials,” ACI Structural Journal, March-April 2004, pp. 165-175.
- [39] Sakai, J., and Kawashima, K., “Effect of Residual Strain of Hoops on the Lateral Confinement of Concrete,” The third Japan-UK Workshop on Implications of Recent Earthquakes on Seismic Risk, pp. 1-11.
- [40] Kowalsky, M.J., Priestley, M.J.N., and Seible, F., “Shear and Flexural Behaviour of Lightweight Concrete Bridge Columns in Seismic Regions,” ACI Structural Journal, January-February 1999, pp. 136-148.

- [41] Chai, Y.H., Priestley, M.J.N., and Seible, F., "Seismic Retrofit of Circular Bridge Columns for Enhanced Flexural Performance," *ACI Structural Journal*, September-October 1991, pp. 572-584.
- [42] Bruneau, M., and Marson, J., "Seismic Design of Concrete-Filled Circular Steel Bridge Piers," *Journal of Bridge Engineering*, ASCE, January-February 2004, pp. 24-34.
- [43] Fujimoto, T., Mukai, A., Nishiyama, I., and Sakino, K., "Behavior of Eccentrically Loaded Concrete-Filled Steel Tubular Columns," *Journal of Structural Engineering*, ASCE, February 2004, pp. 203-212.
- [44] Marson, J., and Bruneau, M., "Cyclic Testing of Concrete-Filled Circular Steel Bridge Piers Having Encased Fixed-Based Detail," *Journal of Bridge Engineering*, ASCE, January-February 2004, pp.14-23.
- [45] Sakino, K., Nakahara, H., Morino, S., and Nishiyama, I., "Behavior of Centrally Loaded Concrete-Filled Steel-Tube Short Columns," *Journal of Structural Engineering*, ASCE, February 2004, pp. 180-188.
- [46] Priestley, M.J.N., and Benzoni, G., "Seismic Performance of Circular Columns with Low Longitudinal Reinforcement Ratios," *ACI Structural Journal*, July-August 1996, pp. 1-12.
- [47] Boyd, P.F., Cofer, W.F., and McLean, D.I., "Seismic Performance of Steel-Encased Concrete Columns under Flexural Loading," *ACI Structural Journal*, May-June 1995, pp. 355-364.
- [48] Kowalsky, M.J., and Priestley, M.J.N., "Improved Analytical Model for Shear Strength of Circular Reinforced Concrete Columns in Seismic Regions," *ACI Structural Journal*, May-June 2000, pp. 388-396.
- [49] Assa, B., Nishiyama, M., and Watanabe, F., "New Approach for Modeling Confined Concrete. I: Circular Columns," *Journal of Structural Engineering*, ASCE, July 2001, pp. 743-750.
- [50] Inai, E., Mukai, A., Kai, M., Tokinoya, H., Fukumoto, T., and Mori, K., "Behavior of Concrete-Filled Steel Tube Beam Columns," *Journal of Structural Engineering*, ASCE, February 2004, pp. 189-202.

- [51] Moyer, M.J., and Kowalsky, M.J., "Influence of Tension Strain on Buckling of Reinforcement in Concrete Columns," *ACI Structural Journal*, January-February 2003, pp. 75-85.
- [52] Cheek, G.S., and Stone W.C., "Behavior of 1/6 Scale Model Columns Subjected to Inelastic Cyclic Loading," *ACI Structural Journal*, November-December 1990, pp. 630-638.
- [53] Verma, R., Priestley, M.J.N., and Seible, F., "Assessment of Seismic Response and Steel Jacket Retrofit of Squat Circular Reinforced Concrete Bridge Columns," Report SSRP-93/05, Structures Division, University of California, San Diego, California, 1993.
- [54] Vu, N.H., Priestley, M.J.N., Seible, F., and Benzoni, G., "The Seismic Response of Well-Confined Circular Reinforced Concrete Columns with Low Aspect Ratios," Report SSRP-97/15, Structures Division, University of California, San Diego, California, 1996.
- [55] Ohtaki, T., Benzoni, G., and Priestley, M.J.N., "Seismic Performance of a Full-Scale Bridge Column-As Built and As Repaired," Report SSRP-96/07, Structures Division, University of California, San Diego, California, 1996.
- [56] Priestley, M.J.N., Seible, F., and Benzoni, G., "Seismic Performance of Circular Columns with Low Longitudinal Steel Ratios," Report SSRP-94/08, Structures Division, University of California, San Diego, California, 1994.
- [57] Benzoni, G., Ohtaki, T., Priestley, M.J.N., and Seible, F., "Seismic Performance of Circular Reinforced Concrete Columns Under Varying Axial Load," Report SSRP-96/04, Structures Division, University of California, San Diego, California, 1996.
- [58] Kunnath, S.K., El-Bahy, A., Taylor, A., and Stone, W., "Cumulative Seismic Damage of Reinforced Concrete Bridge Piers," Technical Report NCEER-97-0006, National Center for Earthquake Engineering Research, September 1997.
- [59] Lehman, D.E., and Moehle, J.P., "Seismic Performance of Well-Confined Concrete Bridge Columns," Pacific Earthquake Engineering Research Center, PEER 1998/01, December 2000.
- [60] Calderone, A.J., Lehman, D.E., and Moehle, J.P., "Behavior of Reinforced Concrete Bridge Columns Having Varying Aspect Ratios and Varying Lengths of Confinement," Pacific Earthquake Engineering Research Center, Report 2000/08, January 2001.

- [61] Pessiki, S., Graybeal, B., and Mudlock, M., "Proposed Design of High-Strength Spiral Reinforcement in Compression Members," *ACI Structural Journal*, November-December 2001, pp. 799-810.
- [62] Xiao, Y., He, W.H., Mao, X.Y., Choi, K.K., and Zhu, P.S., "Confinement Design of CFT Columns for Improved Seismic Performance," *Proceedings of the International Workshop on Steel and Concrete Composite Construction (IWSCCC-2003)*, Taipei, R. China, October 2003, pp. 217-226.
- [63] Berry, M., Parrish, M., and Eberhard, M., "PEER Structural Performance Database User's Manual (Version 1.0)," Pacific Earthquake Engineering Research Center, University of California, Berkeley, January 2004.
- [64] University of Washington, "Structural Performance Database," <http://www.ce.washington.edu/~peera/>, September 2004 (Last Date Accessed).
- [65] Hu, H.T., Huang, C.S., Wu, M.H., and Wu, Y.M., "Nonlinear Analysis of Axially Loaded Concrete-Filled Tube Columns with Confinement Effect," *Journal of Structural Engineering*, ASCE, October 2003, pp. 1322-1329.
- [66] Esmaily, A., and Xiao, Y., "Seismic Behaviour of Bridge Columns Subjected to Various Loading Patterns," Pacific Earthquake Research Center, PEER 2002/15, December 2002.
- [67] Elkin, S.J., Nacamuli, A.M., Lehman, D.E., and Moehle, J.P., "Seismic Performance of Damaged Bridge Columns," *Earthquake Engineering and Engineering Seismology*, Volume 1, Number 1, September 1999, pp. 39-50.

APPENDIX A

MOMENT-CURVATURE COMPARISONS

(Effect of Volumetric Ratio of Spiral Steel on Section Behaviour (NSC))

In Appendix A, Moment-Curvature curves of the 28 sections having spiral ratios according to Eqs. (3.11), (3.12), (4.20) and (4.21) are presented. Detailed information can be found in Section 5.1. Detailed information about sections can be found in Table 4.1 and Table 5.1.

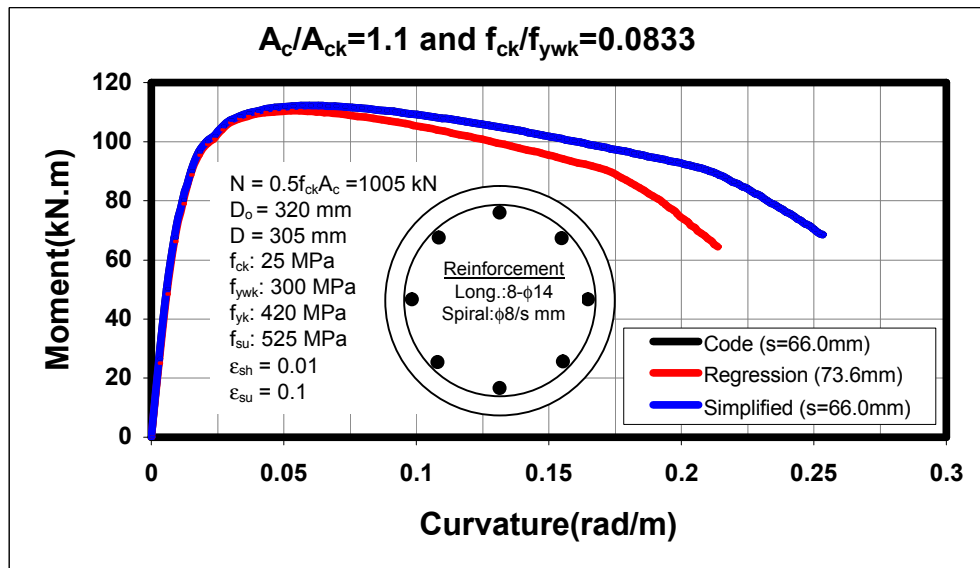


Figure A.1. Comparison of Proposed and Code Equations for Section 1

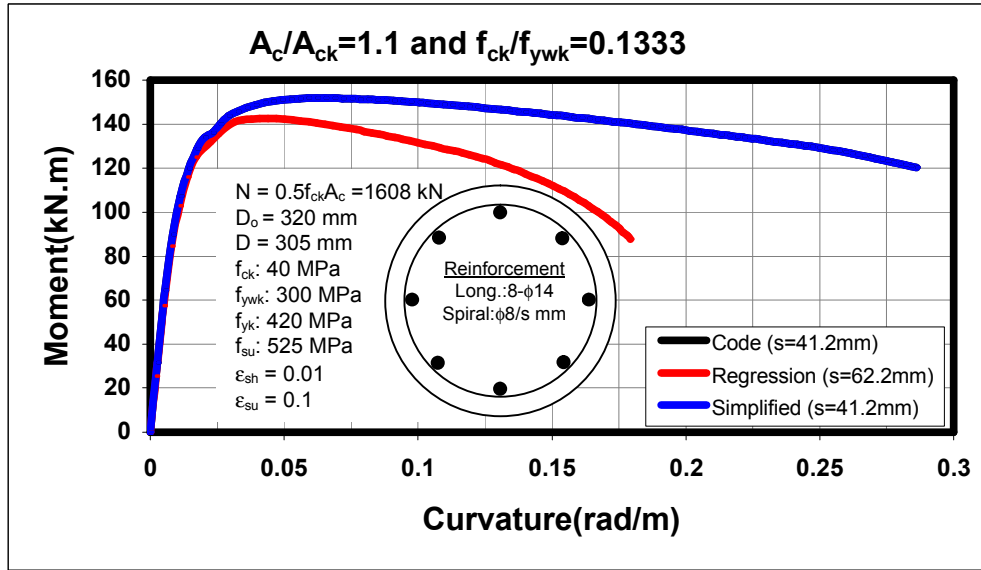


Figure A.2. Comparison of Proposed and Code Equations for Section 2

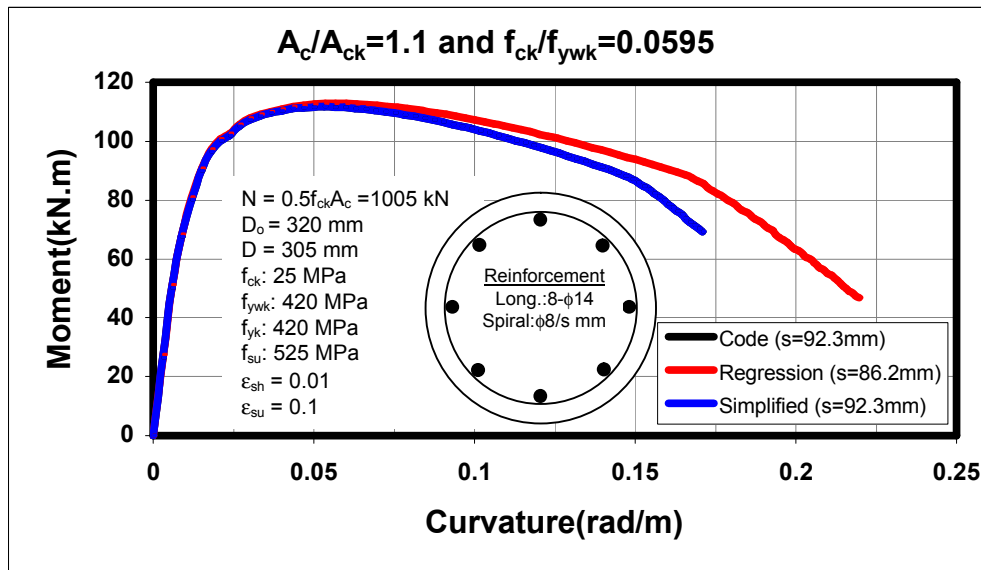


Figure A.3. Comparison of Proposed and Code Equations for Section 3

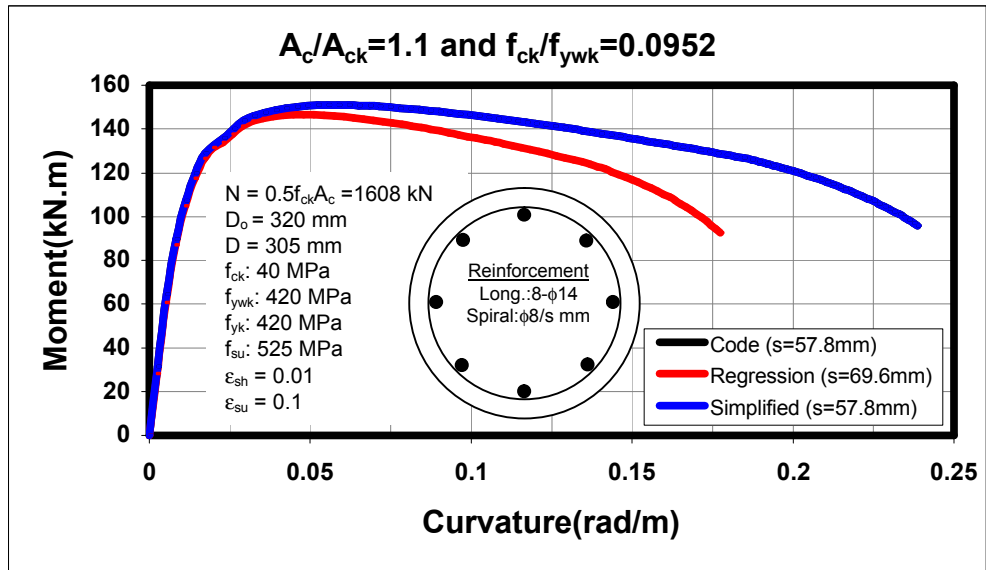


Figure A.4. Comparison of Proposed and Code Equations for Section 4

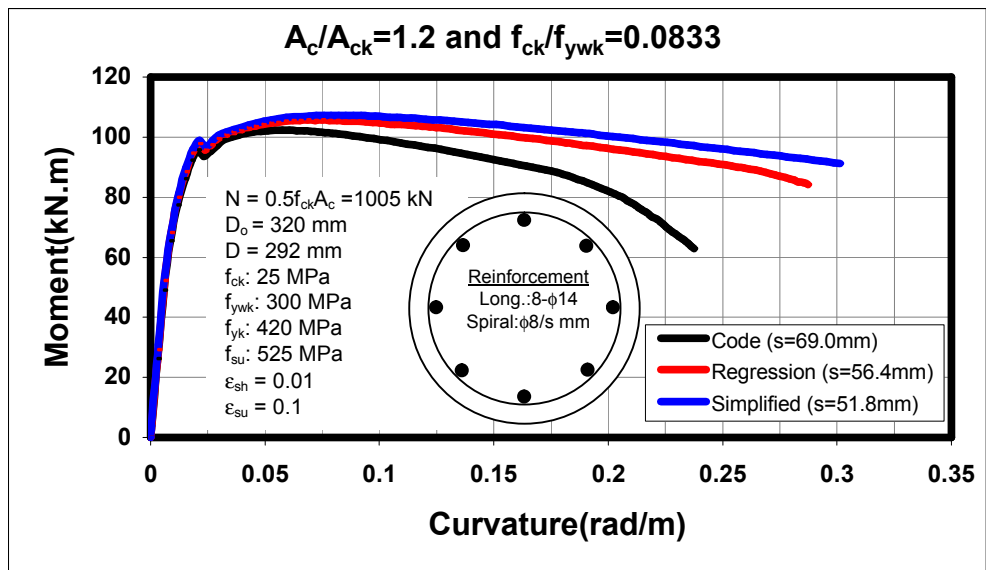


Figure A.5. Comparison of Proposed and Code Equations for Section 5

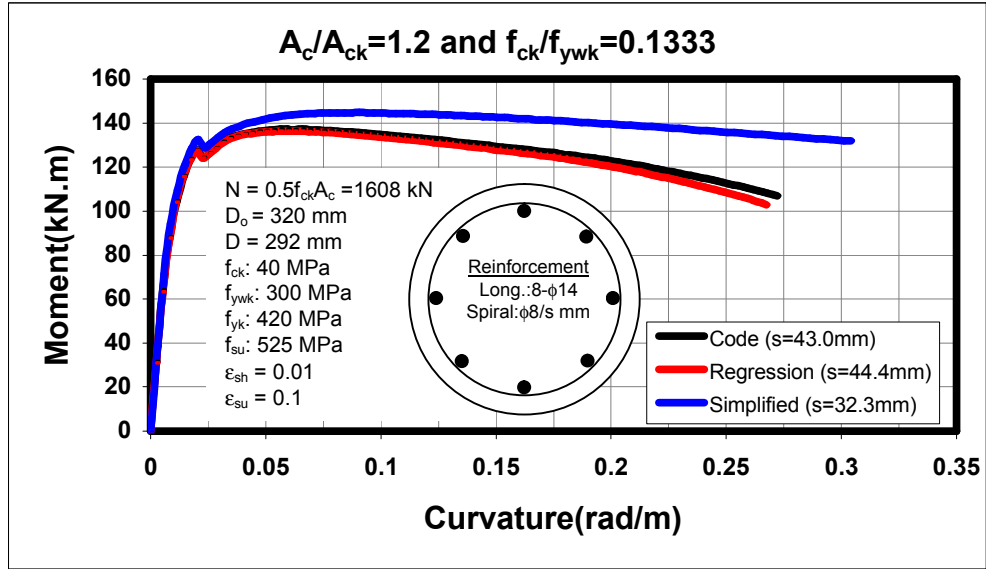


Figure A.6. Comparison of Proposed and Code Equations for Section 6

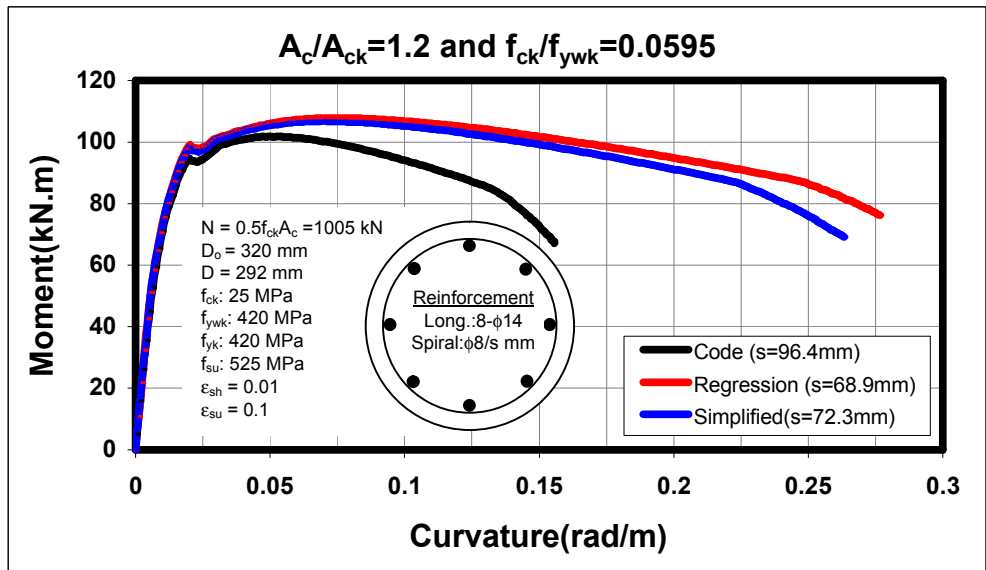


Figure A.7. Comparison of Proposed and Code Equations for Section 7

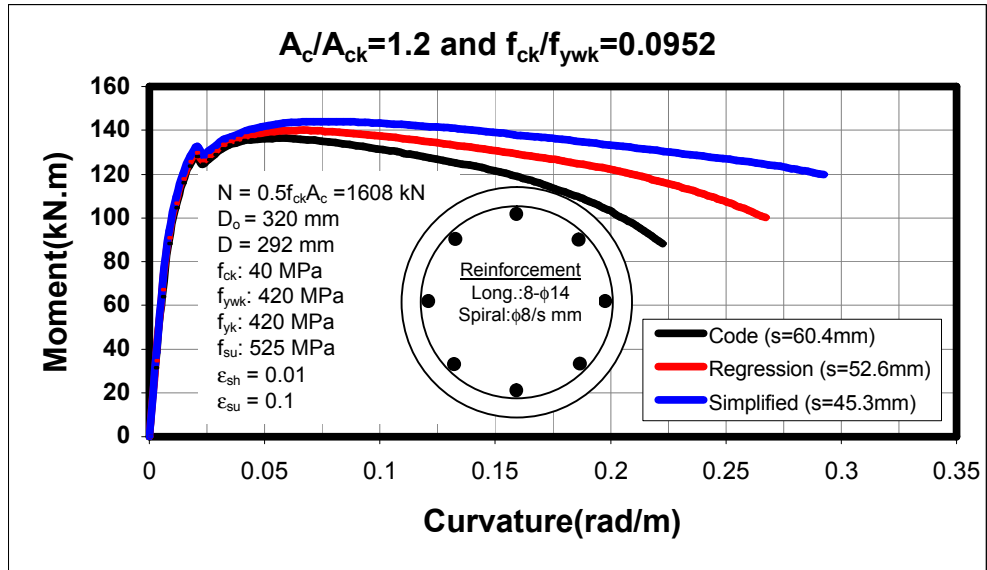


Figure A.8. Comparison of Proposed and Code Equations for Section 8

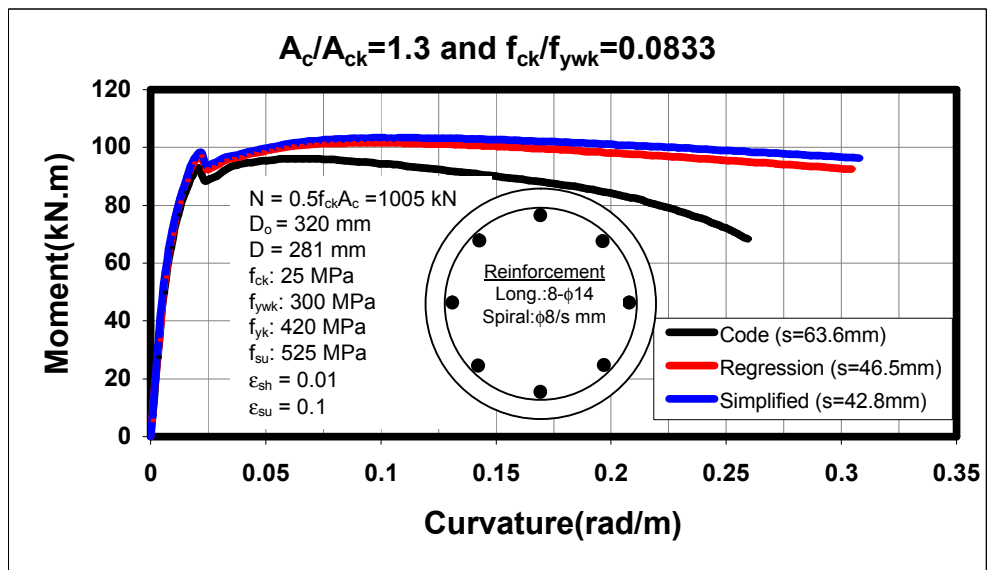


Figure A.9. Comparison of Proposed and Code Equations for Section 9

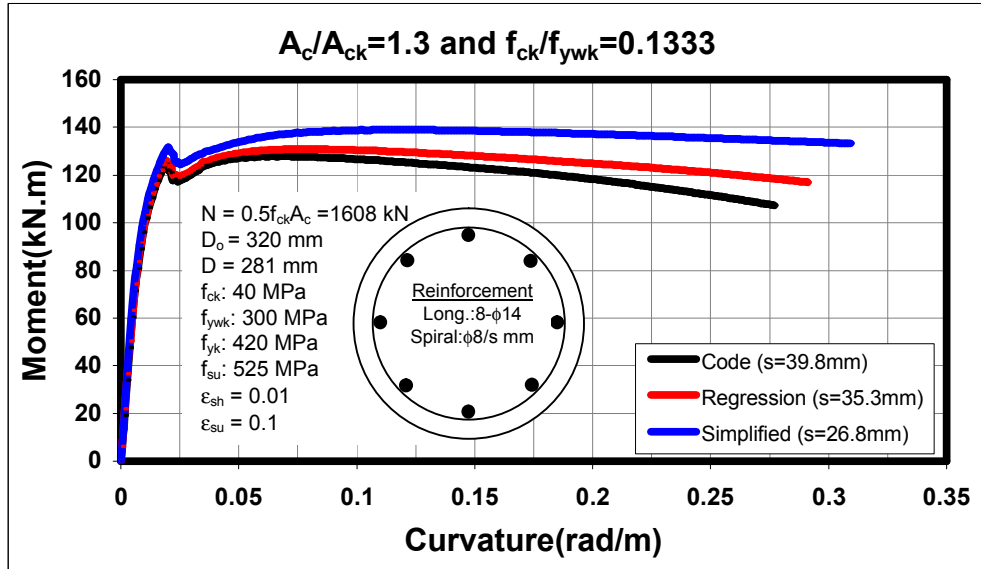


Figure A.10. Comparison of Proposed and Code Equations for Section 10

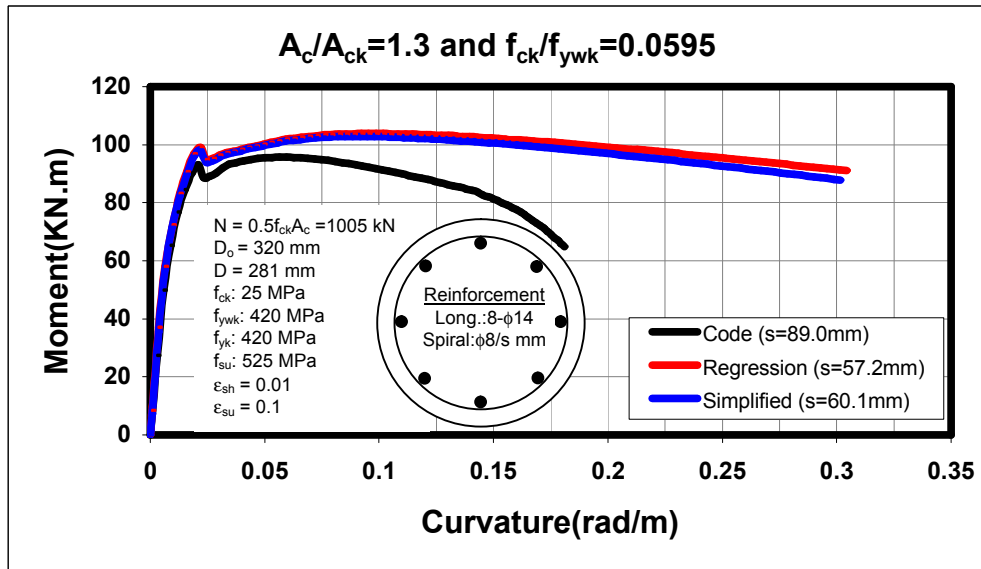


Figure A.11. Comparison of Proposed and Code Equations for Section 11

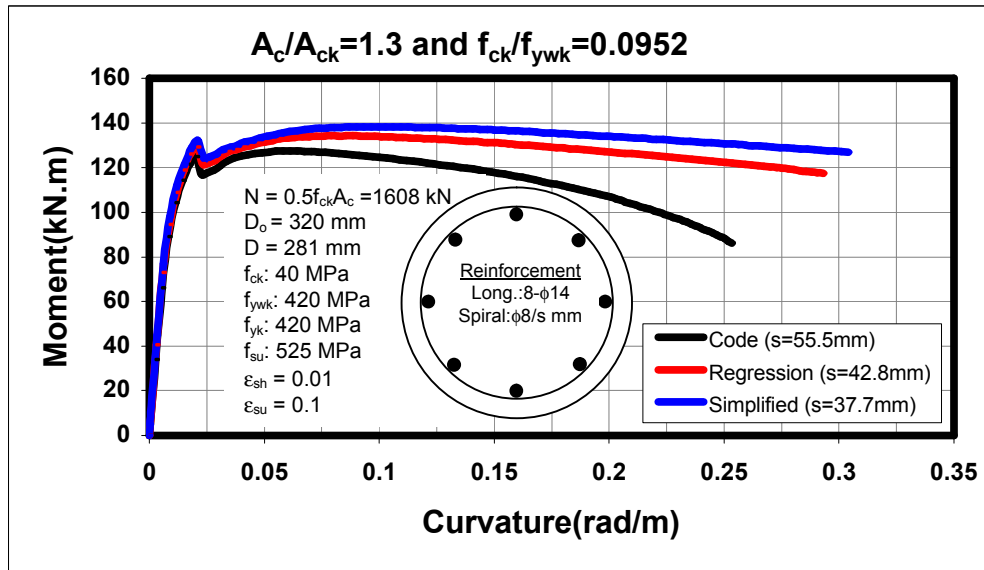


Figure A.12. Comparison of Proposed and Code Equations for Section 12

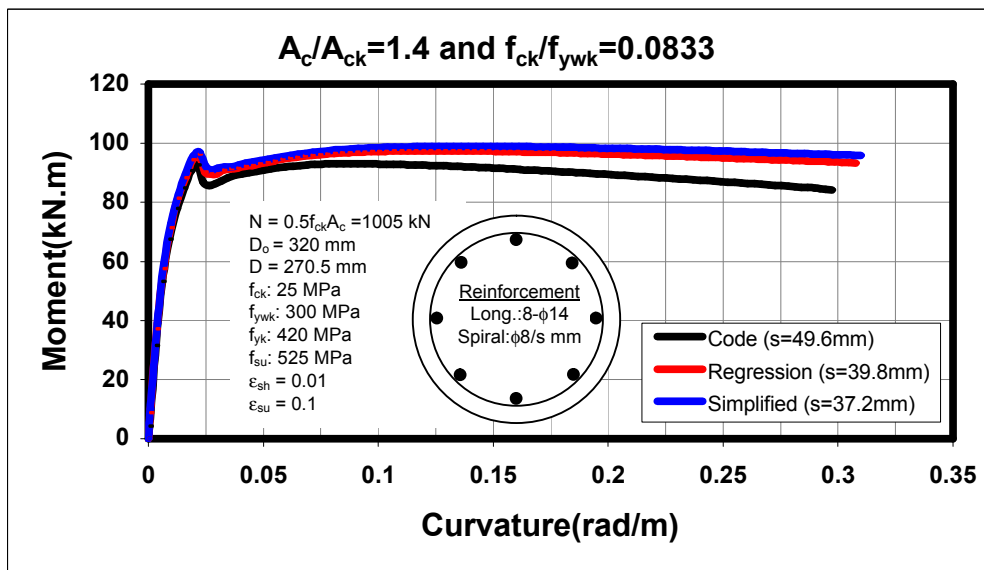


Figure A.13. Comparison of Proposed and Code Equations for Section 13

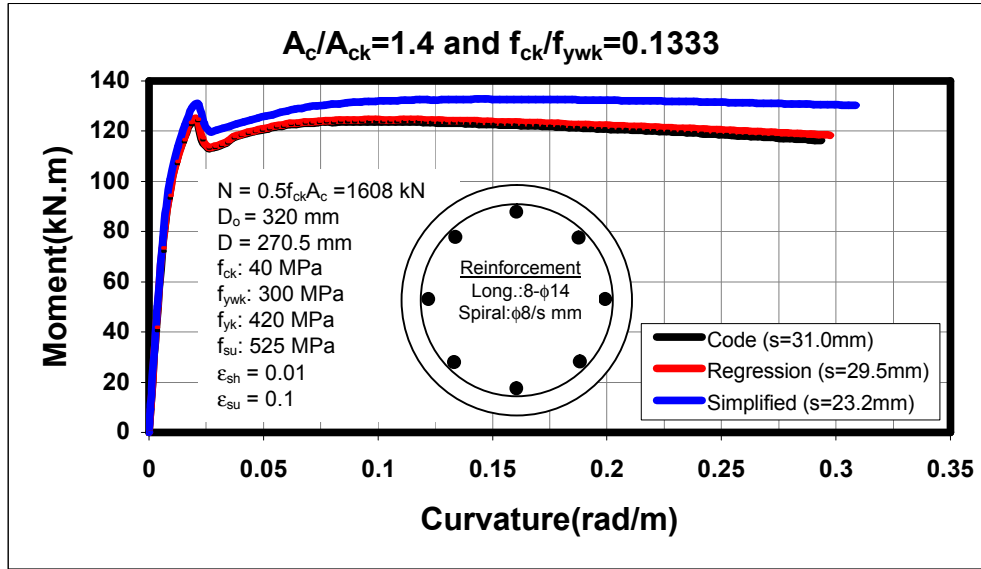


Figure A.14. Comparison of Proposed and Code Equations for Section 14

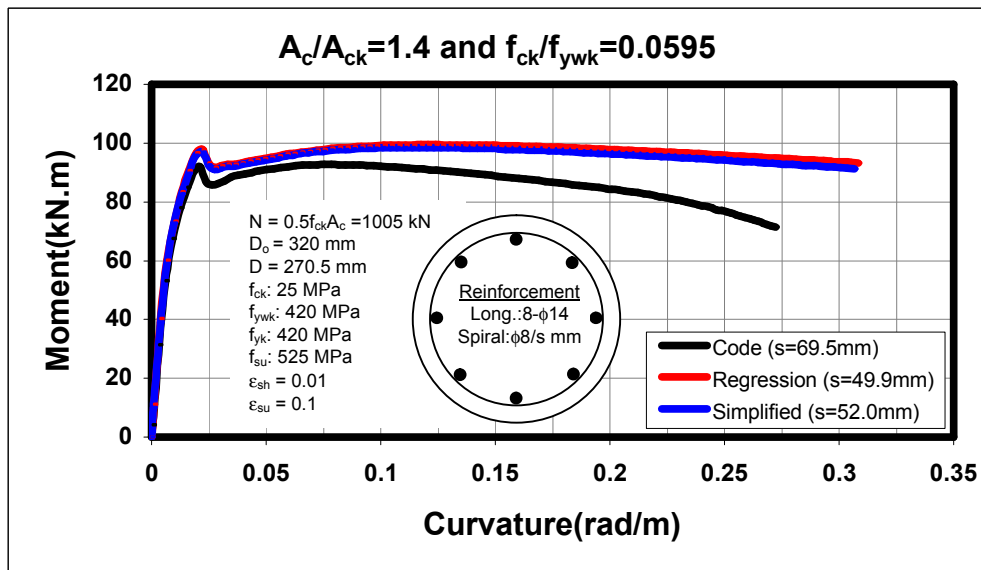


Figure A.15. Comparison of Proposed and Code Equations for Section 15

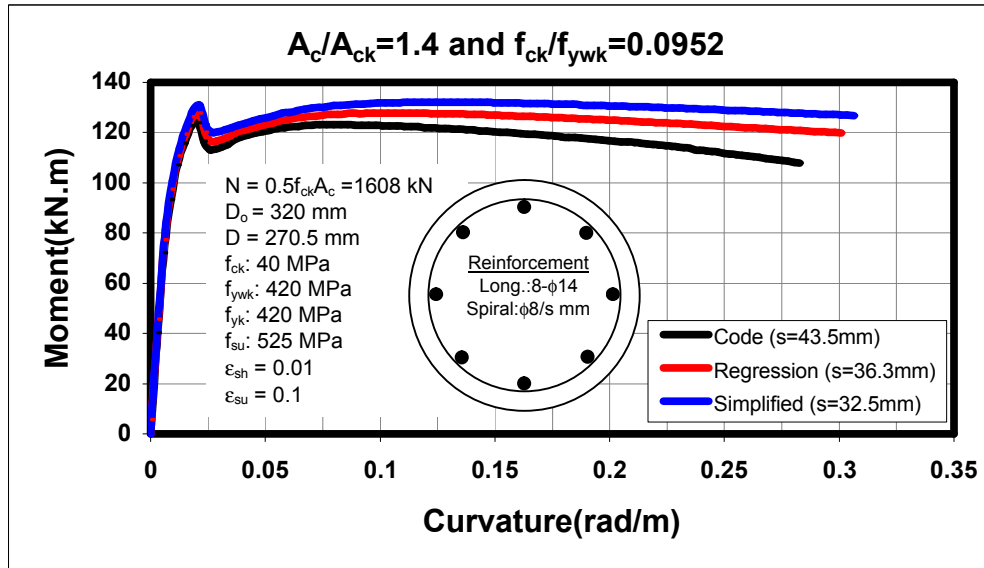


Figure A.16. Comparison of Proposed and Code Equations for Section 16

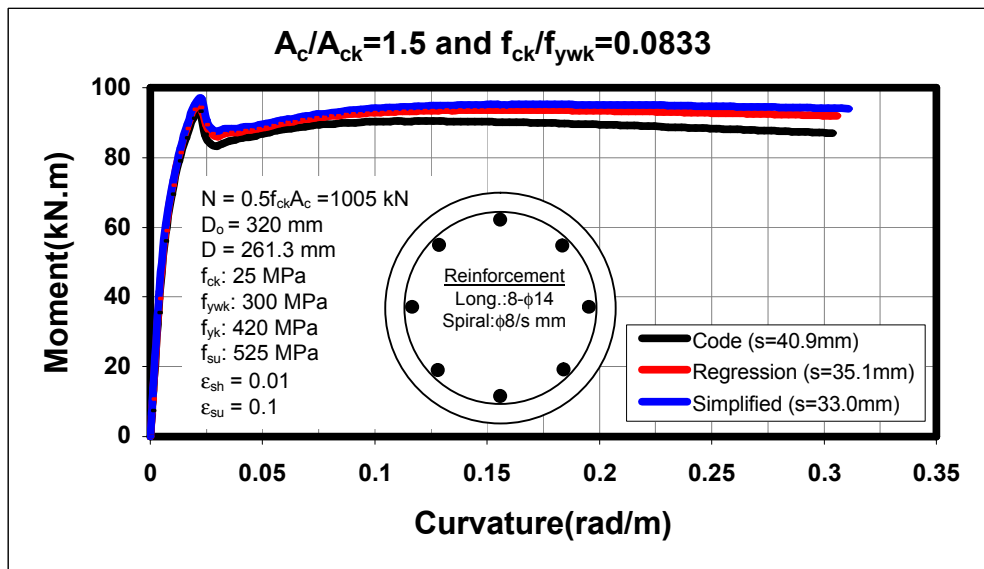


Figure A.17. Comparison of Proposed and Code Equations for Section 17

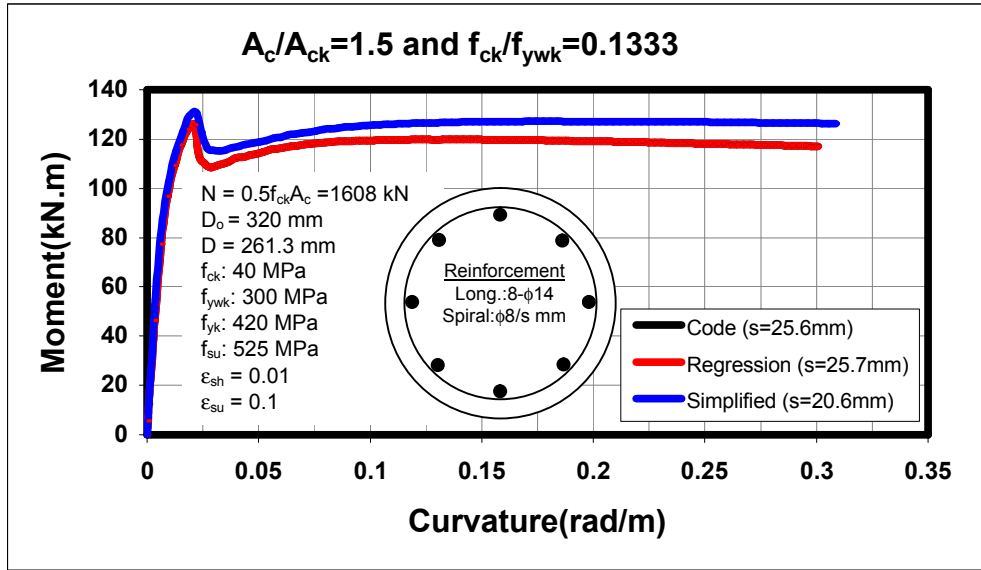


Figure A.18. Comparison of Proposed and Code Equations for Section 18

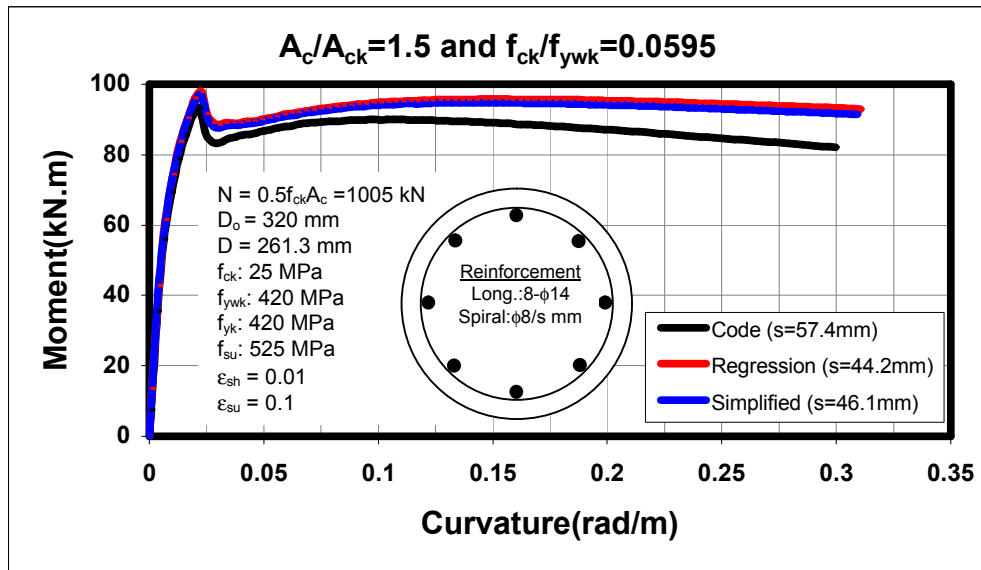


Figure A.19. Comparison of Proposed and Code Equations for Section 19

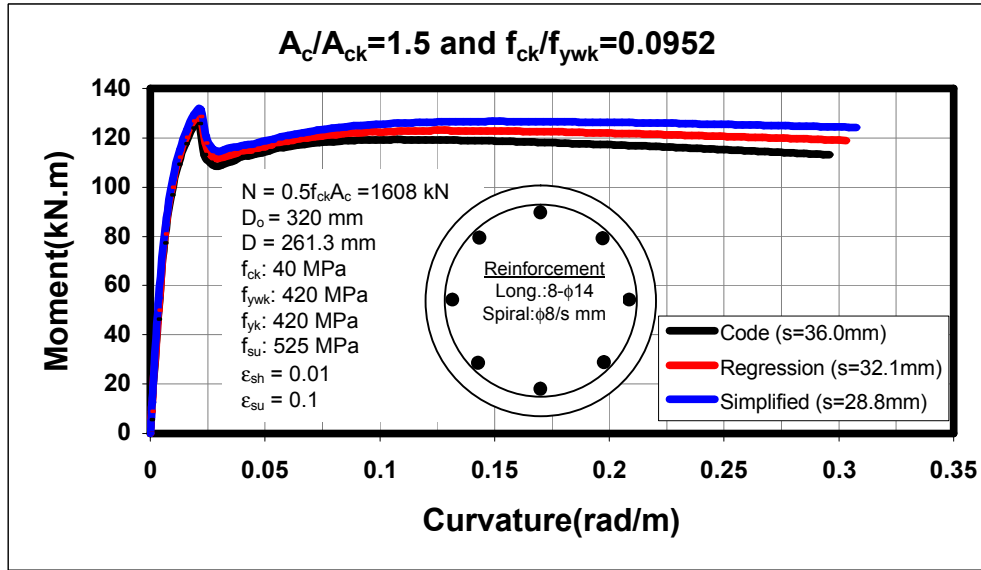


Figure A.20. Comparison of Proposed and Code Equations for Section 20

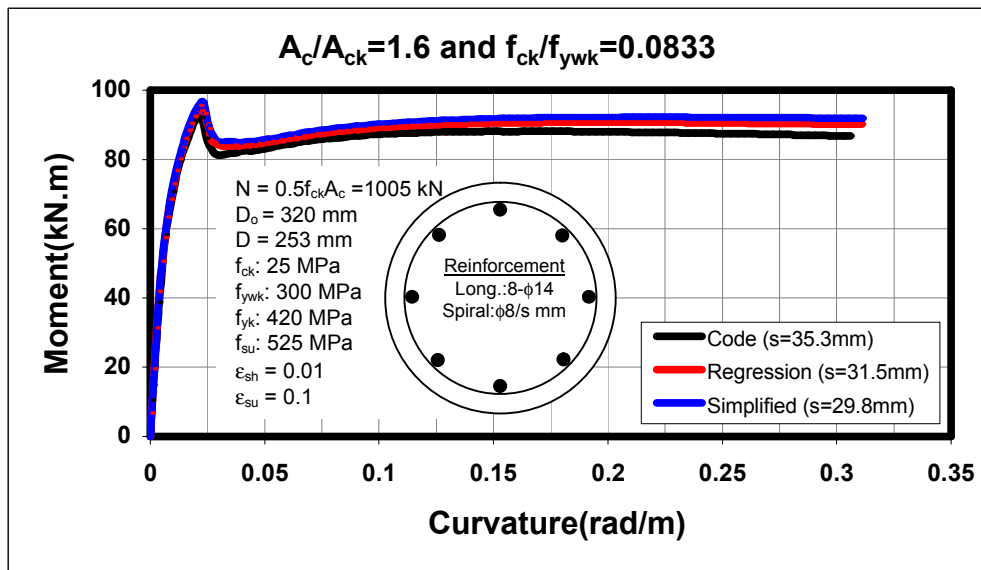


Figure A.21. Comparison of Proposed and Code Equations for Section 21

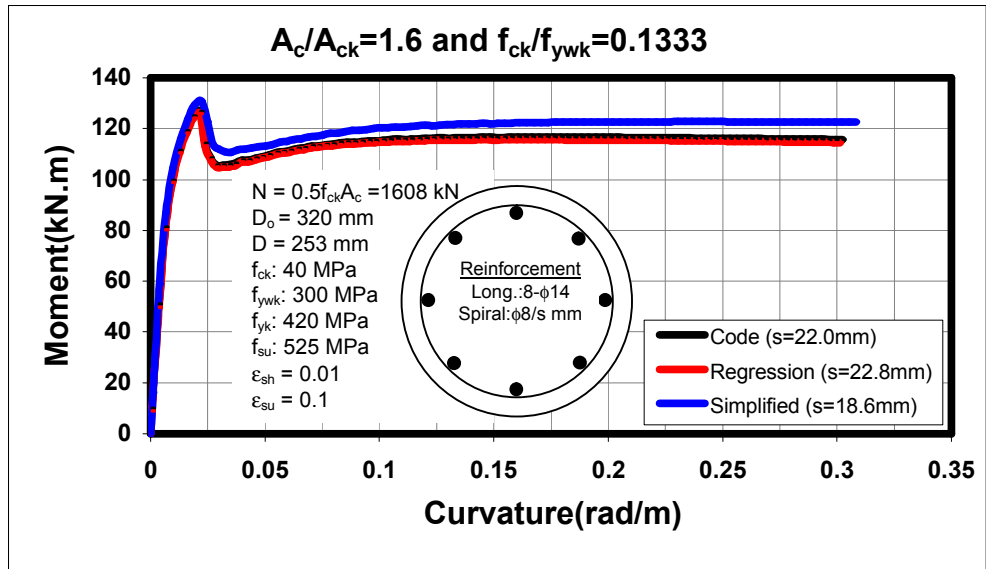


Figure A.22. Comparison of Proposed and Code Equations for Section 22

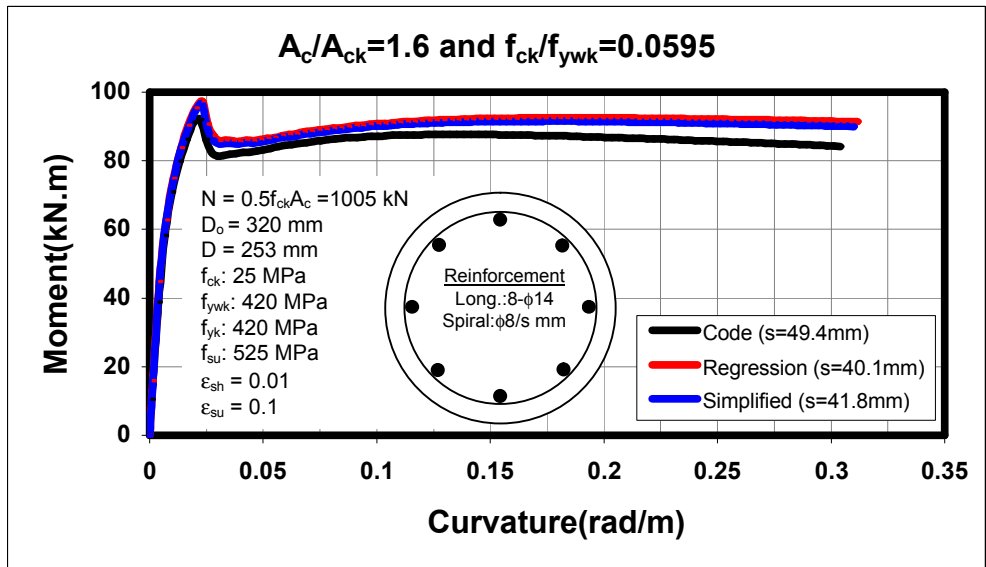


Figure A.23. Comparison of Proposed and Code Equations for Section 23

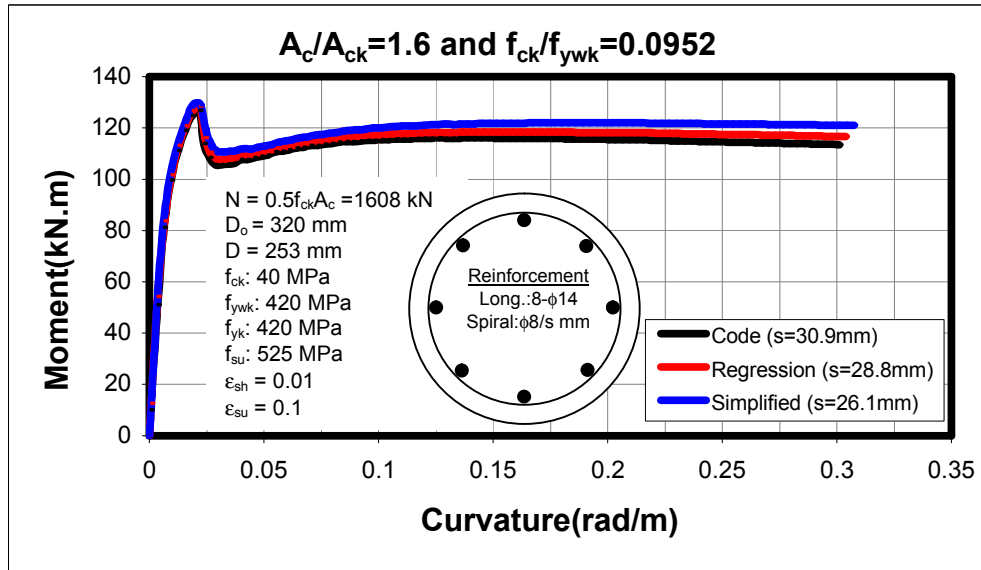


Figure A.24. Comparison of Proposed and Code Equations for Section 24

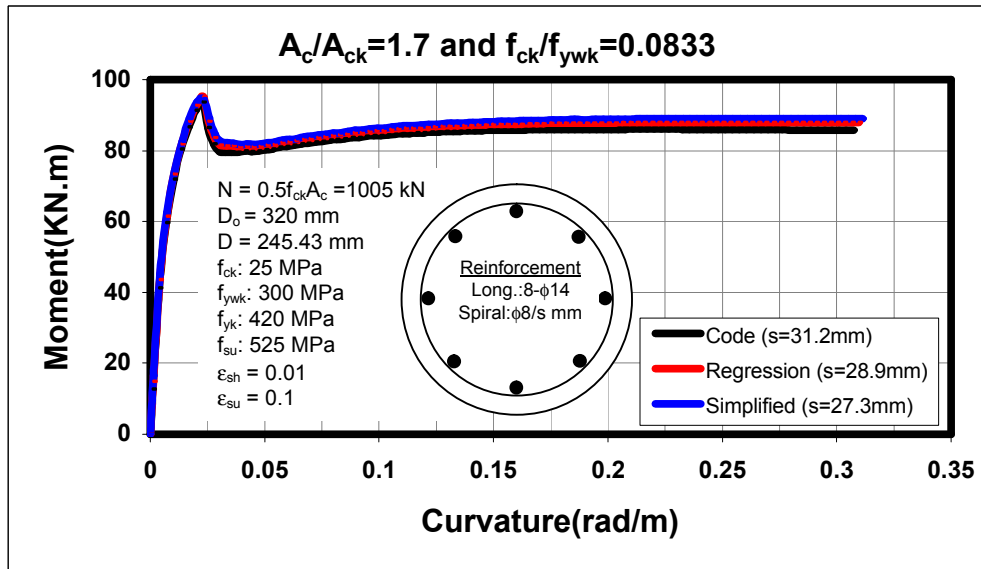


Figure A.25. Comparison of Proposed and Code Equations for Section 25

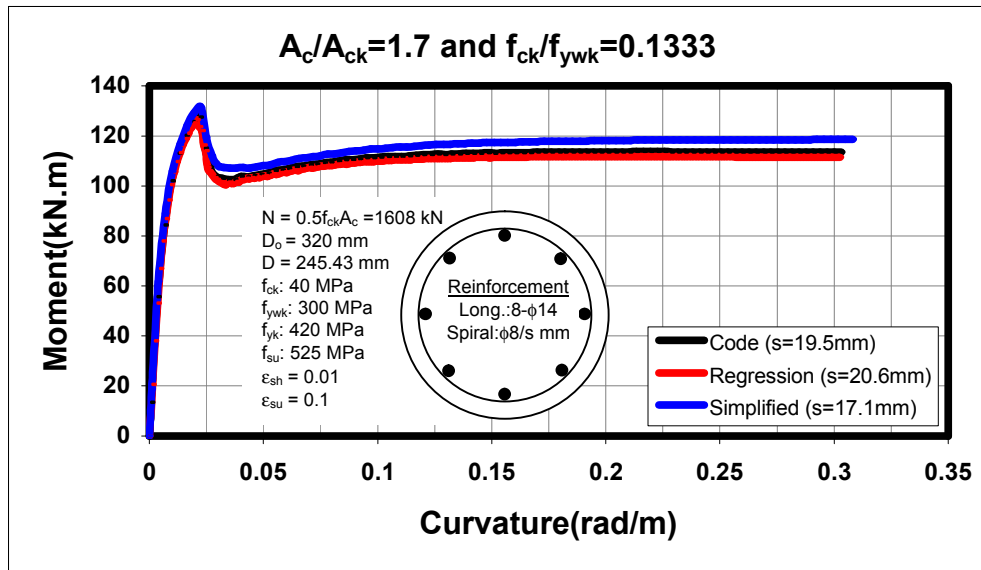


Figure A.26. Comparison of Proposed and Code Equations for Section 26

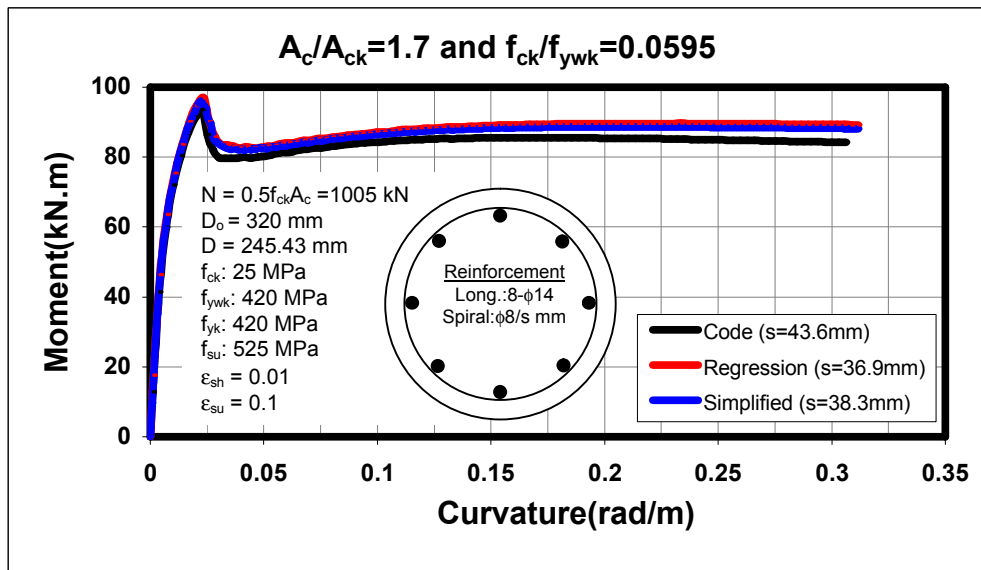


Figure A.27. Comparison of Proposed and Code Equations for Section 27

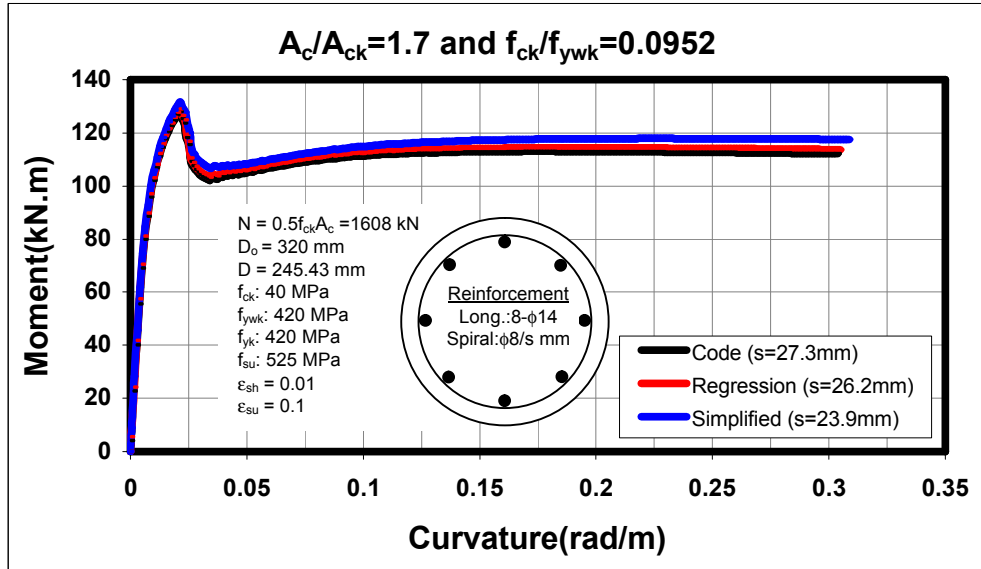


Figure A.28. Comparison of Proposed and Code Equations for Section 28

APPENDIX B

MOMENT-CURVATURE COMPARISONS

(Effect of Longitudinal Steel Percentage and Axial Load Level)

In Appendix B, Moment-Curvature curves are presented in order to investigate the effect of longitudinal steel percentage and axial load level on section behaviour. It is of paramount importance to find out whether Eq. (4.20) and Eq. (4.21) yield consistent results as longitudinal steel percentage and axial load level is changed. Also, effect of longitudinal steel percentage on section ductility is investigated. Detailed information can be found in Section 5.2. Detailed information about sections can be found in Table 4.1, Table 4.2 and Table 5.6.

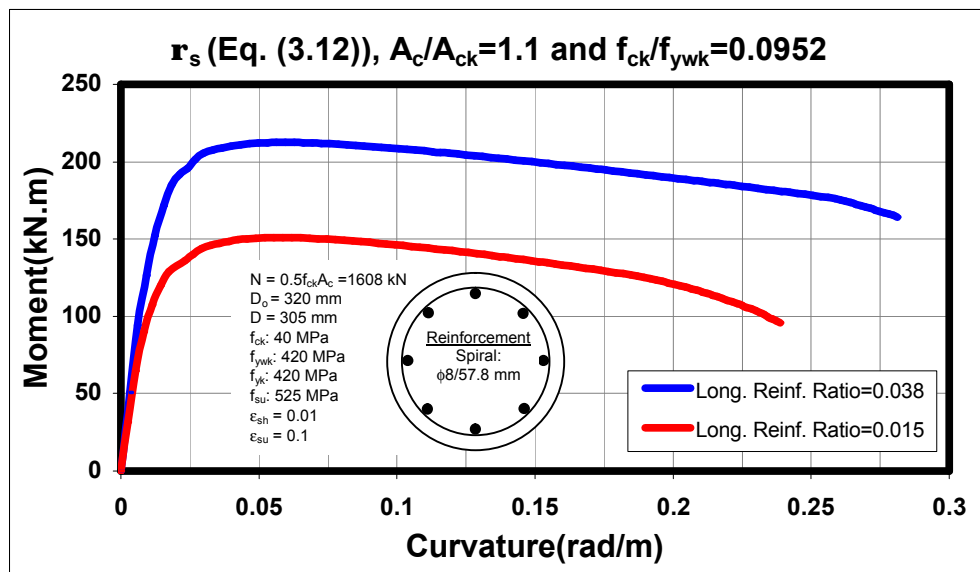


Figure B.1. Effect of Longitudinal Steel Percentage on Ductility [Section 4]

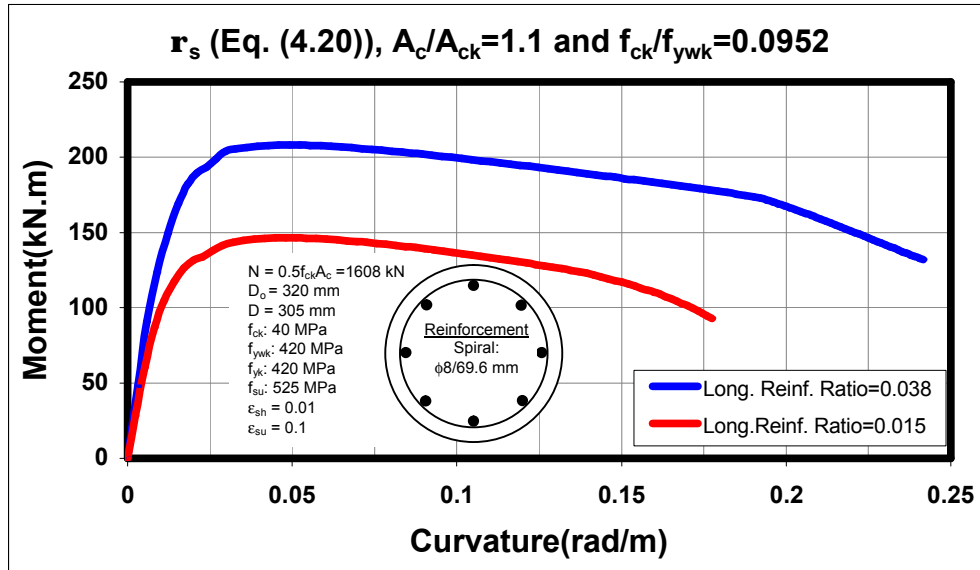


Figure B.2. Effect of Longitudinal Steel Percentage on Ductility [Section 4]

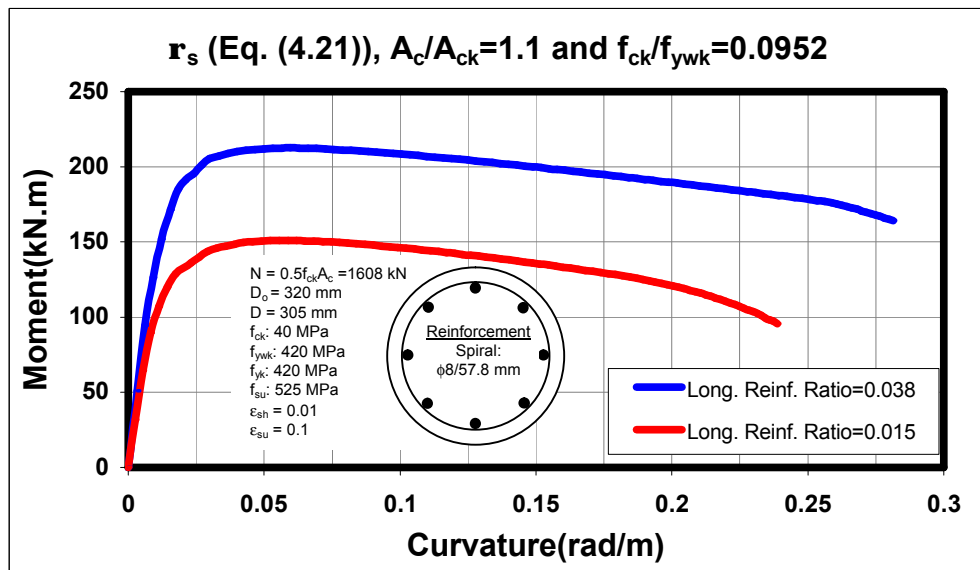


Figure B.3. Effect of Longitudinal Steel Percentage on Ductility [Section 4]

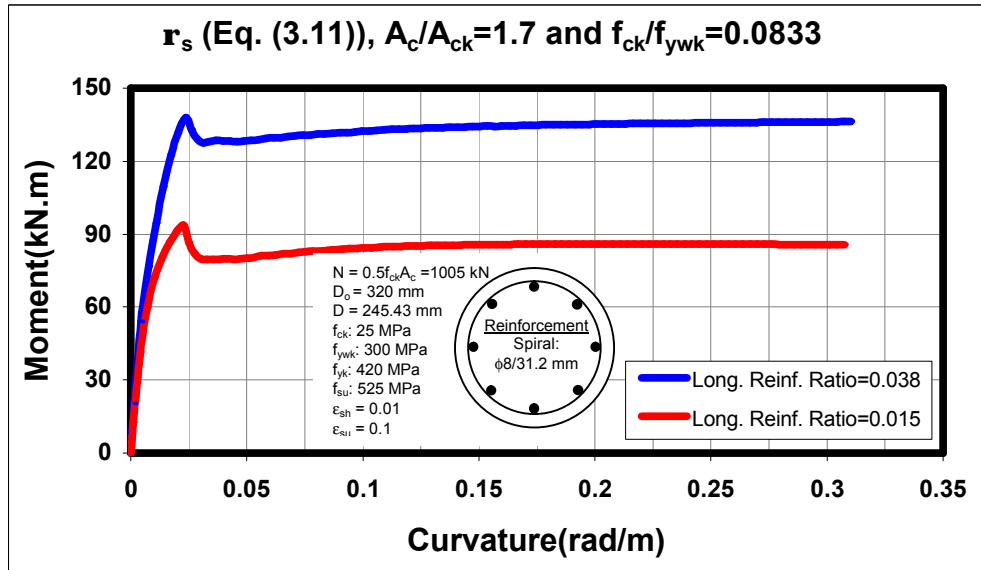


Figure B.4. Effect of Longitudinal Steel Percentage on Ductility [Section 25]

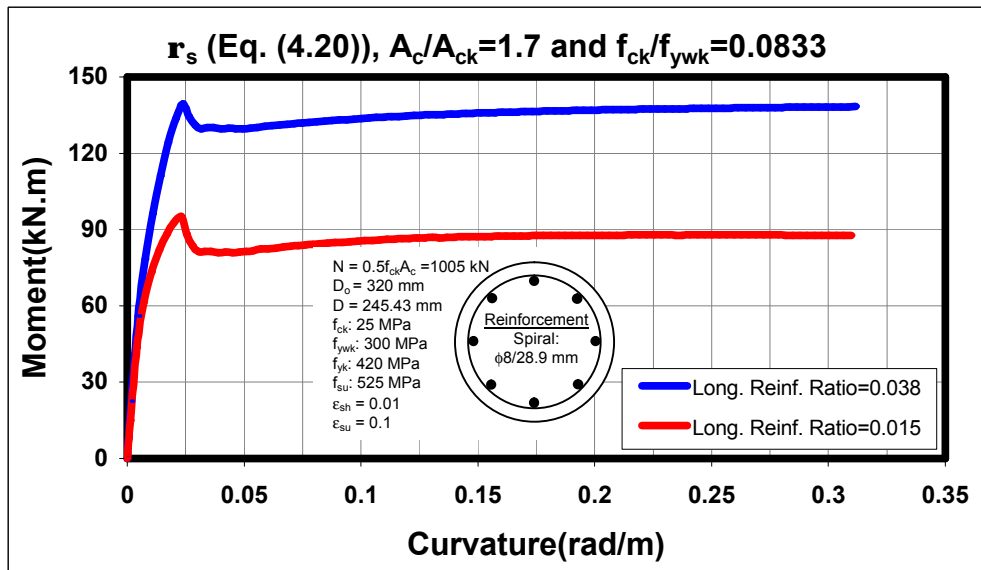


Figure B.5. Effect of Longitudinal Steel Percentage on Ductility [Section 25]

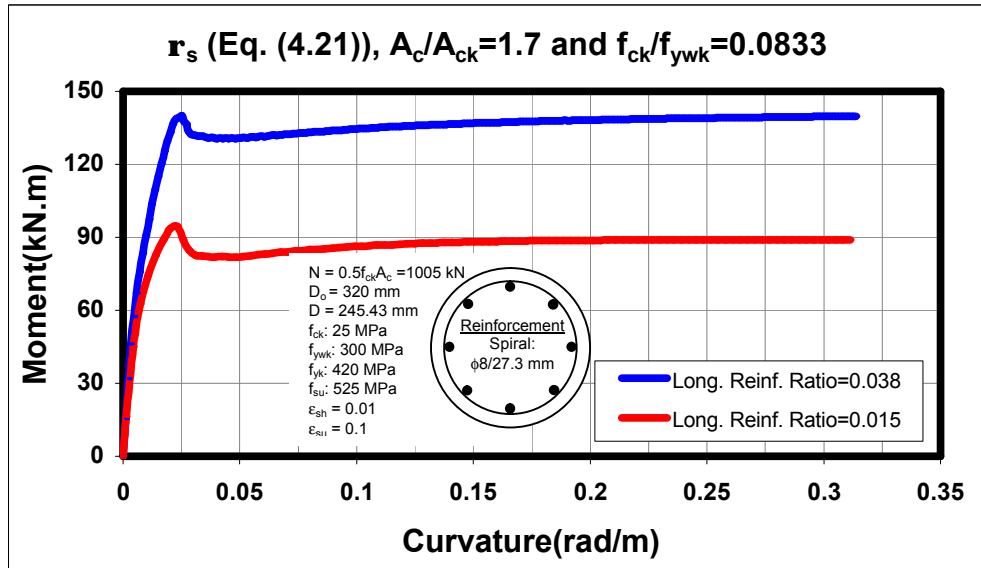


Figure B.6. Effect of Longitudinal Steel Percentage on Ductility [Section 25]

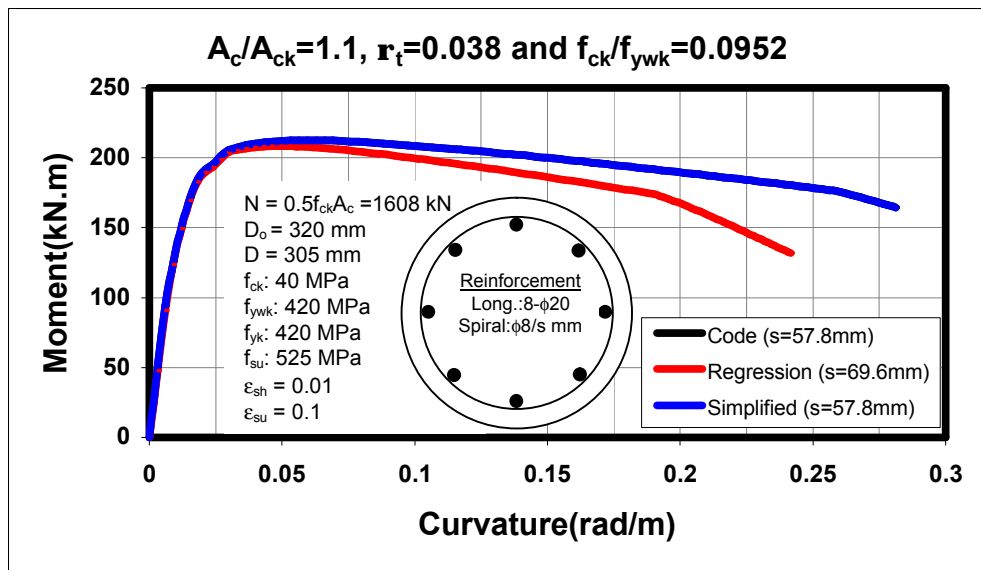


Figure B.7. Comparison of Proposed and Code Equations for Section 4

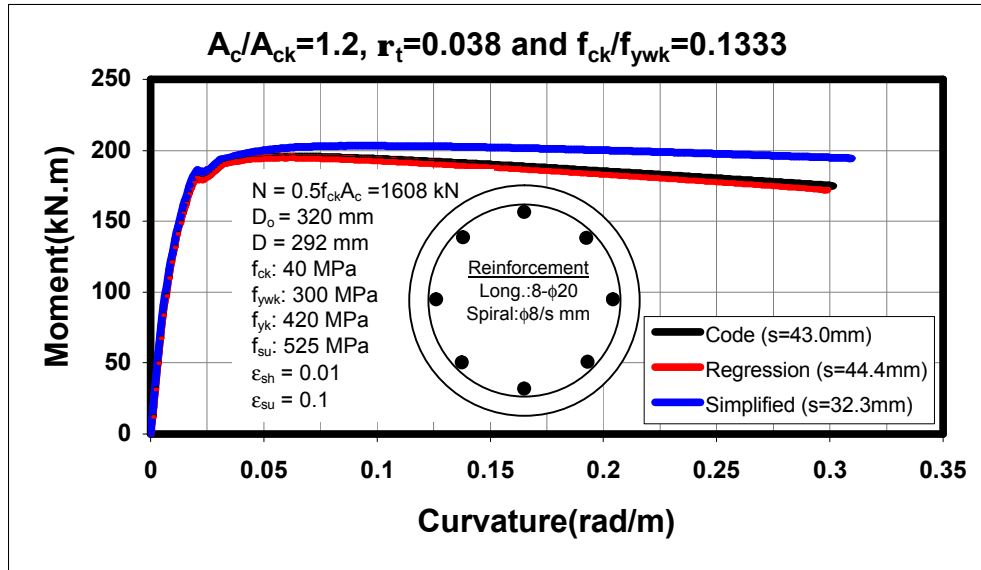


Figure B.8. Comparison of Proposed and Code Equations for Section 6

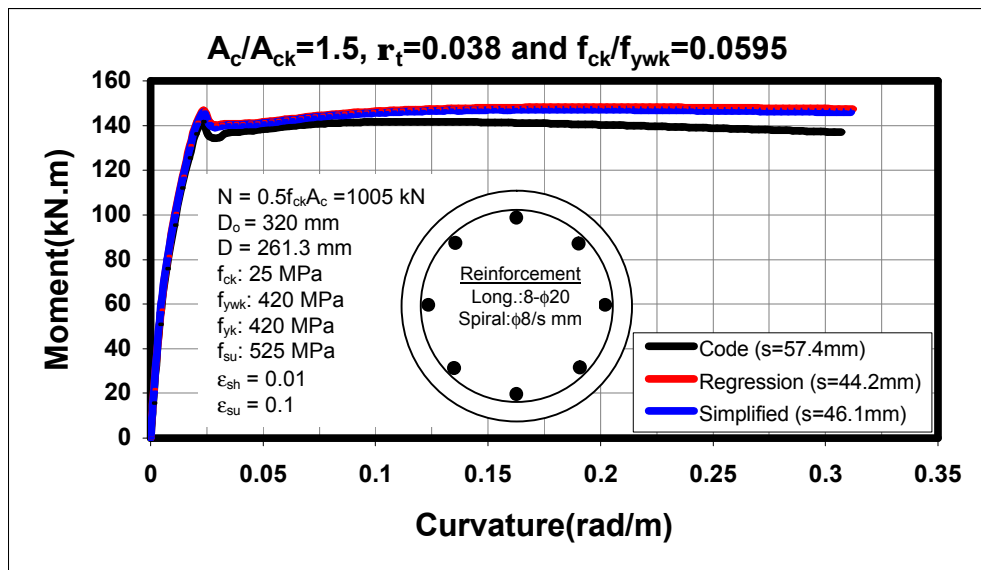


Figure B.9. Comparison of Proposed and Code Equations for Section 19

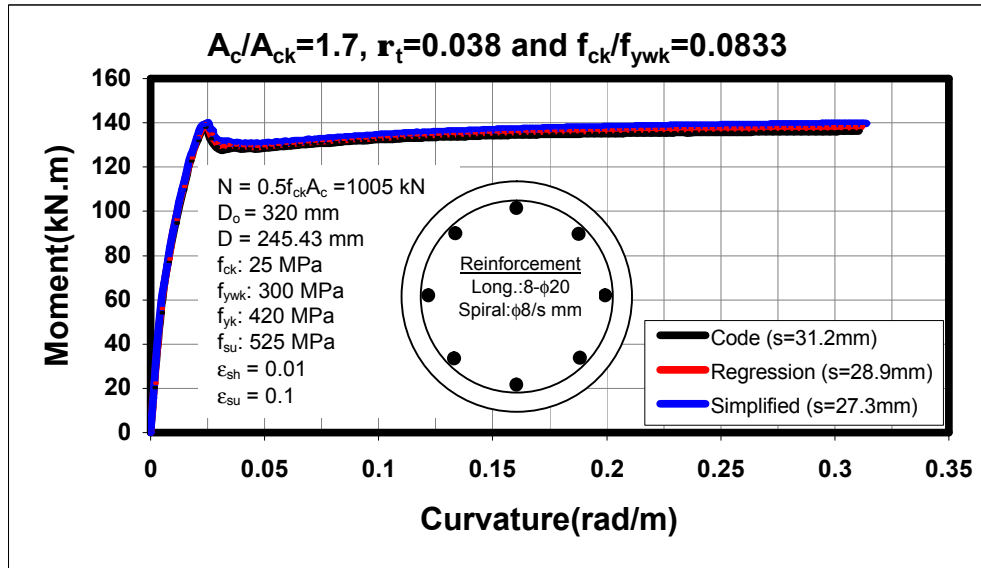


Figure B.10. Comparison of Proposed and Code Equations for Section 25

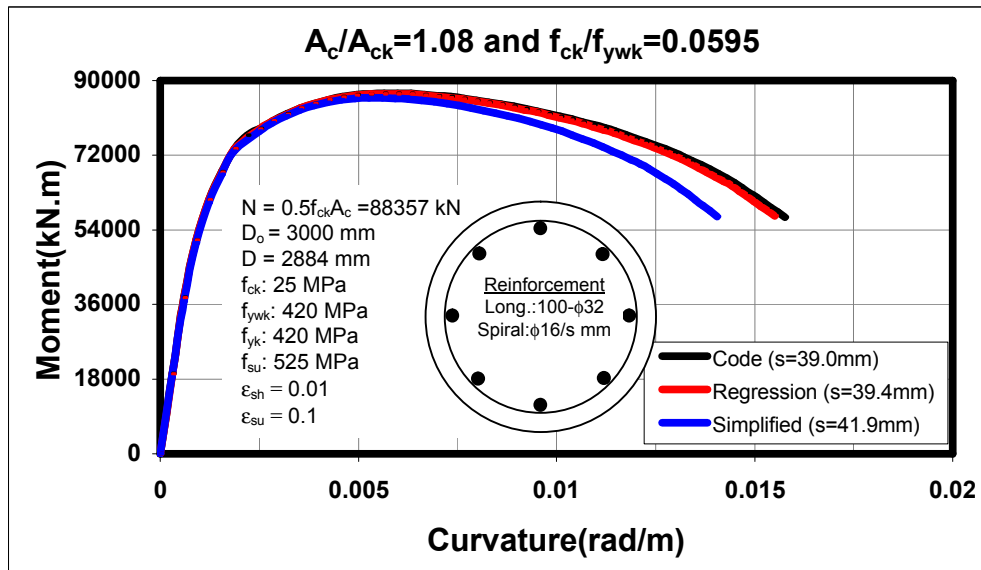


Figure B.11. Comparison of Proposed and Code Equations for Section 57

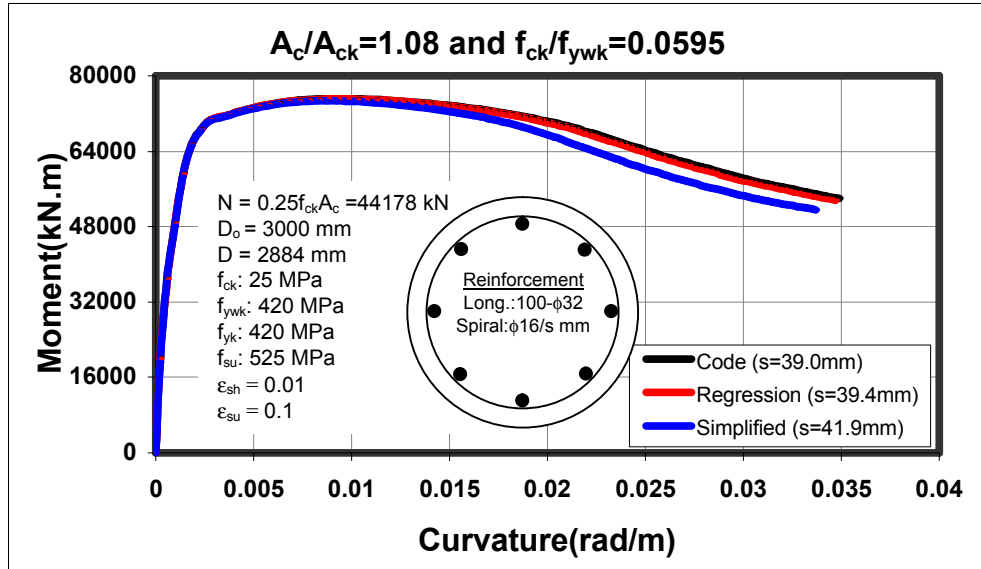


Figure B.12. Effect of Axial Load on Ductility [Section 57]

APPENDIX C

MOMENT-CURVATURE COMPARISONS

(Effect of Number and Orientation of Longitudinal Bars)

In Appendix C, effect of number and orientation of longitudinal bars on section behaviour is presented. Section analyses were carried out with longitudinal steel orientations of 6Φ16, 8Φ14 and 12Φ11.5. Two analysis styles were carried out for 6 bars case. Details can be found in Section 5.3. Details about section properties can be found in Table 4.1 and Table 5.1. In case of six longitudinal bars, axis A or B appearing on titles of some Moment-Curvature curves means that section is bent about axis A or B respectively. If there is no additional information with 6Φ16, it means that section is bent about axis A.

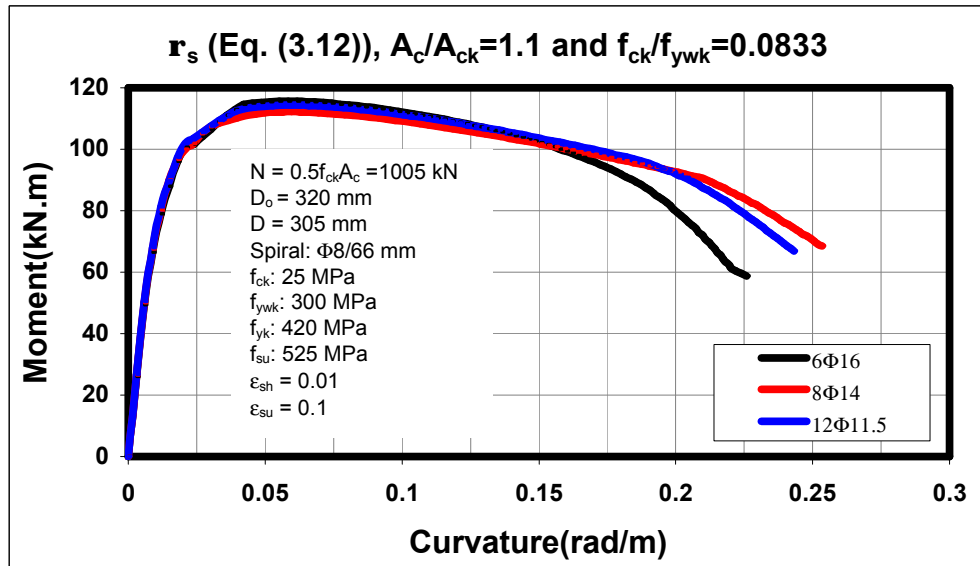


Figure C.1. Comparison of Different Number and Orientation of Longitudinal Bars for Section 1

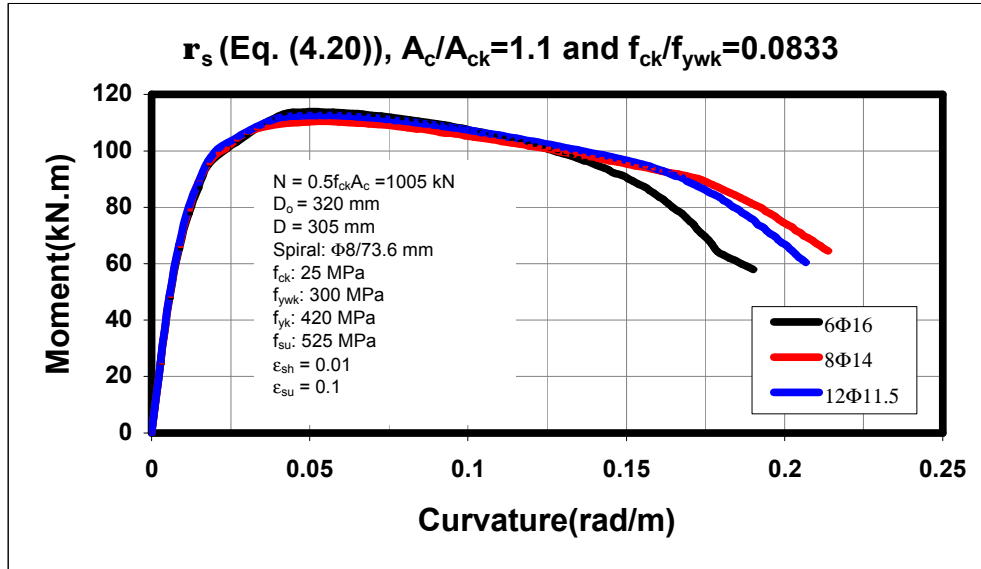


Figure C.2. Comparison of Different Number and Orientation of Longitudinal Bars for Section 1

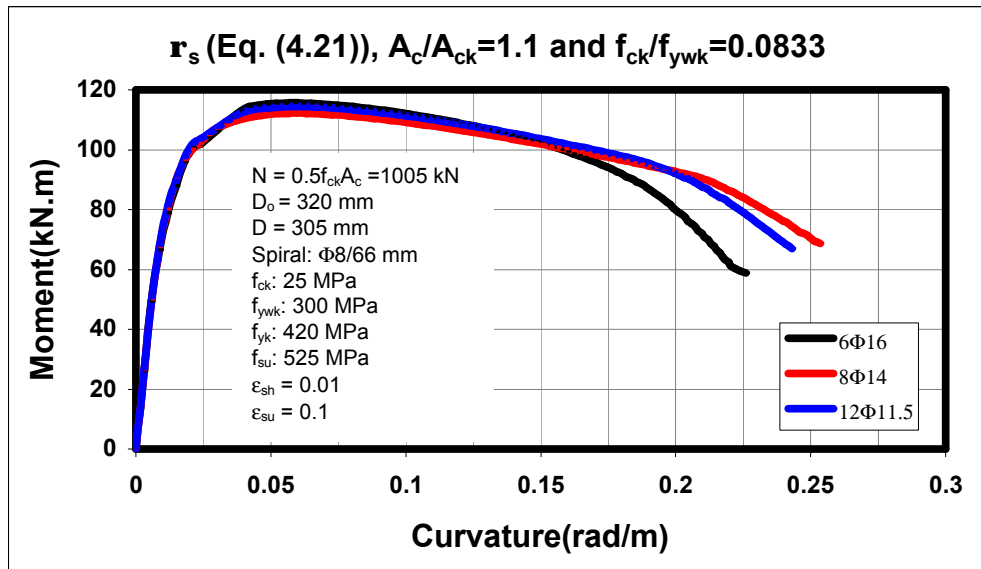


Figure C.3. Comparison of Different Number and Orientation of Longitudinal Bars for Section 1

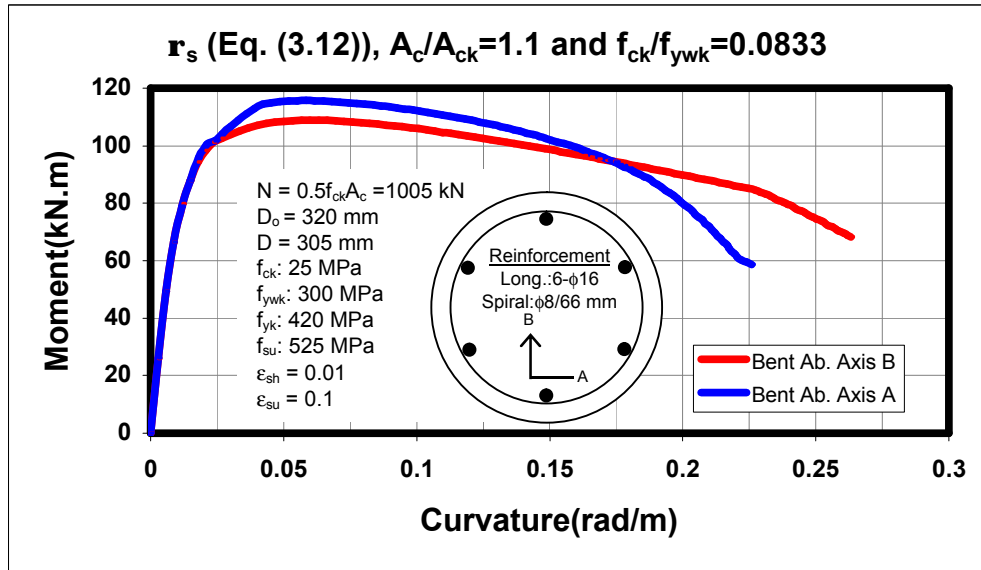


Figure C.4. Comparison of Different Number and Orientation of Longitudinal Bars for Section 1

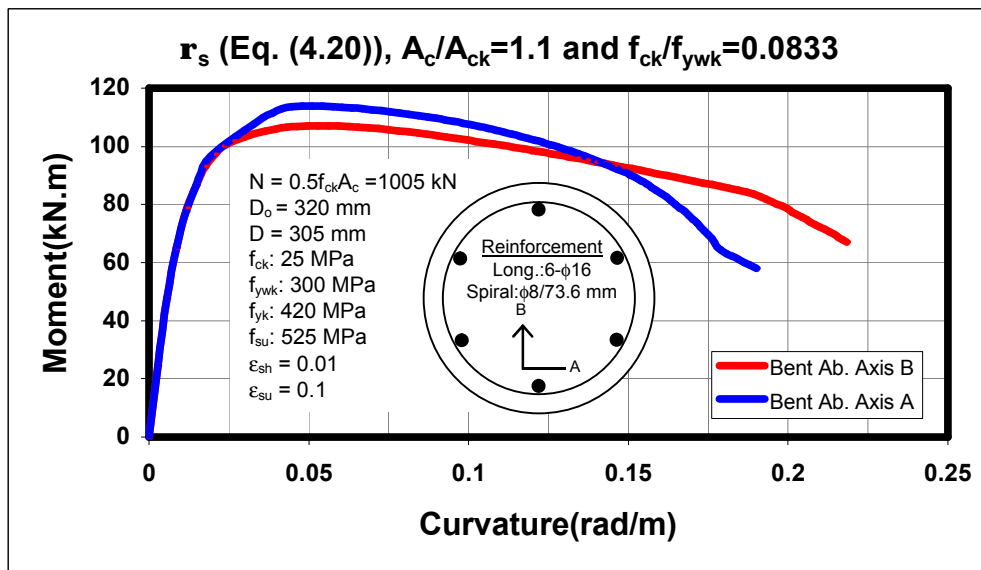


Figure C.5. Comparison of Different Number and Orientation of Longitudinal Bars for Section 1

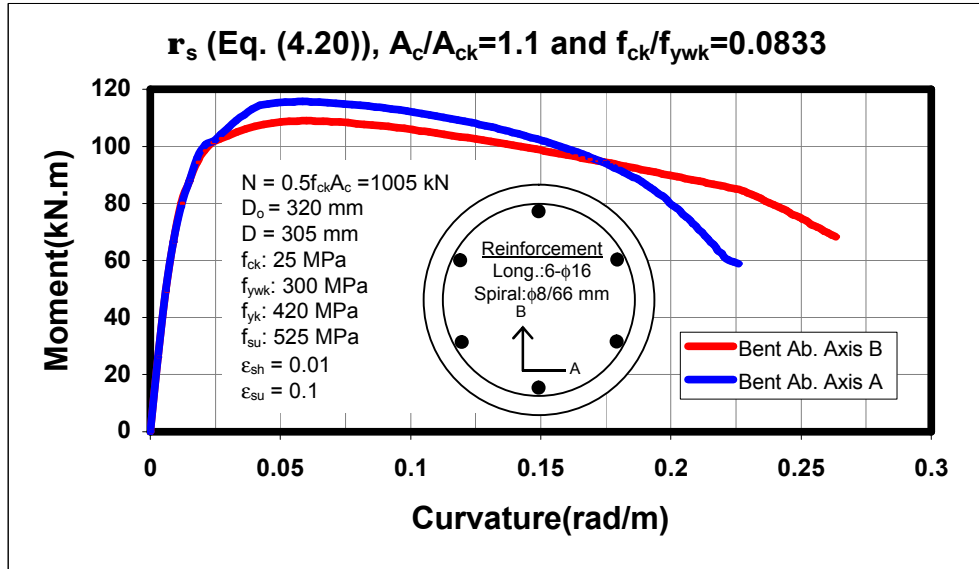


Figure C.6. Comparison of Different Number and Orientation of Longitudinal Bars for Section 1

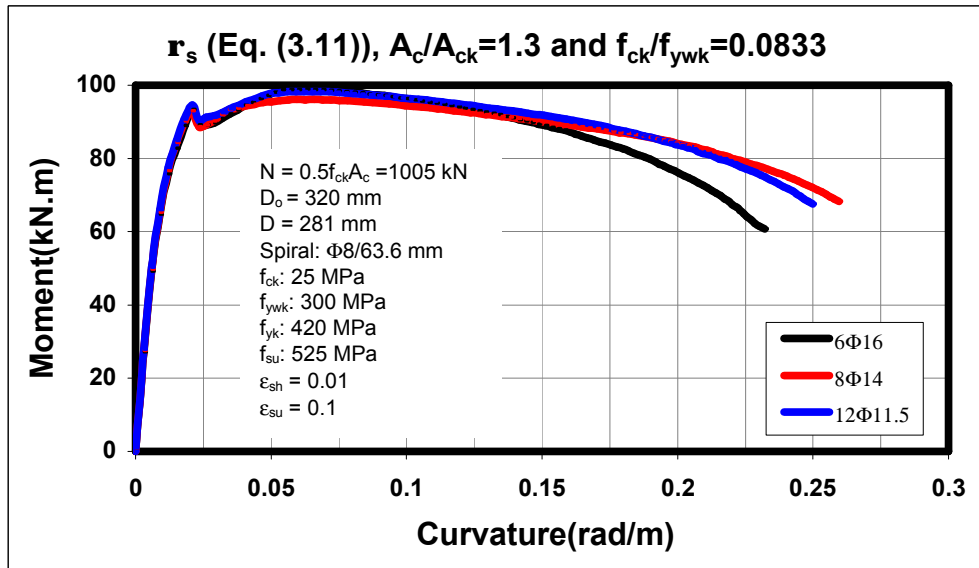


Figure C.7. Comparison of Different Number and Orientation of Longitudinal Bars for Section 9

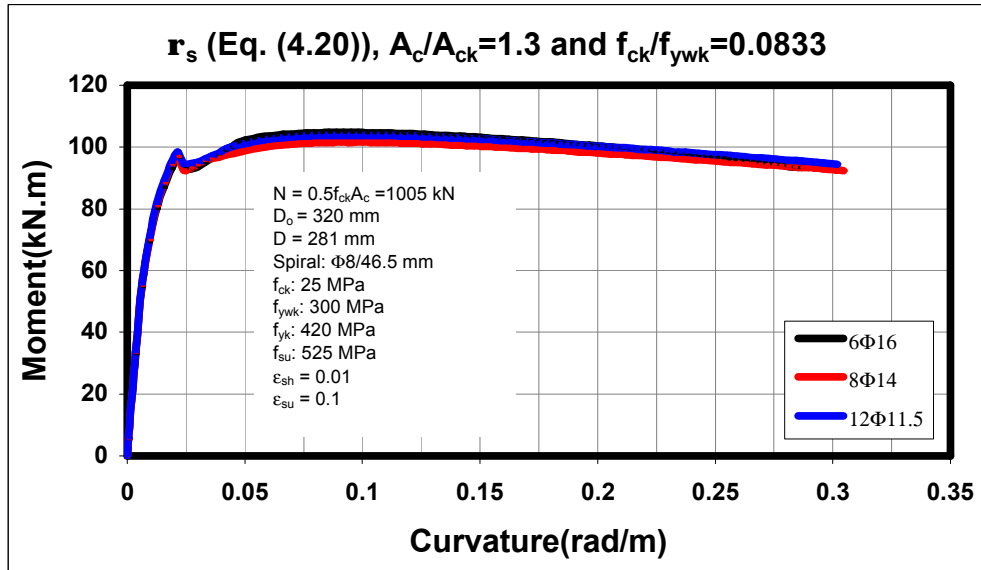


Figure C.8. Comparison of Different Number and Orientation of Longitudinal Bars for Section 9

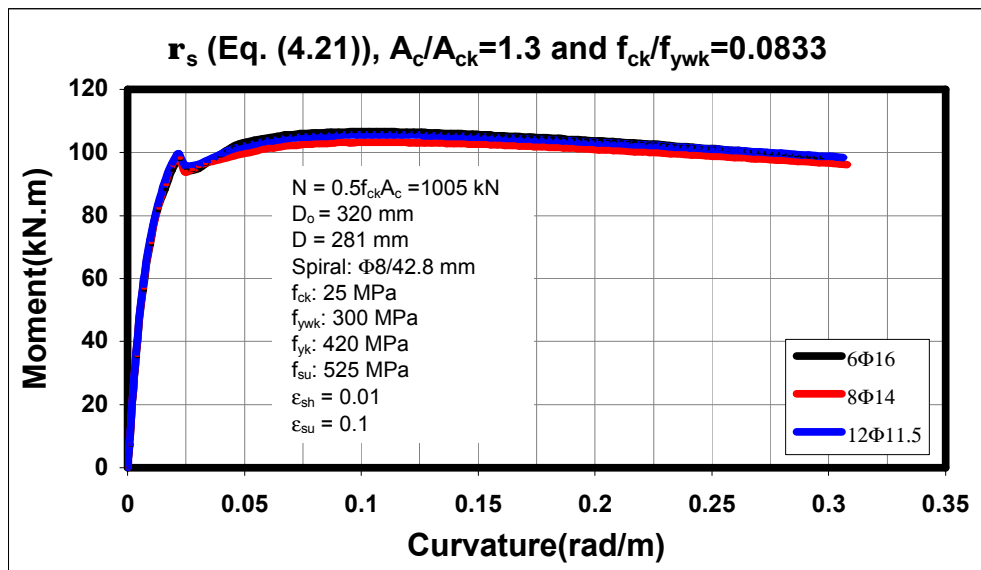


Figure C.9. Comparison of Different Number and Orientation of Longitudinal Bars for Section 9

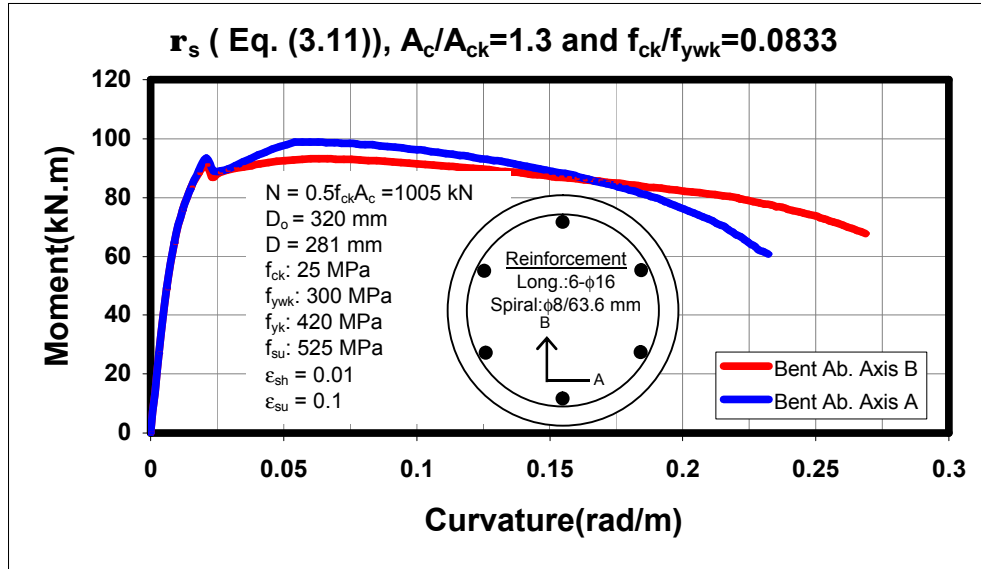


Figure C.10. Comparison of Different Number and Orientation of Longitudinal Bars for Section 9

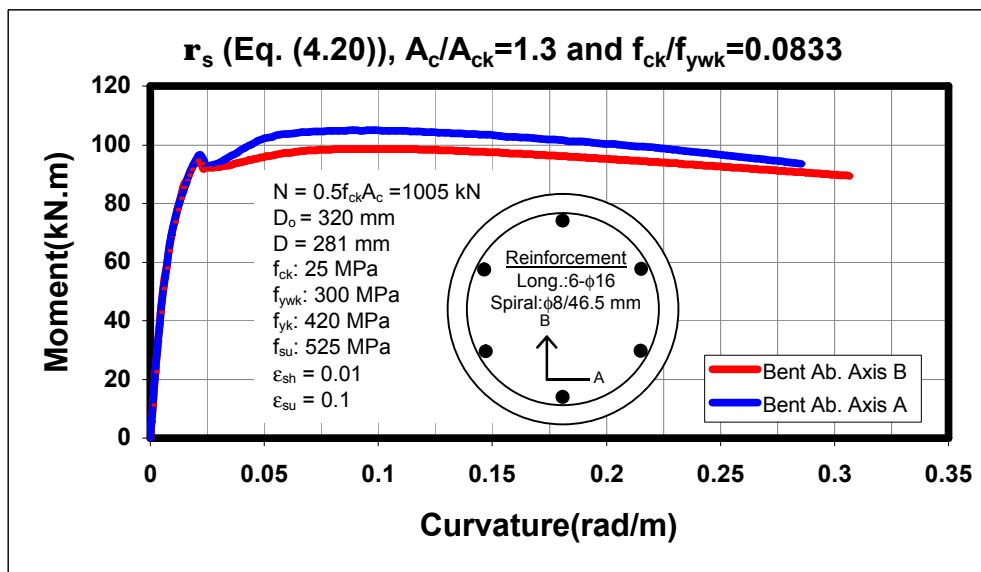


Figure C.11. Comparison of Different Number and Orientation of Longitudinal Bars for Section 9

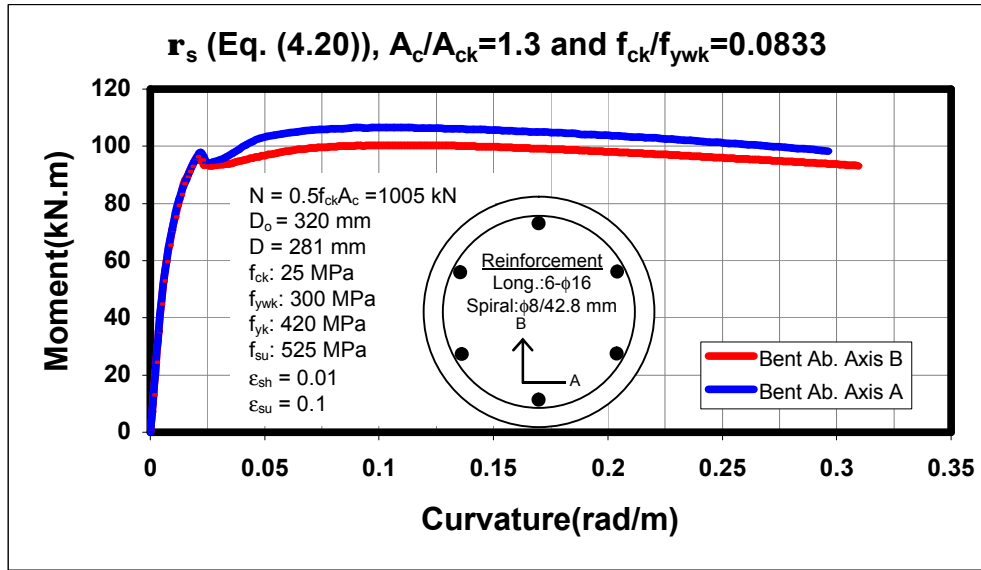


Figure C.12. Comparison of Different Number and Orientation of Longitudinal Bars for Section 9

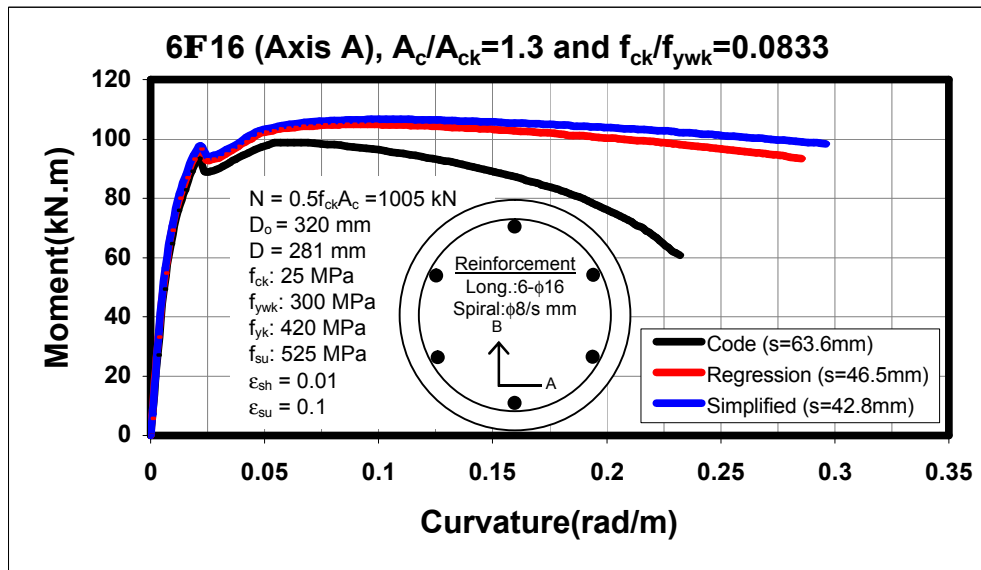


Figure C.13. Comparison of Different Number and Orientation of Longitudinal Bars for Section 9

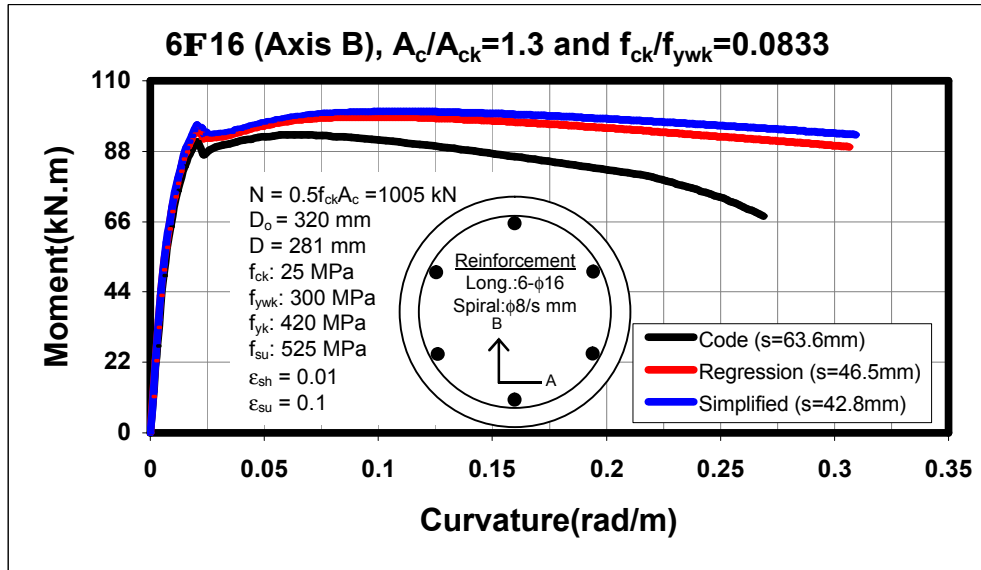


Figure C.14. Comparison of Different Number and Orientation of Longitudinal Bars for Section 9

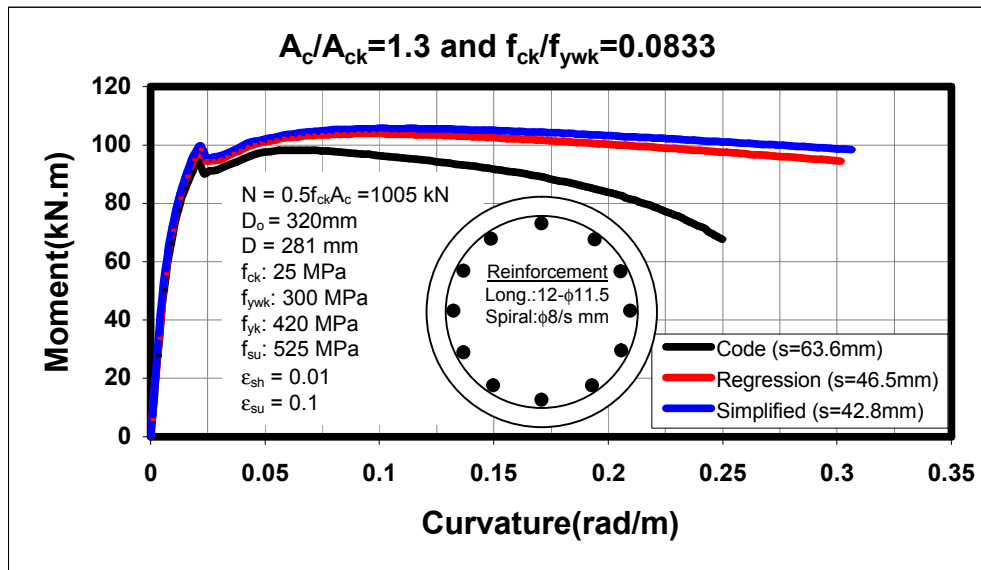


Figure C.15. Comparison of Different Number and Orientation of Longitudinal Bars for Section 9

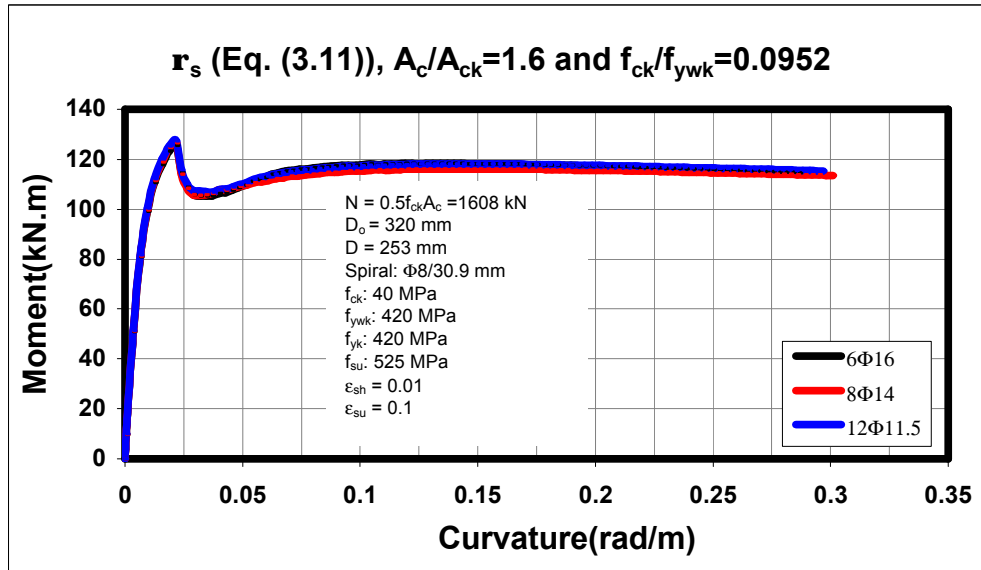


Figure C.16. Comparison of Different Number and Orientation of Longitudinal Bars for Section 24

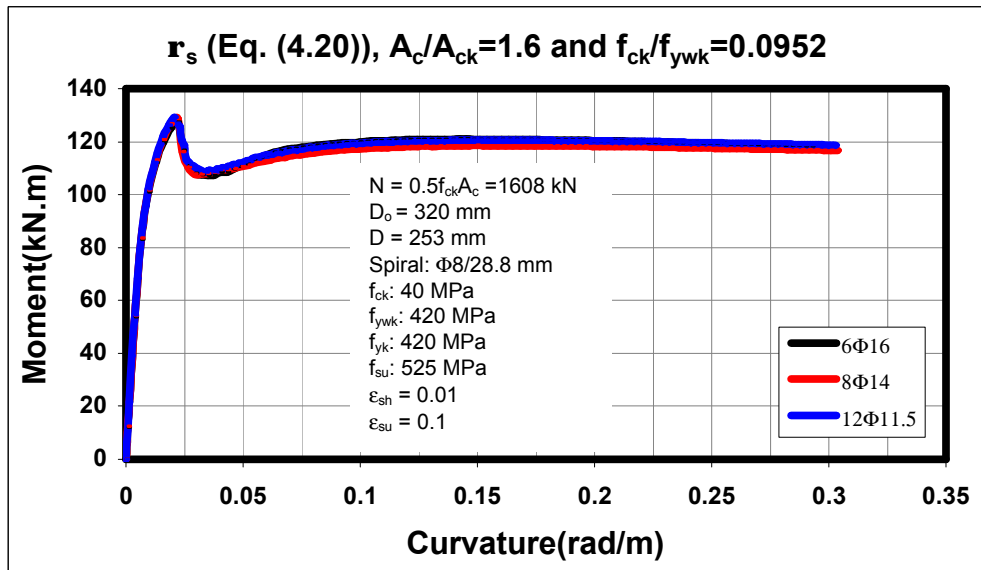


Figure C.17. Comparison of Different Number and Orientation of Longitudinal Bars for Section 24

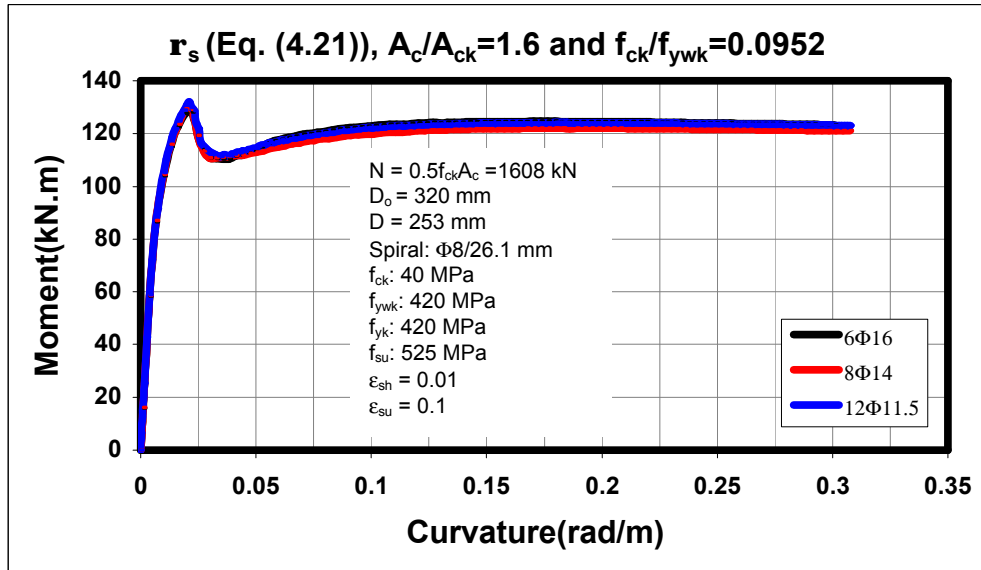


Figure C.18. Comparison of Different Number and Orientation of Longitudinal Bars for Section 24

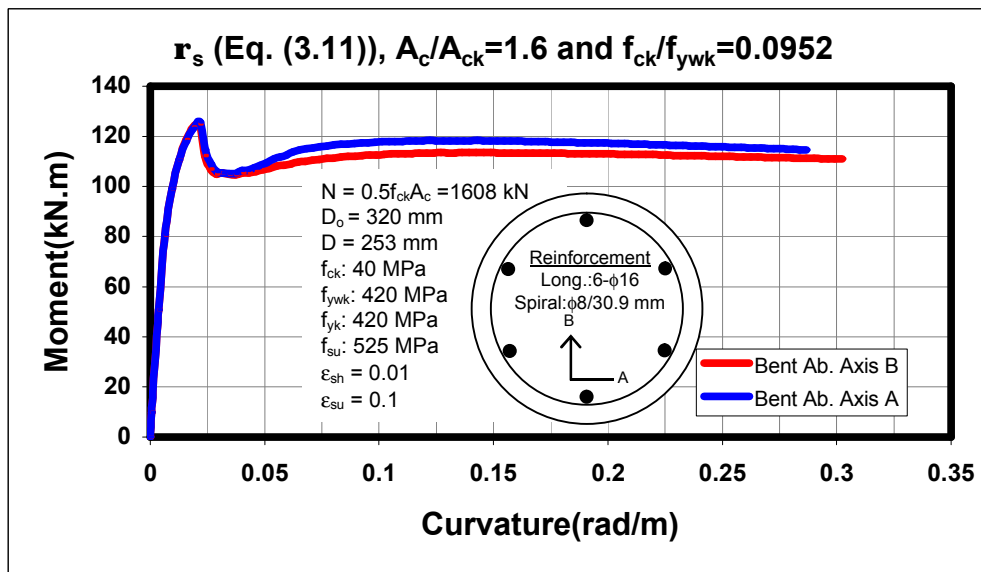


Figure C.19. Comparison of Different Number and Orientation of Longitudinal Bars for Section 24

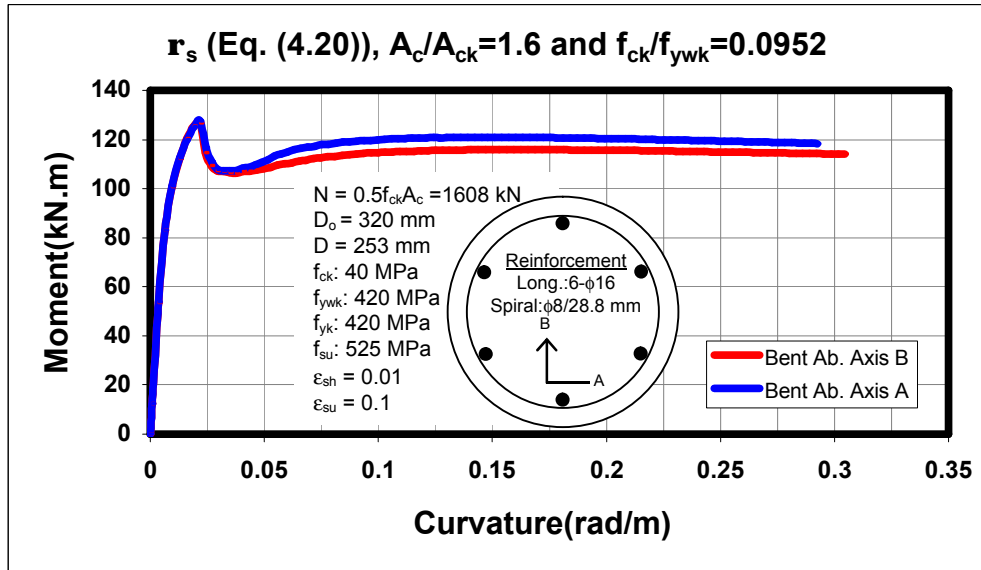


Figure C.20. Comparison of Different Number and Orientation of Longitudinal Bars for Section 24

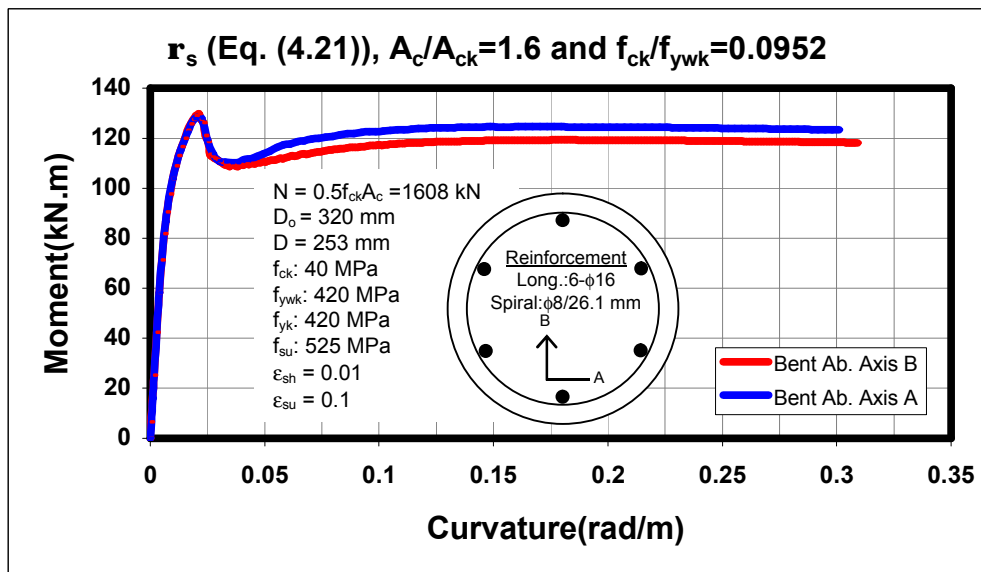


Figure C.21. Comparison of Different Number and Orientation of Longitudinal Bars for Section 24

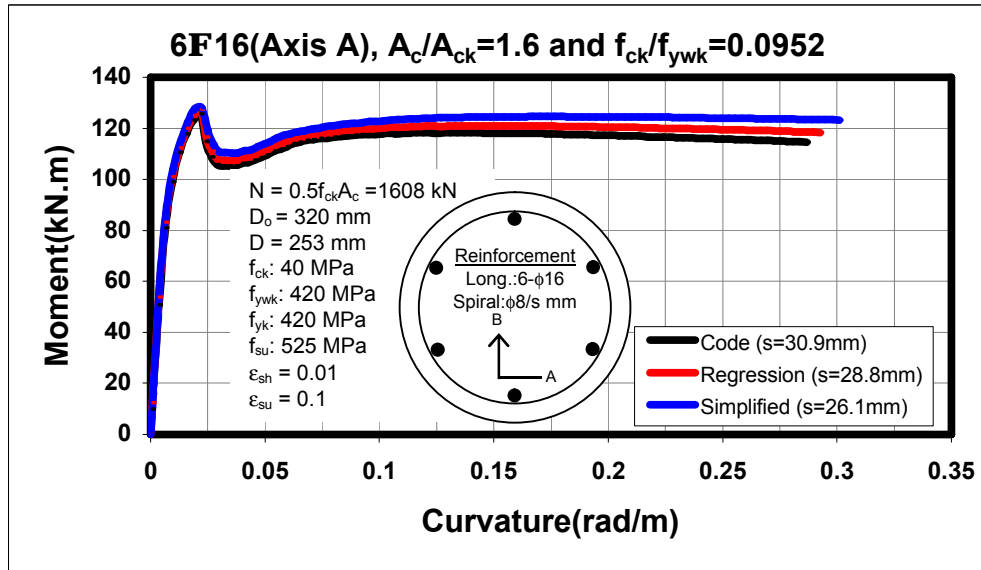


Figure C.22. Comparison of Different Number and Orientation of Longitudinal Bars for Section 24

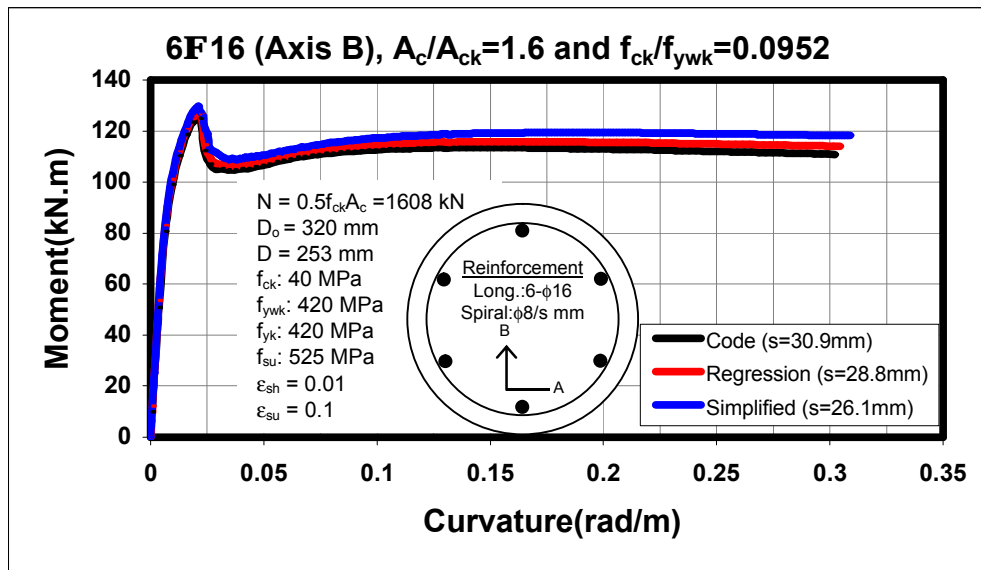


Figure C.23. Comparison of Different Number and Orientation of Longitudinal Bars for Section 24

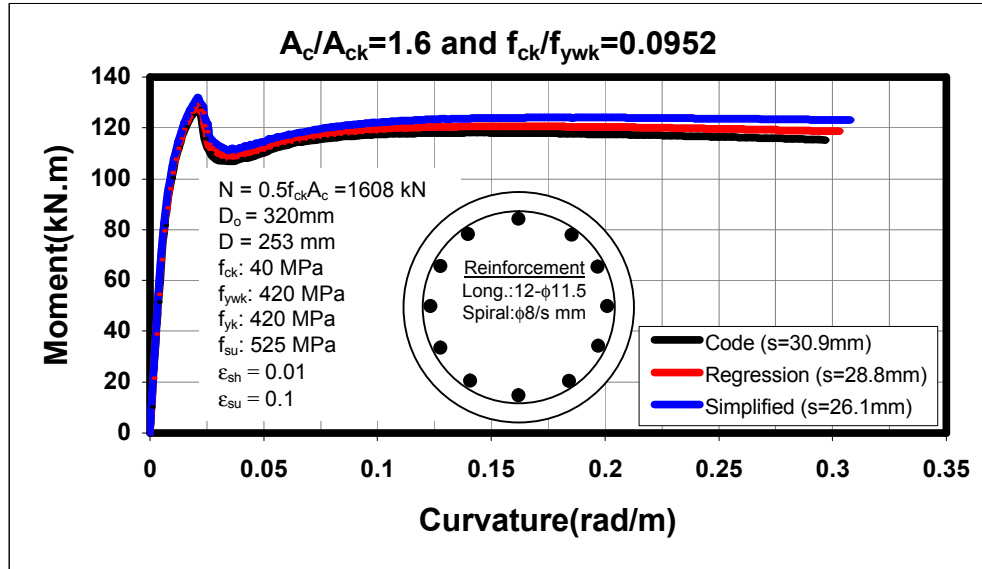


Figure C.24. Comparison of Different Number and Orientation of Longitudinal Bars for Section 24

APPENDIX D

MOMENT-CURVATURE COMPARISONS

(Effect of Volumetric Ratio of Spiral Steel on Section Behaviour (HSC))

In Appendix D, Moment-Curvature curves of the 28 sections having spiral ratios according to Eqs. (3.11), (3.12), (4.41) and (4.21) are presented. Detailed information can be found in Section 5.4. Detailed information about sections can be found in Table 4.1 and Table 5.9.

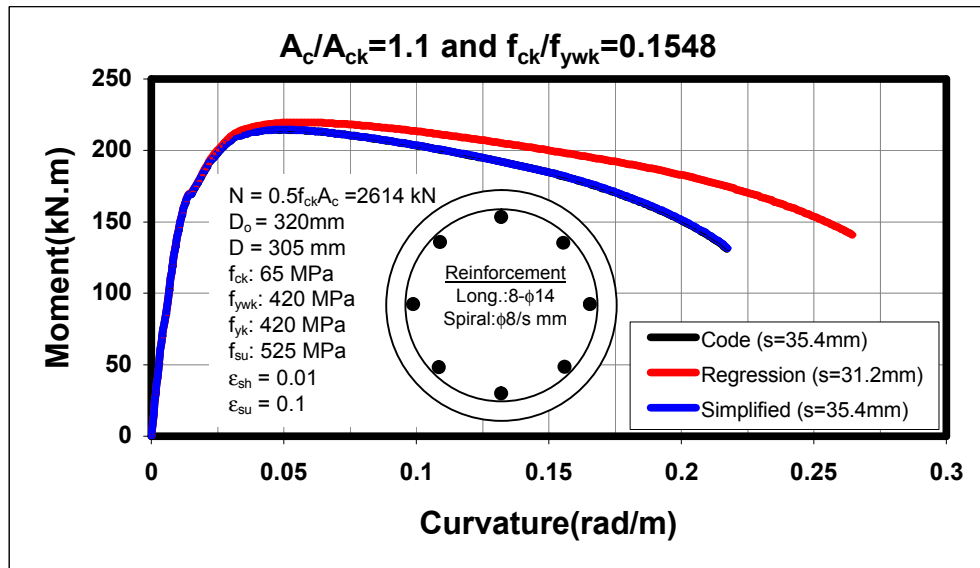


Figure D.1. Comparison of Proposed and Code Equations for Section 29

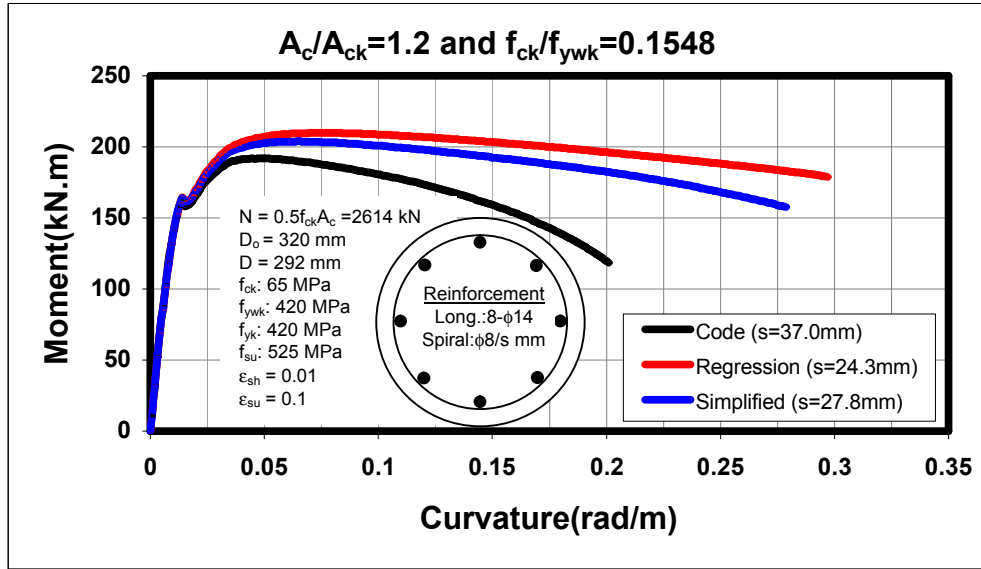


Figure D.2. Comparison of Proposed and Code Equations for Section 30

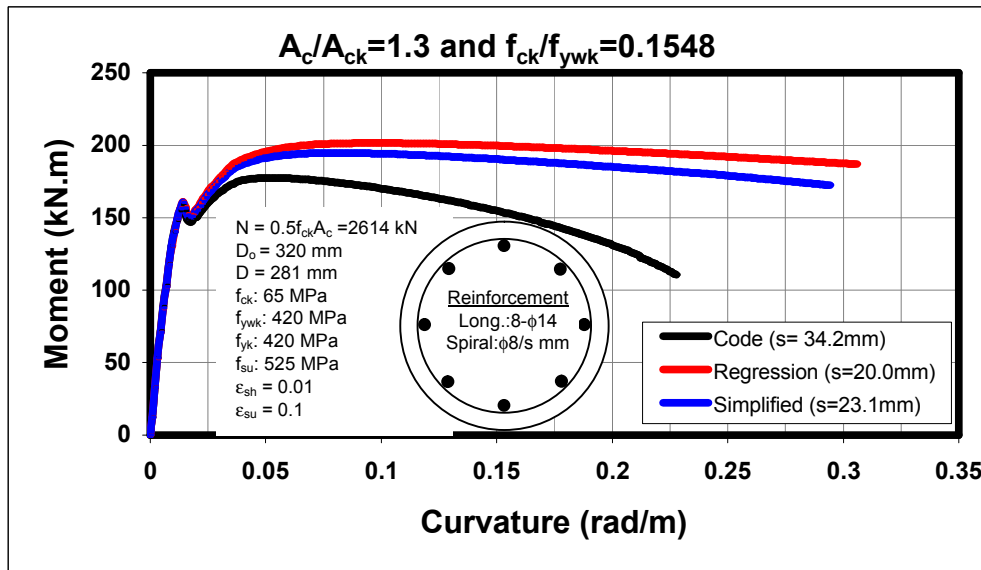


Figure D.3. Comparison of Proposed and Code Equations for Section 31

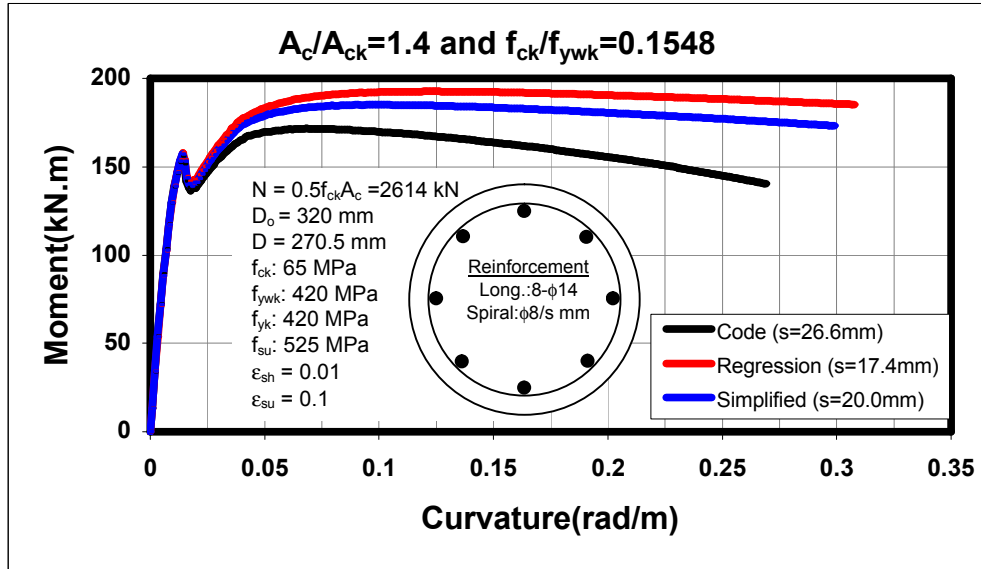


Figure D.4. Comparison of Proposed and Code Equations for Section 32

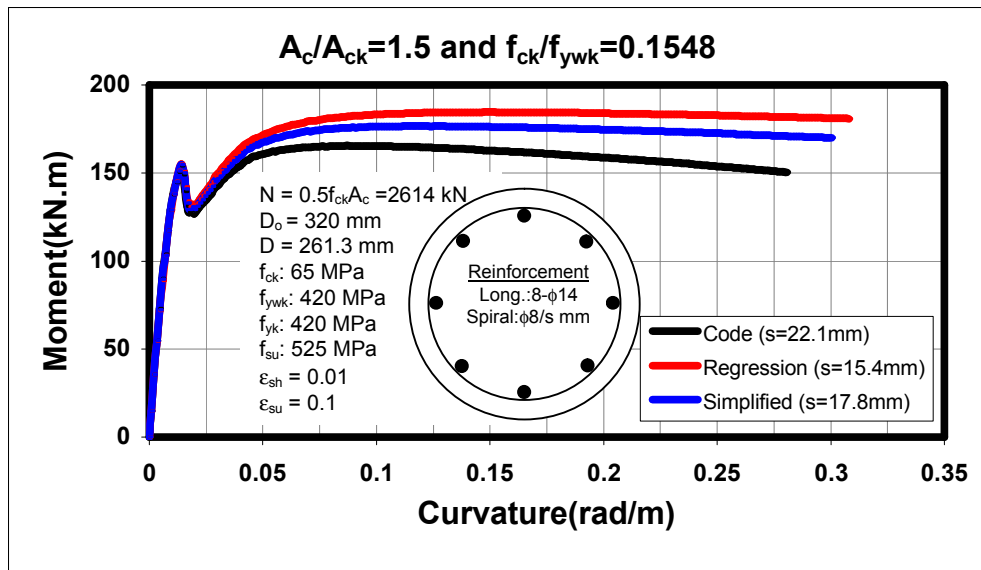


Figure D.5. Comparison of Proposed and Code Equations for Section 33

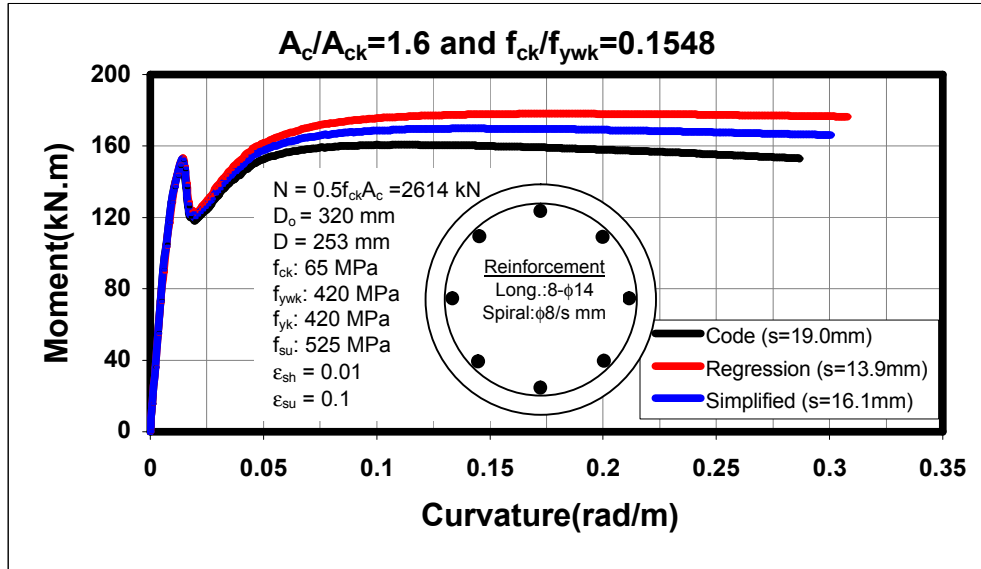


Figure D.6. Comparison of Proposed and Code Equations for Section 34

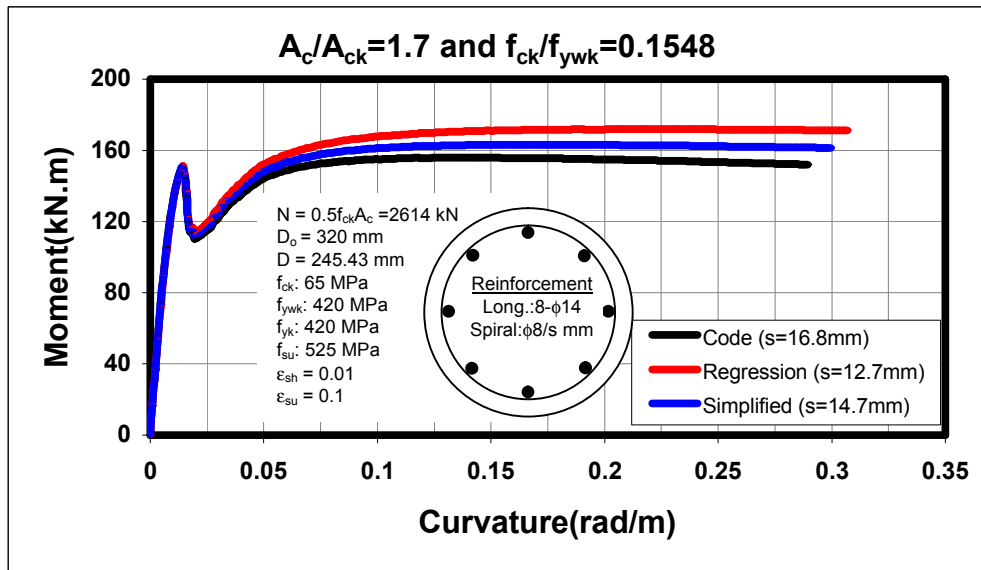


Figure D.7. Comparison of Proposed and Code Equations for Section 35

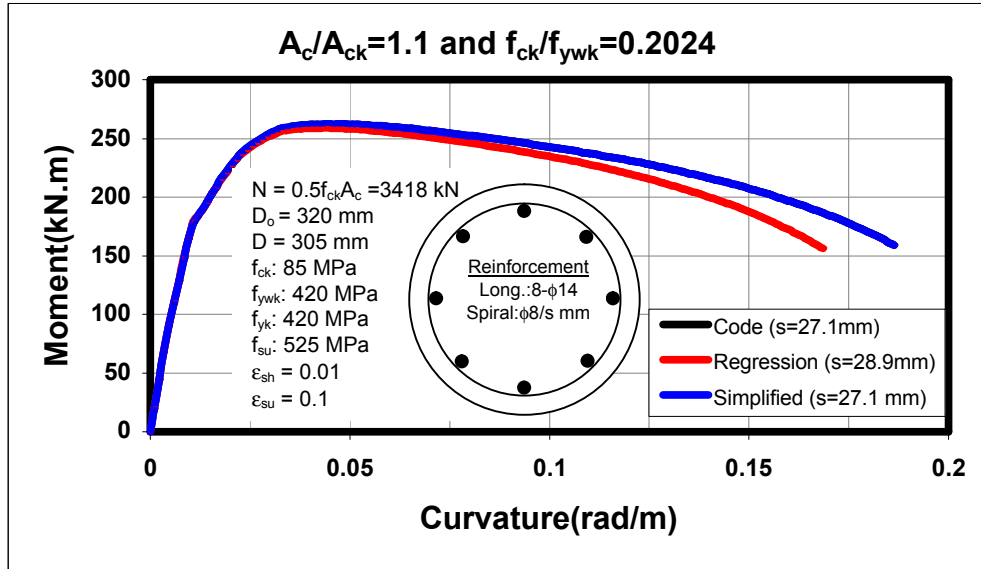


Figure D.8. Comparison of Proposed and Code Equations for Section 36

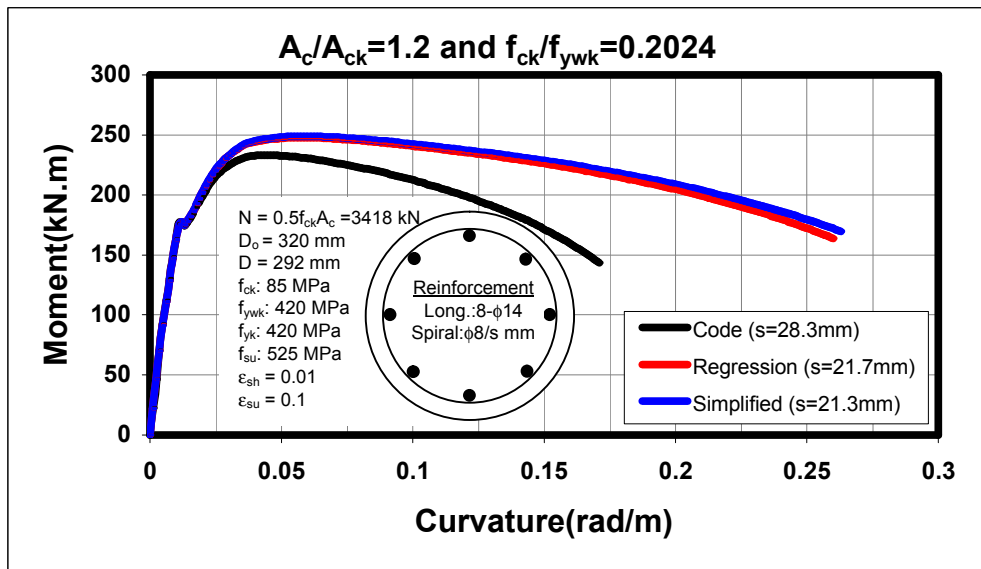


Figure D.9. Comparison of Proposed and Code Equations for Section 37

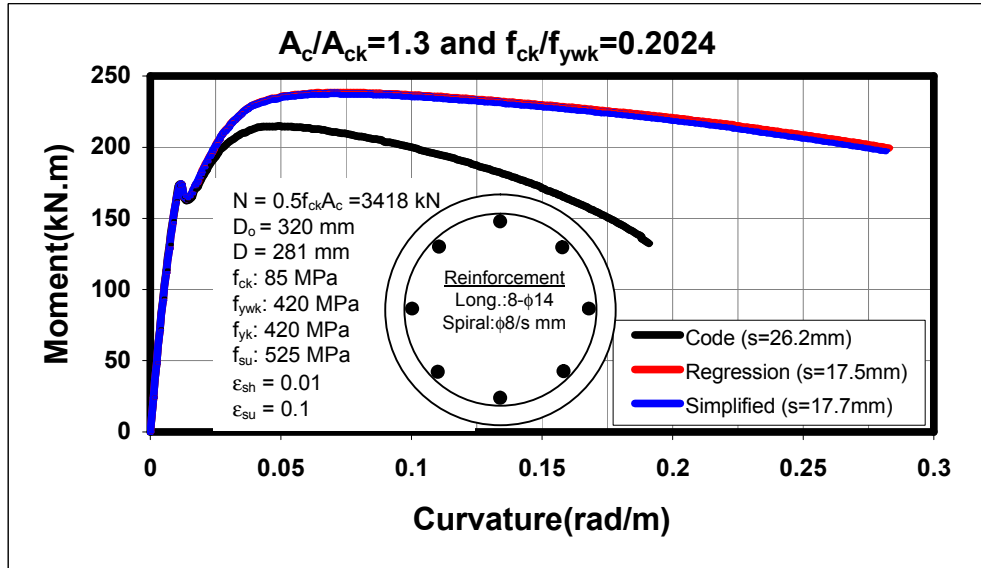


Figure D.10. Comparison of Proposed and Code Equations for Section 38

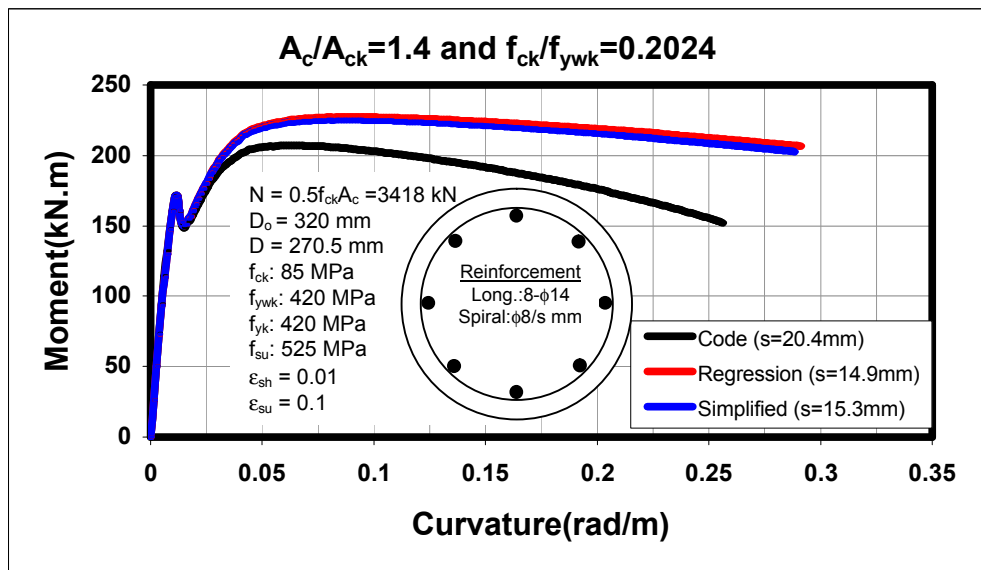


Figure D.11. Comparison of Proposed and Code Equations for Section 39

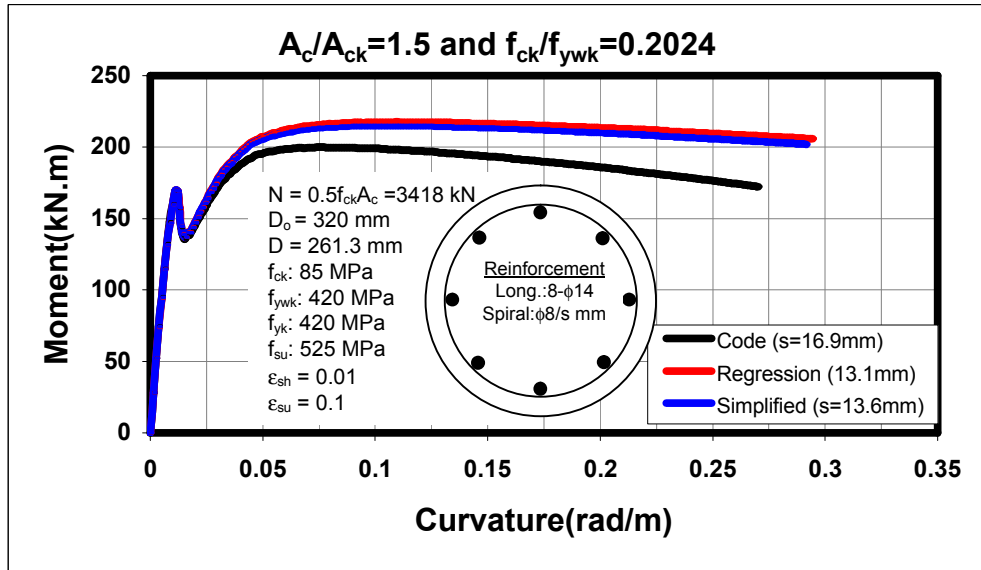


Figure D.12. Comparison of Proposed and Code Equations for Section 40

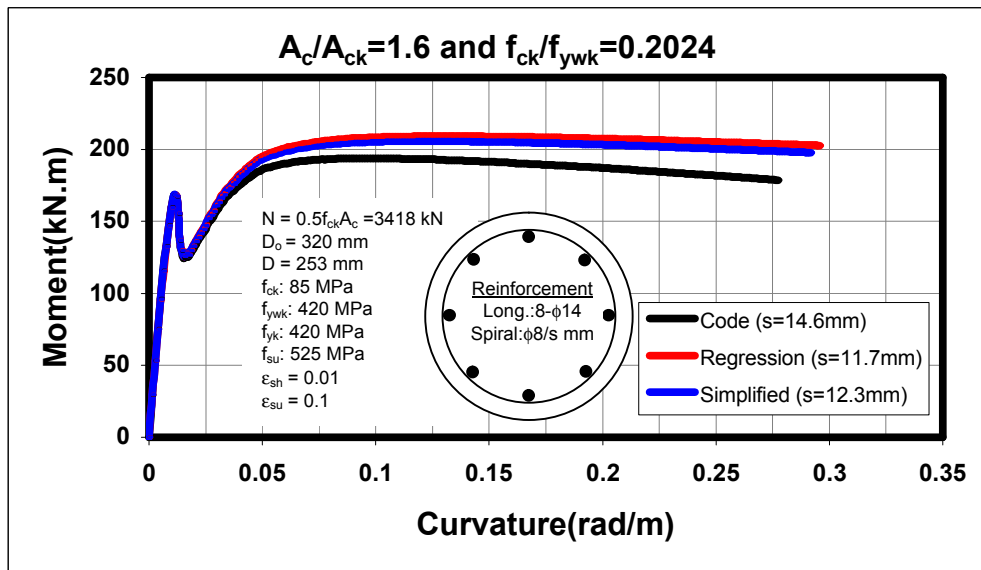


Figure D.13. Comparison of Proposed and Code Equations for Section 41

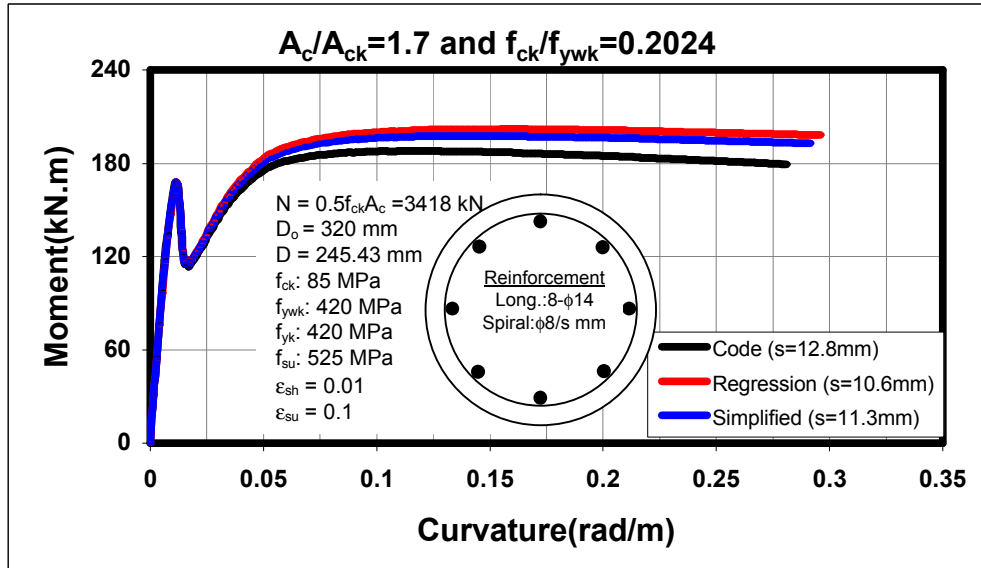


Figure D.14. Comparison of Proposed and Code Equations for Section 42

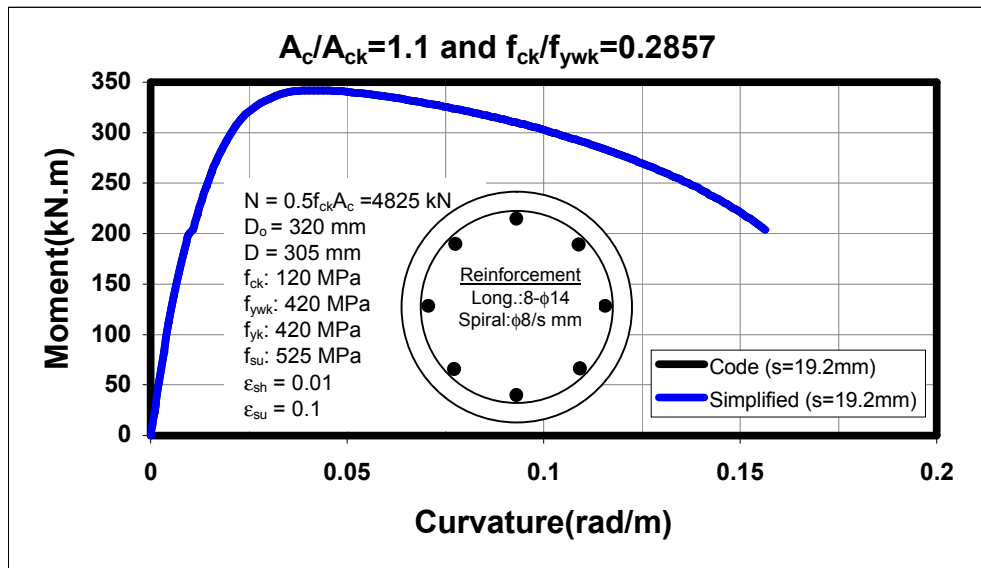


Figure D.15. Comparison of Proposed and Code Equations for Section 43

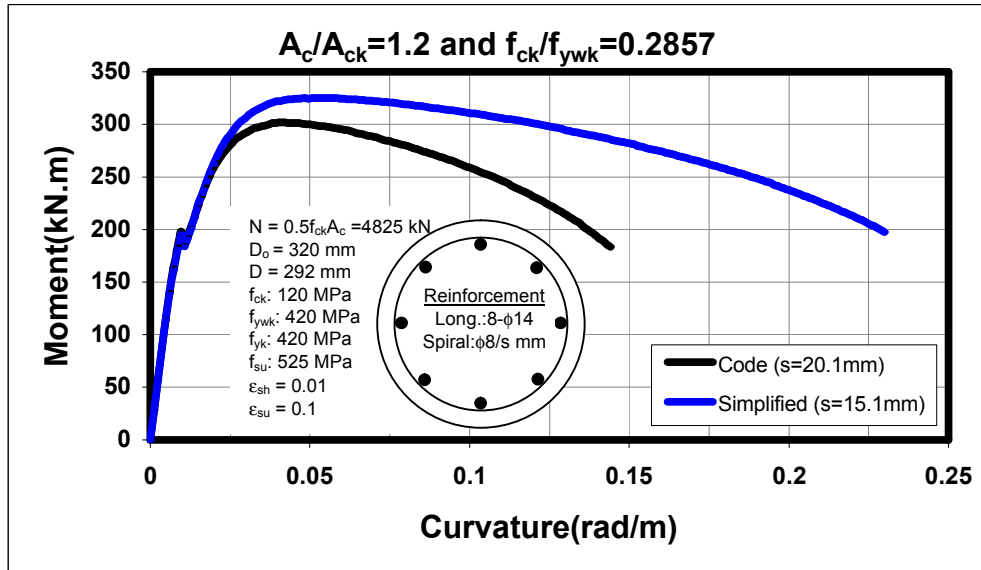


Figure D.16. Comparison of Proposed and Code Equations for Section 44

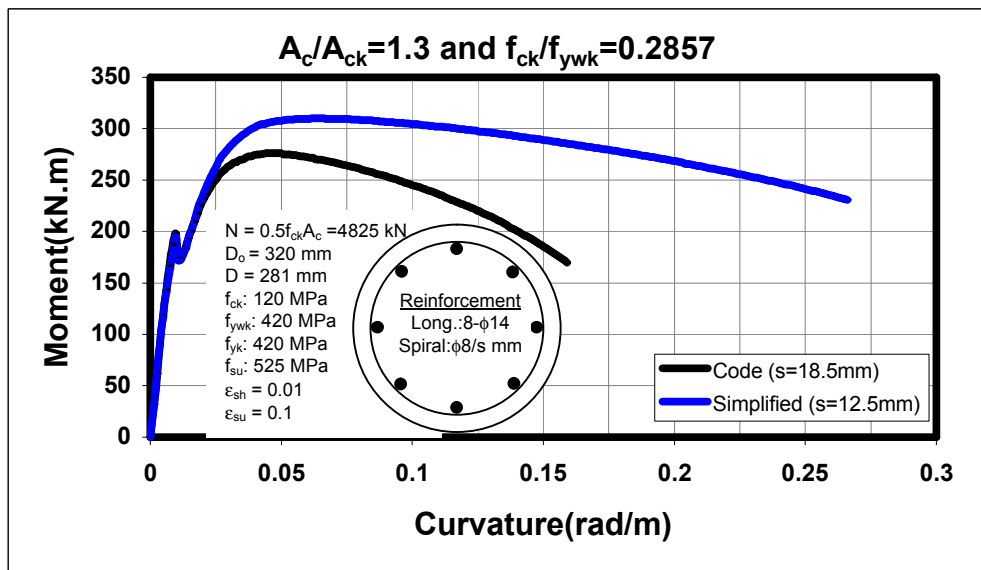


Figure D.17. Comparison of Proposed and Code Equations for Section 45

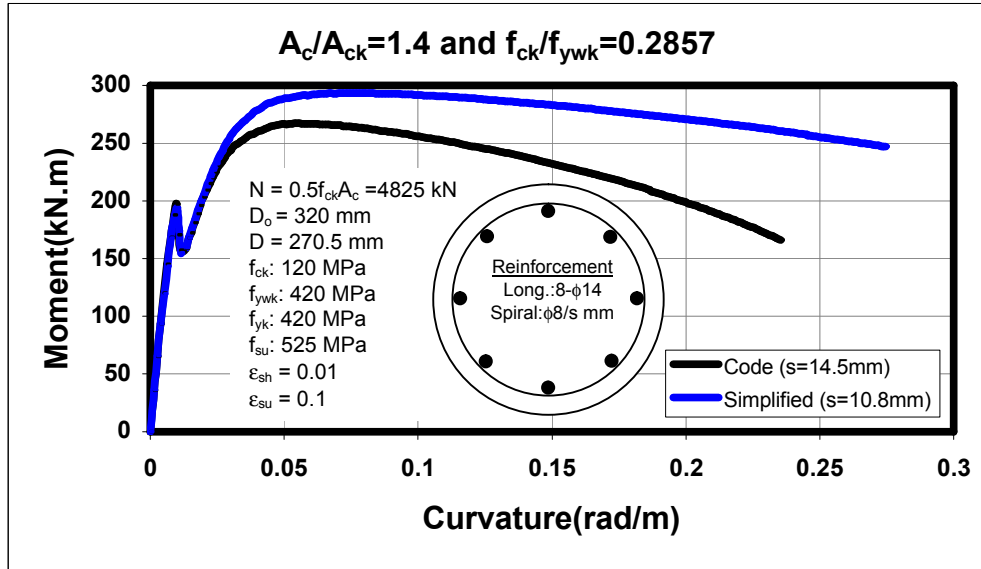


Figure D.18. Comparison of Proposed and Code Equations for Section 46

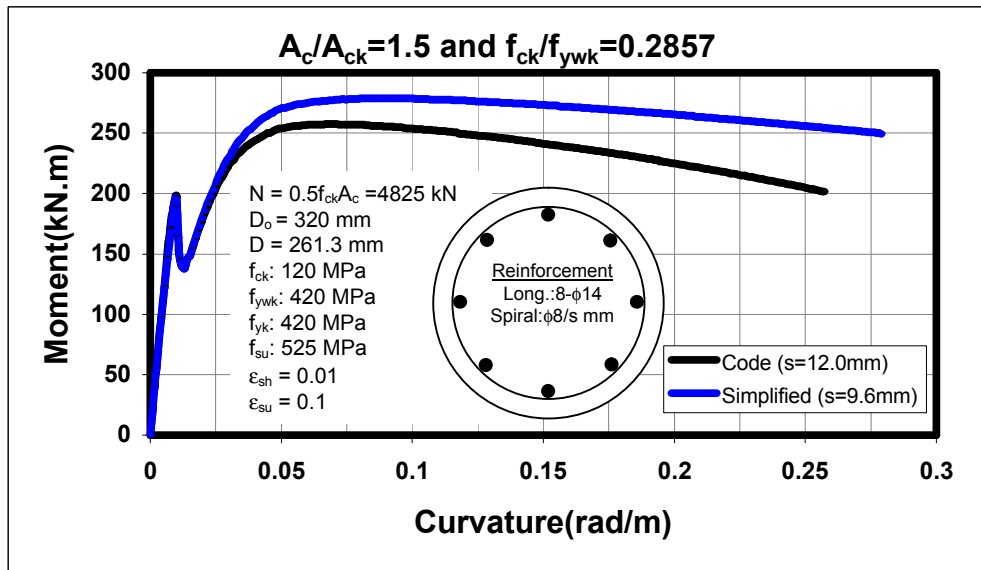


Figure D.19. Comparison of Proposed and Code Equations for Section 47

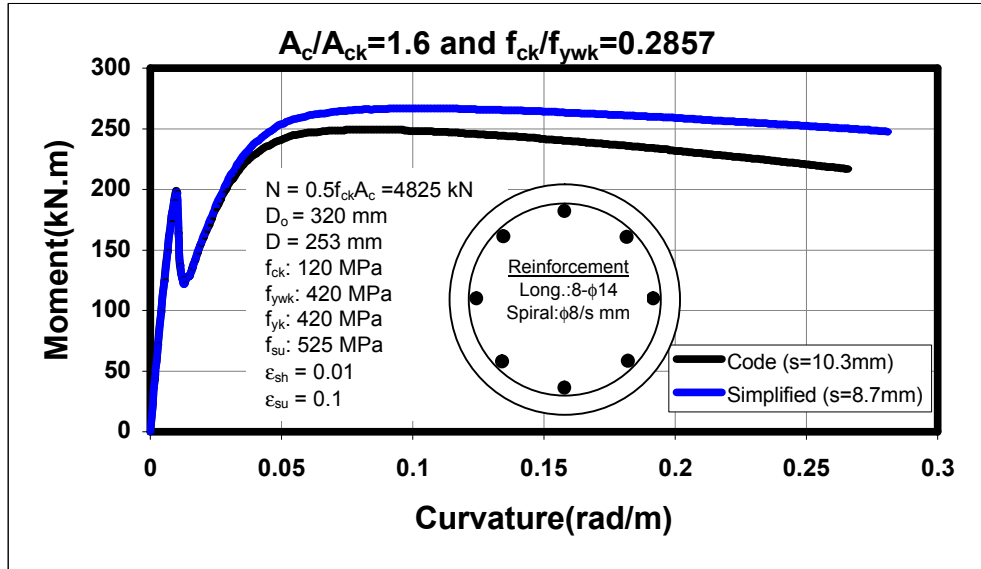


Figure D.20. Comparison of Proposed and Code Equations for Section 48

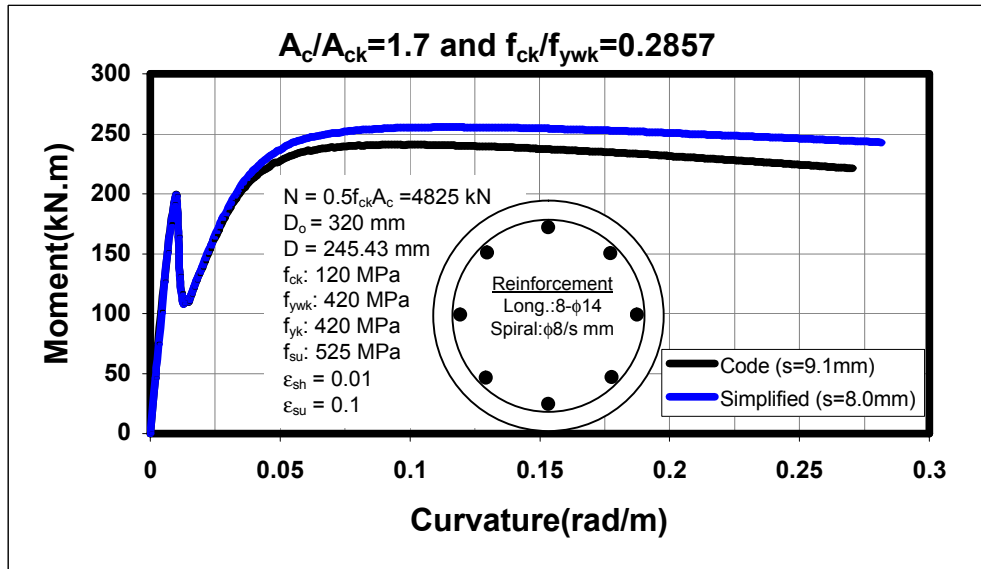


Figure D.21. Comparison of Proposed and Code Equations for Section 49

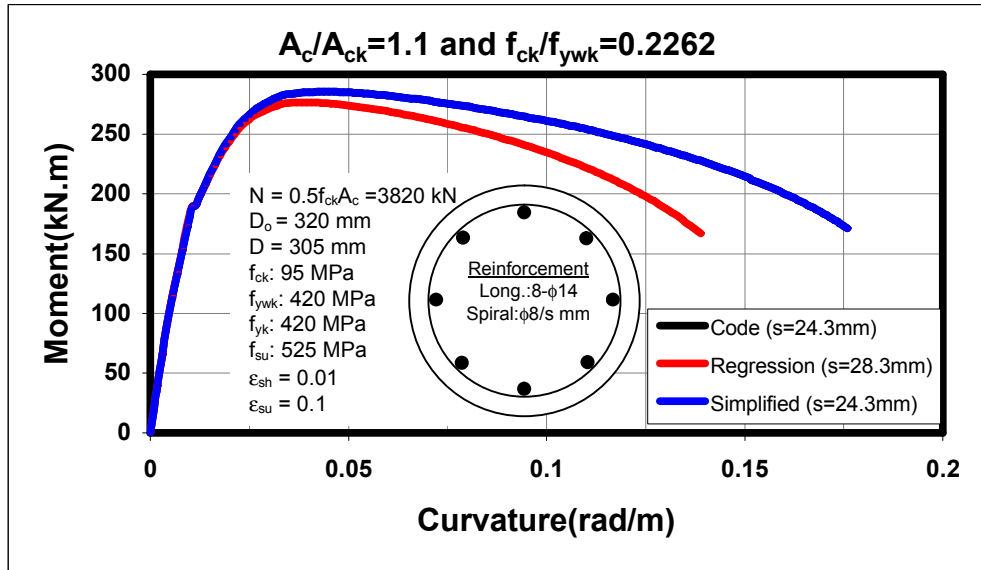


Figure D.22. Comparison of Proposed and Code Equations for Section 50

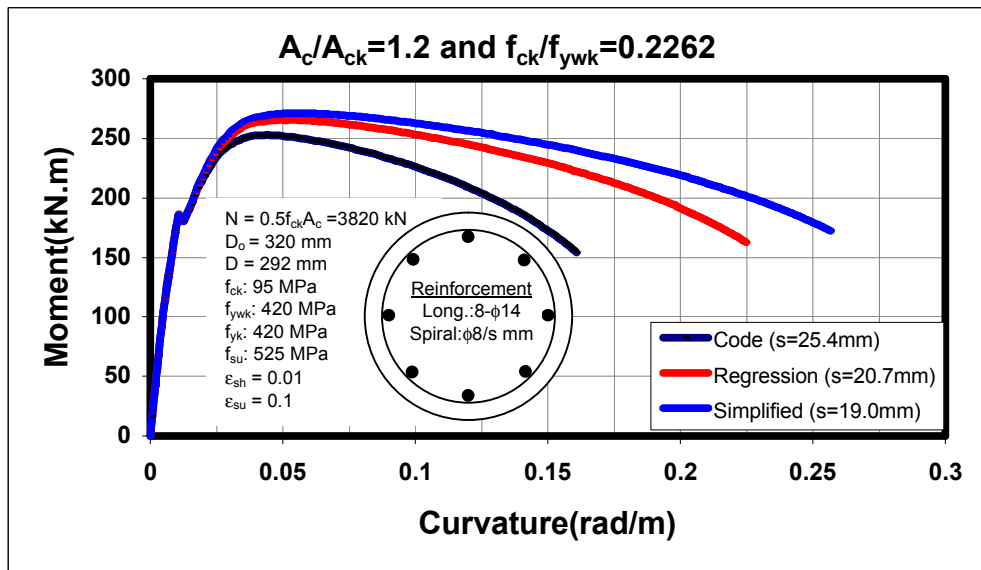


Figure D.23. Comparison of Proposed and Code Equations for Section 51

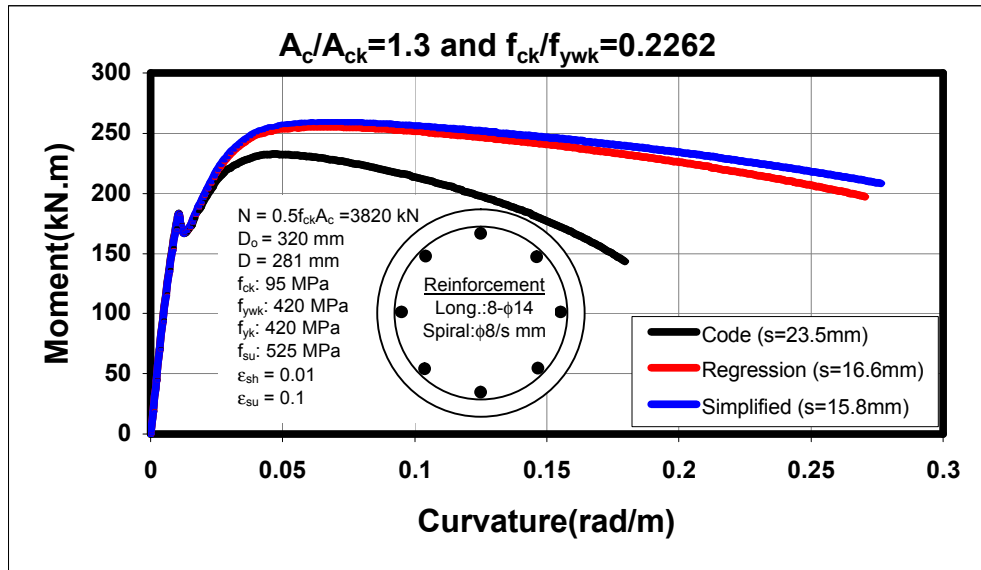


Figure D.24. Comparison of Proposed and Code Equations for Section 52

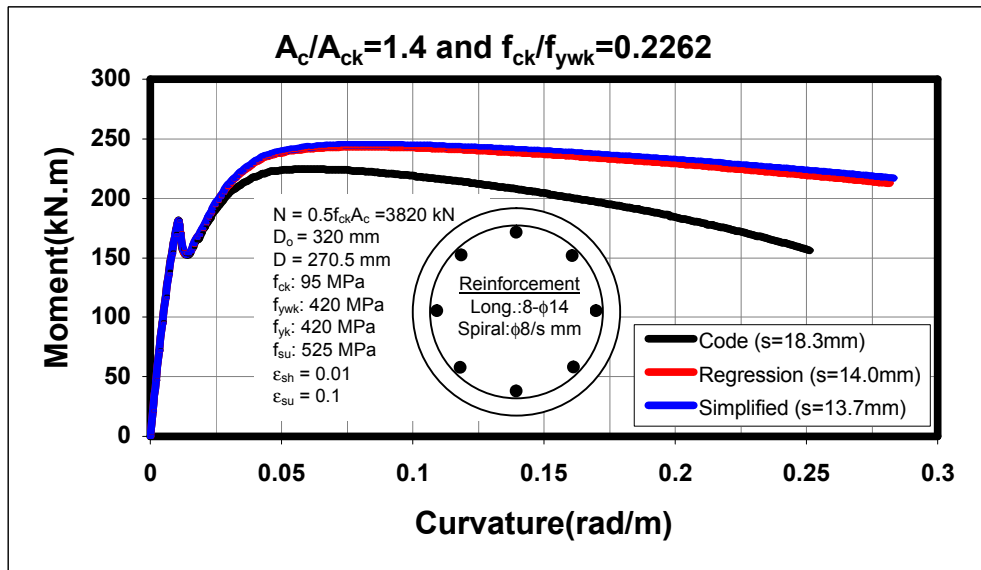


Figure D.25. Comparison of Proposed and Code Equations for Section 53

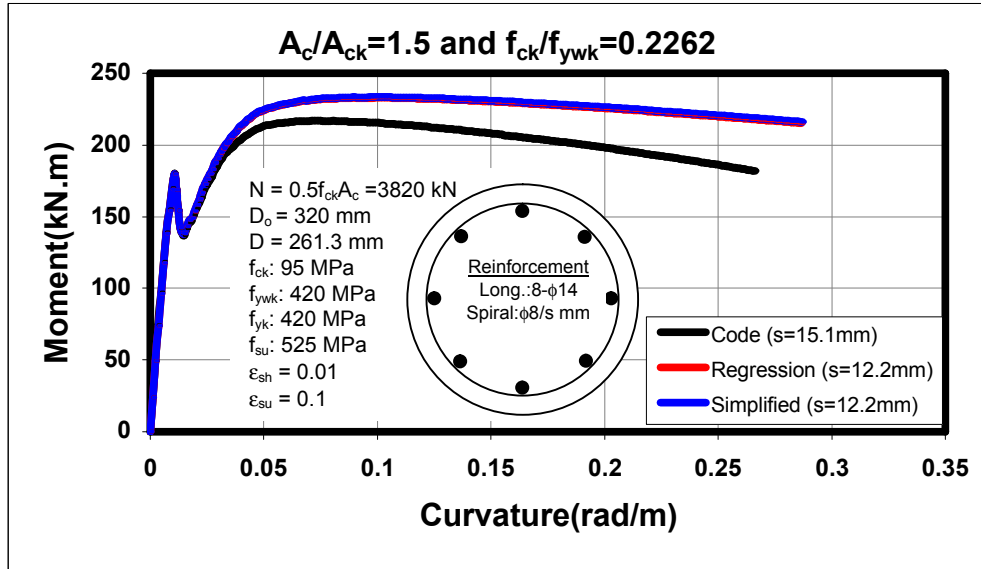


Figure D.26. Comparison of Proposed and Code Equations for Section 54

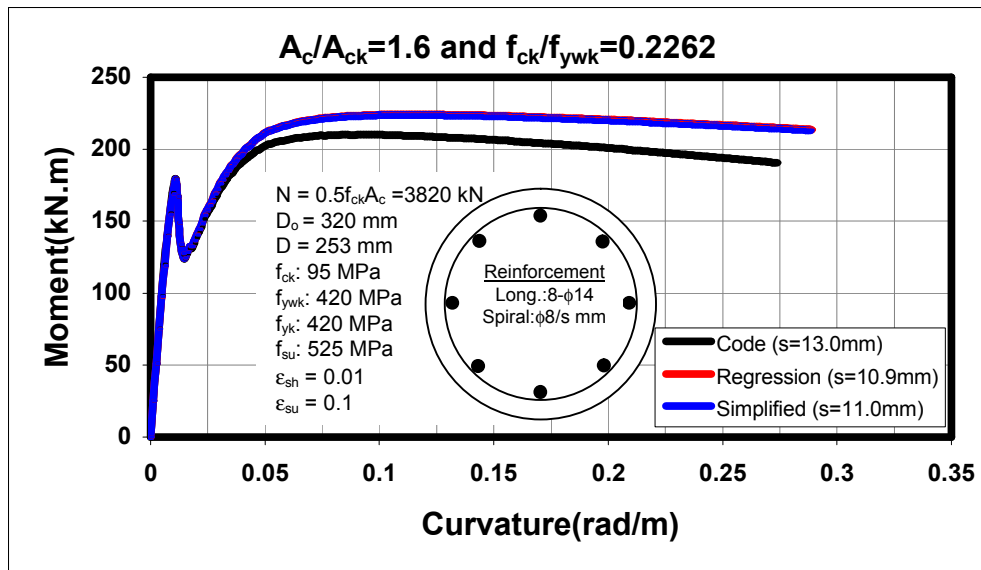


Figure D.27. Comparison of Proposed and Code Equations for Section 55

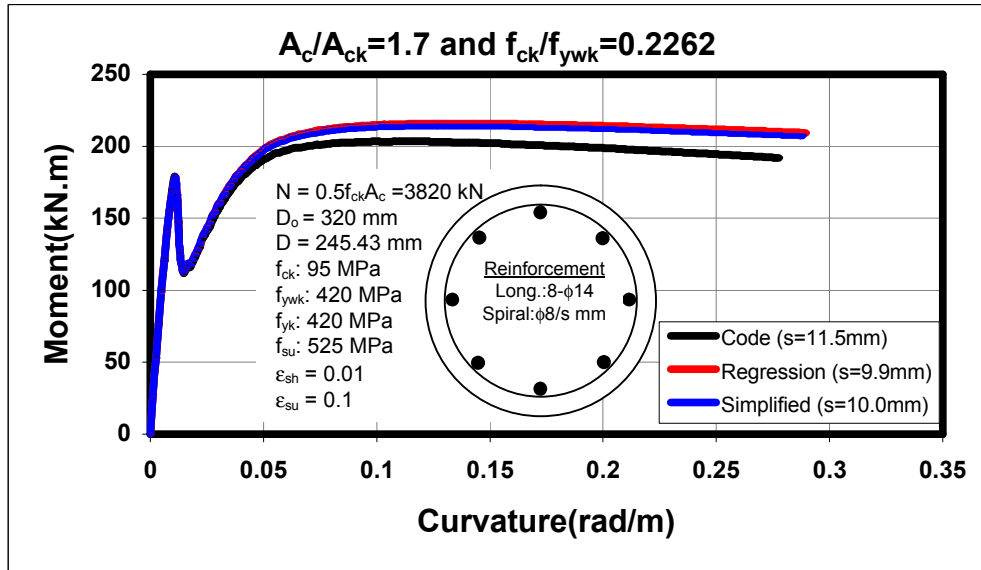


Figure D.28. Comparison of Proposed and Code Equations for Section 56